High-$E_{\rm T}$ isolated-photon plus jets production in pp collisions at $\sqrt s=$ 8 TeV with the ATLAS detector

ATLAS Collaboration

Link to publication on Research at Birmingham portal

High-E_T isolated-photon plus jets production in pp collisions at $\sqrt{s}$ = 8 TeV with the ATLAS detector

The ATLAS Collaboration

The dynamics of isolated-photon plus one-, two- and three-jet production in pp collisions at a centre-of-mass energy of 8 TeV are studied with the ATLAS detector at the LHC using a data set with an integrated luminosity of 20.2 fb^{-1}. Measurements of isolated-photon plus jets cross sections are presented as functions of the photon and jet transverse momenta. The cross sections as functions of the azimuthal angle between the photon and the jets, the azimuthal angle between the jets, the photon–jet invariant mass and the scattering angle in the photon–jet centre-of-mass system are presented. The pattern of QCD radiation around the photon and the leading jet is investigated by measuring jet production in an annular region centred on each object; enhancements are observed around the leading jet with respect to the photon in the directions towards the beams. The experimental measurements are compared to several different theoretical calculations, and overall a good description of the data is found.

arXiv:1611.06586v1 [hep-ex] 20 Nov 2016

Contents

1 Introduction

The production of prompt photons in association with jets in proton–proton collisions, $pp \rightarrow \gamma + \text{jets} + X$, provides a testing ground for perturbative QCD (pQCD) with a hard colourless probe less affected by hadronisation effects than jet production. The measurements of the angular correlations between the photon and the jets can be used to probe the dynamics of the hard-scattering process. Since the dominant production mechanism in pp collisions at the Large Hadron Collider (LHC) proceeds via the $qg \rightarrow q\gamma$ process, measurements of prompt-photon plus jet production are useful in constraining the gluon density in the proton [1, 2]. These measurements can also be used to tune the Monte Carlo (MC) models and to test t-channel quark exchange [3].

At leading order (LO) in pQCD, the reaction $pp \rightarrow \gamma + \text{jet} + X$ is understood to proceed via two separate production mechanisms: direct photons (D), which originate from the hard process, and fragmentation photons (F), which arise from the fragmentation of a coloured, high transverse momentum (p_T) parton [4, 5]. The direct and fragmentation contributions are only well defined at LO; at higher orders such distinction is no longer possible. Measurements of prompt-photon production in a final state with accompanying hadrons require isolation of photons to avoid the large contribution from neutral-hadron decays into photons. The production of inclusive isolated photons in pp collisions was studied by the ATLAS [6–9] and CMS [10, 11] collaborations. The cross section for isolated photons in association with jets as a function of the photon transverse energy[1] (E_T^γ) in different regions of rapidity of the highest-p_T jet was measured by ATLAS [12]. The production of isolated photons in association with jets was also measured by CMS [13–15].

The dynamics of the underlying processes in $2 \rightarrow 2$ hard scattering can be investigated using the variable θ^*, where $\cos\theta^* \equiv \tanh(\Delta y/2)$ and Δy is the difference between the rapidities of the two final-state particles. The variable θ^* coincides with the scattering angle in the centre-of-mass frame for collinear scattering of massless particles, and its distribution is sensitive to the spin of the exchanged particle. For processes dominated by t-channel gluon exchange, such as dijet production in pp collisions, the cross section behaves as $(1-|\cos\theta^*|)^{-2}$ when $|\cos\theta^*| \rightarrow 1$. In contrast, processes dominated by t-channel quark exchange, such as W/Z + jet production, are expected to have an asymptotic $(1-|\cos\theta^*|)^{-1}$ behaviour. This prediction from QCD can be tested in photon plus jet production in high-energy hadron–hadron collisions. The direct-photon contribution, as shown in Figure 1(a), is expected to exhibit a $(1-|\cos\theta^*|)^{-1}$ dependence when $|\cos\theta^*| \rightarrow 1$, whereas that of fragmentation processes, as shown in Figure 1(b), is predicted to be the same as in dijet production, namely $(1-|\cos\theta^*|)^{-2}$. For both processes, there are also s-channel contributions which are, however, non-singular when $|\cos\theta^*| \rightarrow 1$. At higher orders, direct processes such as $qq \rightarrow qq\gamma$ are dominated by t-channel gluon exchange and contribute to the distribution in $|\cos\theta^*|$ with a component similar to that of fragmentation. However, a measurement of the cross section for prompt-photon plus jet production as a function of $|\cos\theta^*|$ is still sensitive to the relative contributions of the direct and fragmentation components and allows a test of the dominance of the t-channel quark exchange, such as that shown in Figure 1(a).

---

[1] ATLAS uses a right-handed coordinate system with its origin at the nominal interaction point (IP) in the centre of the detector and the z-axis along the beam pipe. The x-axis points from the IP to the centre of the LHC ring, and the y-axis points upwards. Cylindrical coordinates (r, ϕ) are used in the transverse plane, ϕ being the azimuthal angle around the z-axis. The pseudorapidity is defined in terms of the polar angle θ as $\eta = -\ln\tan(\theta/2)$. Angular distance is measured in units of $\Delta R \equiv \sqrt{(\Delta\eta)^2 + (\Delta\phi)^2}$. The rapidity is defined as $y = 0.5\ln[(E + p_z)/(E - p_z)]$, where E is the energy and p_z is the z-component of the momentum, and transverse energy is defined as $E_T = E\sin\theta$.
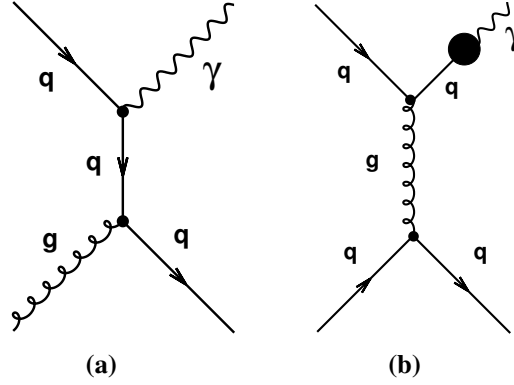
Figure 1: Examples of diagrams for (a) γ + jet production through direct-photon processes and (b) γ + jet production through fragmentation processes.

Colour connection between the partons in the initial and final states modifies the pattern of QCD radiation around the final-state partons. Colour-coherence effects were studied at the Tevatron [16, 17] using dijet events by comparing the measurements with predictions with and without such effects. Photon plus two-jet events are optimal for investigating jet production around the photon and the highest-p_T jet: the partons are colour-connected while the photon is colourless.

The results presented in this paper include measurements of cross sections for isolated-photon plus one-, two- and three-jet final states as functions of E_T^γ and the transverse momentum of the leading jet (jet1, p_T^{jet1}), the second-highest-p_T jet (jet2, p_T^{jet2}) and the third-highest-p_T jet (jet3, p_T^{jet3}) [5, 18–20]. The analysis is performed using a dataset with an integrated luminosity of 20.2 fb^{-1} of pp collisions at $\sqrt{s}$ = 8 TeV. The dynamics of the photon plus one-jet system are studied by measuring the photon–jet invariant mass ($m^{\gamma-jet1}$) and $\cos\theta^*$ [5]. In addition, the azimuthal angles between the photon and each jet ($\Delta\phi^{\gamma-jet2}$, $\Delta\phi^{\gamma-jet3}$) and between the jets ($\Delta\phi^{jet1-jet2}$, $\Delta\phi^{jet1-jet3}$, $\Delta\phi^{jet2-jet3}$) are measured for photon plus two- and three-jet events [19, 20]. The production of jet2 around the photon and jet1 is measured separately to investigate the differences between the two configurations. The scale evolution of the photon plus one-jet system is studied by measuring the cross sections as functions of $\cos\theta^*$ in different regions of $m^{\gamma-jet1}$. For photon plus two- and three-jet events, the scale evolution is investigated by measuring the angular correlations in different regions of E_T^γ.

The predictions from the event generators PYTHIA [21] and SHERPA [22] are compared with the measurements. The next-to-leading-order (NLO) QCD predictions from JETPHOX [23, 24] are compared with the photon plus one-jet measurements, whereas those from BLACKHAT [25, 26] are compared with the photon plus two-jet and photon plus three-jet measurements.

2 The ATLAS detector

The ATLAS detector [27] at the LHC covers nearly the entire solid angle around the collision point. It consists of an inner tracking detector surrounded by a thin superconducting solenoid, electromagnetic and hadronic calorimeters, and a muon spectrometer incorporating three large superconducting toroidal magnets.

The inner-detector system (ID) is immersed in a 2 T axial magnetic field and provides charged-particle tracking in the range $|\eta| < 2.5$. A high-granularity silicon pixel detector covers the interaction region and typically provides three measurements per track. It is followed by a silicon microstrip tracker, which provides eight two-dimensional measurement points per track. These silicon detectors are complemented by a transition radiation tracker, which enables radially extended track reconstruction up to $|\eta| = 2.0$. The transition radiation tracker also provides electron identification information based on the fraction of the typically 30 total hits which are above a higher energy-deposit threshold corresponding to transition radiation.

The calorimeter system covers the pseudorapidity range $|\eta| < 4.9$. Within the region $|\eta| < 3.2$, electromagnetic calorimetry is provided by barrel and endcap high-granularity lead/liquid-argon (LAr) electromagnetic calorimeters, with an additional thin LAr presampler covering $|\eta| < 1.8$ to correct for energy loss in material upstream of the calorimeters; for $|\eta| < 2.5$ the LAr calorimeter is divided into three layers in depth, which are finely segmented in η and ϕ. Hadronic calorimetry is provided by a steel/scintillator-tile calorimeter, segmented into three barrel structures within $|\eta| < 1.7$, and two copper/LAr hadronic endcap calorimeters, which cover $1.5 < |\eta| < 3.2$. The solid angle coverage is completed with forward copper/LAr and tungsten/LAr calorimeter modules optimised for electromagnetic and hadronic measurements, respectively.

The muon spectrometer (MS) comprises separate trigger and high-precision tracking chambers measuring the deflection of muons in a magnetic field generated by superconducting air-core toroids. The tracking chamber system covers the region $|\eta| < 2.7$ with three layers of monitored drift tubes, complemented by cathode-strip chambers in the forward region. The muon trigger system covers the range $|\eta| < 2.4$ with resistive-plate chambers in the barrel and thin-gap chambers in the endcap regions.

A three-level trigger system is used to select interesting events [28]. The level-1 trigger is implemented in hardware and uses a subset of detector information to reduce the event rate to at most 75 kHz. This is followed by two software-based trigger levels which together reduce the event rate to about 400 Hz.

3 Data selection

The data used in this analysis were collected during the proton–proton collision running period of 2012, when the LHC operated at a centre-of-mass energy of $\sqrt{s} = 8$ TeV. Only events taken in stable beam conditions and passing detector and data-quality requirements are considered. Events were recorded using a single-photon trigger, with a nominal transverse energy threshold of 120 GeV; this trigger is used offline to select events in which the photon transverse energy, after reconstruction and calibration, is greater than 130 GeV. For isolated photons with $E_T^\gamma > 130$ GeV and pseudorapidity $|\eta^\gamma| < 2.37$ the trigger efficiency is higher than 99.8%. The integrated luminosity of the collected sample is 20.2 ± 0.4 fb^{-1} [29].

The sample of isolated-photon plus jets events is selected using offline criteria similar to those reported in previous publications [3, 9]. Events are required to have a reconstructed primary vertex consistent with the average beam-spot position, with at least two associated charged-particle tracks with $p_T > 400$ MeV. If more than one such vertex is present in the event, the one with the highest sum of the p_T^2 of the associated tracks is selected as the primary vertex.

During the 2012 data-taking period there were on average 19 proton–proton interactions per bunch crossing. The methods used to mitigate the effects of the additional pp interactions (pile-up) on the photon isolation and jet reconstruction are described below.

5

3.1 Photon selection

The selection of photon candidates is based on energy clusters reconstructed in the electromagnetic calorimeter with transverse energies exceeding 2.5 GeV. The clusters matched to charged-particle tracks, based on the distance in (η, ϕ) between the cluster barycentre and the track impact point extrapolated to the second layer of the LAr calorimeter, are classified as electron candidates. Those clusters without matching tracks are classified as unconverted photon candidates, and clusters matched to pairs of tracks originating from reconstructed conversion vertices in the inner detector or to single tracks with no hit in the innermost layer of the pixel detector are classified as converted photon candidates [30]. From MC simulations, 96% of prompt photons with $E_T^\gamma > 25$ GeV are expected to be reconstructed as photon candidates, while the remaining 4% are incorrectly reconstructed as electrons but not as photons. The efficiency to reconstruct photon conversions decreases at high E_T^γ (> 150 GeV), where it becomes more difficult to separate the two tracks from the conversions. Such conversions with very nearby tracks are often not recovered as single-track conversions because of the tighter selections applied to single-track conversion candidates. The overall photon reconstruction efficiency is thus reduced to about 90% for $E_T^\gamma \sim 1$ TeV [30].

The energy measurement is performed using calorimeter and tracking information. A dedicated energy calibration [31] is applied separately for converted and unconverted photon candidates to account for upstream energy loss and both lateral and longitudinal leakage.

The direction of the photon is determined from the barycentre of the energy cluster in the electromagnetic calorimeter and the position of the primary vertex. Events with at least one photon candidate with calibrated $E_T^\gamma > 130$ GeV and $|\eta^\gamma| < 2.37$ are selected; candidates in the region $1.37 < |\eta^\gamma| < 1.56$, which includes the transition region between the barrel and endcap calorimeters, are not considered. The same shower-shape and isolation requirements as described in previous publications [6, 7, 9, 12, 30] are applied to the candidates; these requirements are referred to as "tight" identification criteria. The photon identification efficiency for $E_T^\gamma > 130$ GeV varies in the range (94–100)% depending on η^γ and whether the candidate is classified as an unconverted or converted photon [30].

The photon candidate is required to be isolated based on the amount of transverse energy in a cone of size $\Delta R = 0.4$ around the photon. The isolation transverse energy is computed from three-dimensional topological clusters of calorimeter cells (see Section 3.3) [32] and is denoted by $E_{T,det}^{iso}$. The measured value of $E_{T,det}^{iso}$ is corrected for leakage of the photon's energy into the isolation cone and the estimated contributions from the underlying event and pile-up. The latter correction is performed using the jet-area method [33] to estimate the ambient transverse energy density on an event-by-event basis; this estimate is used to subtract the joint contribution of the underlying event and pile-up to $E_{T,det}^{iso}$ and amounts to 1.5–2 GeV in the 2012 data-taking period. After these corrections, $E_{T,det}^{iso}$ is required to be lower than 4.8 GeV $+ 4.2 \cdot 10^{-3} \cdot E_T^\gamma$ [GeV] [9]; the requirement is E_T^γ-dependent so that in simulation the fraction of identified photons which are isolated stays high as E_T^γ increases. The isolation requirement significantly reduces the main background, which consists of multi-jet events where one jet typically contains a π^0 or η meson that carries most of the jet energy and is misidentified as a prompt photon.

A small fraction of the events contain more than one photon candidate satisfying the selection criteria. In such events, the highest-E_T^γ photon is considered for further study.

3.2 Jet selection

Jets are reconstructed using the anti-k_t algorithm [34] with radius parameter $R = 0.6$. The inputs to the jet reconstruction are three-dimensional topological clusters of calorimeter cells. This method first clusters topologically connected calorimeter cells and classifies these clusters as either electromagnetic or hadronic. The classification uses a local cluster weighting (LCW) calibration scheme based on cell-energy density and longitudinal depth within the calorimeter [35]. Based on this classification, energy corrections derived from single-pion MC simulations are applied. Dedicated corrections are derived for the effects of the non-compensating response of the calorimeter, signal losses due to noise-suppression threshold effects, and energy lost in non-instrumented regions. The jet four-momenta are computed from the sum of the topological cluster four-momenta, treating each as a four-vector with zero mass. These jets are referred to as detector-level jets. The direction of the jet is then corrected such that the jet originates from the selected primary vertex of the event. Prior to the final calibration, the contribution from the underlying event and pile-up is subtracted on a jet-by-jet basis using the jet-area method. An additional jet-energy calibration is derived from MC simulations as a correction relating the calorimeter response to the true jet energy. To determine these corrections, the jet reconstruction procedure applied to the topological clusters is also applied to the generated stable particles, which are defined as those with a lifetime τ longer than 10 ps, including muons and neutrinos; these jets are referred to as particle-level jets. In addition, sequential jet corrections, derived from MC simulated events and using global properties of the jet such as tracking information, calorimeter energy deposits and muon spectrometer information, are applied [36]. Finally, the detector-level jets are further calibrated with additional correction factors derived in situ from a combination of γ + jet, Z + jet and dijet balance methods [35, 37].

Jets reconstructed from calorimeter signals not originating from a pp collision are rejected by applying jet-quality criteria [35, 38]. These criteria suppress spurious jets from electronic noise in the calorimeter, cosmic rays and beam-related backgrounds. Remaining jets are required to have calibrated transverse momenta greater than 50 GeV and rapidity $|y^{\text{jet}}| < 4.4$. Jets overlapping with the candidate photon are not considered if the jet axis lies within a cone of size $\Delta R = 1.0$ around the photon candidate; this requirement prevents any overlap between the photon isolation cone ($\Delta R = 0.4$) and the jet cone ($\Delta R = 0.6$).

3.3 Event categorisation

To investigate the production of jets in association with a photon, six samples are selected; the requirements are listed in Table 1:

- "Photon plus one-jet sample" (P1J): it is used to study the major features of an inclusive sample of events with a photon and at least one jet. In this sample, jet1 is required to have $p_{\text{T}}^{\text{jet1}} > 100$ GeV; asymmetric requirements on E_{T}^{γ} and $p_{\text{T}}^{\text{jet1}}$ are applied to reduce the infrared sensitivity of the NLO QCD calculations [39].

- "Photon plus one-jet $m^{\gamma-\text{jet1}}$ and $\cos\theta^*$ sample" (P1JM): for the measurements of the cross sections as functions of $m^{\gamma-\text{jet1}}$ and $|\cos\theta^*|$ additional constraints are needed to remove biases due to the rapidity and transverse momentum requirements on the photon and jet1 [3]. To perform unbiased measurements, the requirements $|\eta^{\gamma} + y^{\text{jet1}}| < 2.37$, $|\cos\theta^*| < 0.83$ and $m^{\gamma-\text{jet1}} > 467$ GeV are

applied.[2] These selections define a kinematic region where the acceptance is independent of the variables being studied.

- "Photon plus two-jet sample" (P2J): it is used to study the major features of an inclusive sample of events with a photon and at least two jets and the azimuthal correlations between the photon and jet2 as well as between jet1 and jet2. Due to the resolution in p_T the highest- and next-to-highest-p_T particle-level jets can end up being reconstructed as jet2 and jet1, respectively. To suppress such migrations, asymmetric requirements are applied: $p_T^{jet1} > 100$ GeV and $p_T^{jet2} > 65$ GeV.

- "Photon plus three-jet sample" (P3J): it is used to investigate the major characteristics of an inclusive sample of events with a photon and at least three jets; in addition, measurements of the azimuthal correlations between the photon and jet3, jet1 and jet3, as well as between jet2 and jet3 are performed. Asymmetric requirements are applied to suppress the migrations in p_T between the three highest-p_T jets: $p_T^{jet1} > 100$ GeV, $p_T^{jet2} > 65$ GeV and $p_T^{jet3} > 50$ GeV.

To compare the pattern of QCD radiation around the photon and jet1, two additional samples of photon plus two-jet events are selected. The phase-space regions are defined to avoid biases due to different p_T and η requirements on the final-state objects as well as to have no overlap between the two samples. The following requirements are common to the two samples:

- The jets must satisfy $p_T^{jet1} > 130$ GeV, $|\eta^{jet1}| < 2.37$ and $p_T^{jet2} > 50$ GeV. The first two requirements are imposed to be the same as for the photon so as to compare additional jet production in similar regions of phase space. The third requirement is chosen to select jets with the lowest p_T threshold, while suppressing the contribution from the underlying event and pile-up.

- The angular distance between the photon and jet1, $\Delta R^{\gamma-jet1}$, is restricted to $\Delta R^{\gamma-jet1} > 3$ to avoid any overlap between the two samples and any bias within the regions that are used to study additional jet production.

The requirements specific to each of the two samples are listed below:

- "Photon plus two-jet β^γ selection" (P2JBP): it is used to measure the production of jet2 around the photon. The cross section is measured as a function of the observable β^γ [16, 17], which is defined as[3]

$$\beta^\gamma = \tan^{-1} \frac{|\phi^{jet2} - \phi^\gamma|}{\text{sign}(\eta^\gamma) \cdot (\eta^{jet2} - \eta^\gamma)}. \tag{1}$$

The phase space is restricted to $1 < \Delta R^{\gamma-jet2} < 1.5$; the lower requirement avoids the overlap with the photon isolation cone while the upper requirement is the largest value which makes this sample and the next one non-overlapping. In addition, $p_T^{jet2} < E_T^\gamma$ is imposed for comparison with the other sample.

- "Photon plus two-jet β^{jet1} selection" (P2JBJ): it is used to measure the production of jet2 around jet1 using the observable β^{jet1}, defined as

$$\beta^{jet1} = \tan^{-1} \frac{|\phi^{jet2} - \phi^{jet1}|}{\text{sign}(\eta^{jet1}) \cdot (\eta^{jet2} - \eta^{jet1})}. \tag{2}$$

---

[2] The maximal (minimal) value of $|\cos\theta^*|$ ($m^{\gamma-jet1}$) for which the measurement is unbiased corresponds to $\tanh(2.37/2)$ ($2 \cdot E_T^\gamma / \sin\theta^*$) with $E_T^\gamma = 130$ GeV and $\cos\theta^* = 0.83$.

[3] In the definitions of β^γ and β^{jet1}, the arctangent function with two arguments is used to keep track of the proper quadrant.

To compare on equal footing with the measurement of the previous sample, the restriction $1 < \Delta R^{\mathrm{jet1-jet2}} < 1.5$ is applied.

Schematic diagrams for the definitions of β^γ and β^{jet1} are shown in Figure 2. The variable β^γ (β^{jet1}) is defined in such a way that $\beta^\gamma = 0$ or π ($\beta^{\mathrm{jet1}} = 0$ or π) corresponds to a plane in space containing jet2, the beam axis and the photon (jet1); $\beta = 0$ (π) always points to the beam which is closer to (farther from) the photon or jet1 in the η–ϕ plane.

The number of selected events in data for each of the six samples is included in Table 1. The overlap between the different samples is as follows: (a) P3J is contained within P2J, which in turn is a subset of P1J; (b) P1JM is contained within P1J; (c) P2JBP and P2JBJ have no overlap.

	Sample					
	P1J	P1JM	P2J	P2JBP	P2JBJ	P3J
Common requirements	$E_{\mathrm{T}}^\gamma > 130$ GeV and $|\eta^\gamma| < 2.37$, excluding $1.37 < |\eta^\gamma| < 1.56$ $|y^{\mathrm{jet}}| < 4.4$ and $\Delta R^{\gamma-\mathrm{jet}} > 1$					
$p_{\mathrm{T}}^{\mathrm{jet1}}$ [GeV]	> 100	> 100	> 100	> 130	> 130	> 100
$p_{\mathrm{T}}^{\mathrm{jet2}}$ [GeV]	–	–	> 65	> 50	> 50	> 65
$p_{\mathrm{T}}^{\mathrm{jet3}}$ [GeV]	–	–	–	–	–	> 50
$|\eta^\gamma + y^{\mathrm{jet1}}|$	–	< 2.37	–	–	–	–
$|\cos\theta^*|$	–	< 0.83	–	–	–	–
$m^{\gamma-\mathrm{jet1}}$ [GeV]	–	> 467	–	–	–	–
$\Delta R^{\gamma-\mathrm{jet1}}$	–	–	–	> 3	> 3	–
$\Delta R^{\gamma-\mathrm{jet2}}$	–	–	–	$1 < \Delta R^{\gamma-\mathrm{jet2}} < 1.5$	–	–
$\Delta R^{\mathrm{jet1-jet2}}$	–	–	–	–	$1 < \Delta R^{\mathrm{jet1-jet2}} < 1.5$	–
$|\eta^{\mathrm{jet1}}|$	–	–	–	< 2.37	< 2.37	–
$p_{\mathrm{T}}^{\mathrm{jet2}}, E_{\mathrm{T}}^\gamma$	–	–	–	$p_{\mathrm{T}}^{\mathrm{jet2}} < E_{\mathrm{T}}^\gamma$	–	–
Number of Events	2 451 236	344 572	567 796	40 537	37 429	164 062
Normalisation factor SHERPA (PYTHIA)	1.0 (1.1)	1.0 (1.2)	1.1 (1.2)	1.0 (1.2)	1.0 (1.2)	1.1 (1.1)

Table 1: Characteristics of the six samples of γ + jet(s) events: kinematic requirements, number of selected events in data and normalisation factors applied to the MC predictions.

4 Monte Carlo simulations

Samples of MC events were generated to study the characteristics of signal events. The MC samples were also used to determine the response of the detector and the correction factors necessary to obtain the particle-level cross sections. In addition, these samples were used to estimate hadronisation corrections to the NLO QCD calculations.
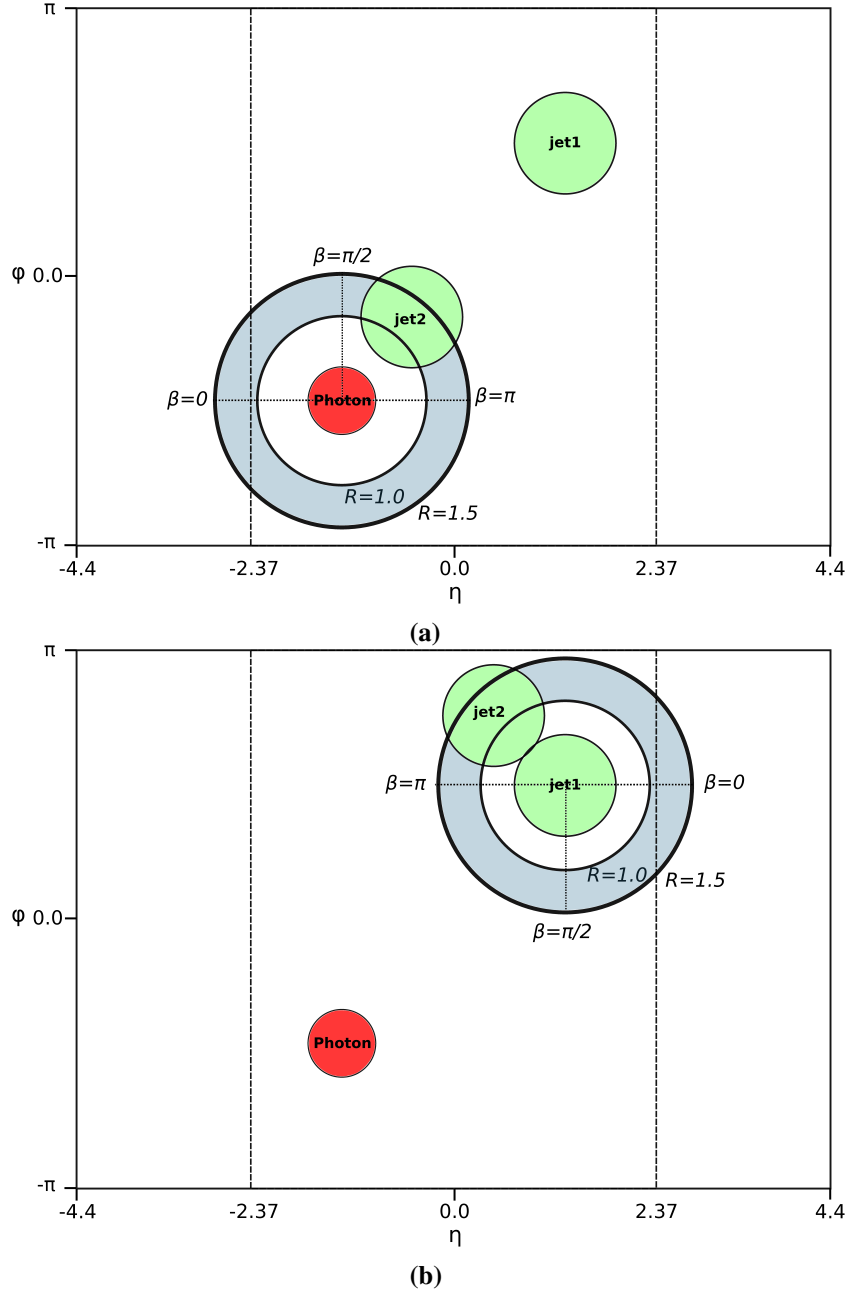
Figure 2: Schematic diagrams that show the definitions of (a) β^{γ} and (b) β^{jet1}.

10

The MC programs Pythia 8.165 [21] and Sherpa 1.4.0 [22] were used to generate the simulated events (see Table 2). In both generators, the partonic processes were simulated using LO matrix elements, with the inclusion of initial- and final-state parton showers. Fragmentation into hadrons was performed using the Lund string model [40] in the case of Pythia, and a modified version of the cluster model [41] in the case of Sherpa, for which it is the default treatment. The LO CTEQ6L1 [42] (NLO CT10 [43]) parton distribution functions (PDF) were used to parameterise the proton structure in Pythia (Sherpa). Both samples included a simulation of the underlying event. The event generator parameters were set according to the "AU2 CTEQ6L1" [44] tune for Pythia and the "CT10" tune for Sherpa. All samples of generated events were passed through the Geant4-based [45] ATLAS detector- and trigger-simulation programs [46]. They were reconstructed and analysed by the same program chain as the data.

The Pythia simulation of the signal included LO photon plus jet events from both direct processes (the hard subprocesses $qg \rightarrow q\gamma$ and $q\bar{q} \rightarrow g\gamma$, called "hard component") and photon bremsstrahlung in QCD dijet events (called "brem component"). The Sherpa samples were generated with LO matrix elements for photon plus jet final states with up to three additional partons, supplemented with parton showers. While the brem component was modelled in Pythia by final-state QED radiation arising from calculations of all $2 \rightarrow 2$ QCD processes, it was accounted for in Sherpa through the matrix elements of $2 \rightarrow n$ processes with $n \geq 3$; in the evaluation of the matrix elements the photon was required to be farther than $\Delta R = 0.3$ from any parton.

All samples were simulated taking into account the effects of the pile-up appropriate for 2012 data. The additional interactions were modelled by overlaying simulated hits from events with exactly one high momentum-transfer (signal) collision per bunch crossing with hits from minimum-bias events that were produced with the Pythia 8.160 program [21] using the A2M tune [44] and the MSTW2008 LO [47] PDF set.

Dedicated Pythia and Sherpa samples of events were generated at particle and parton levels, switching off the mechanisms that account for the underlying event to correct the NLO calculations for hadronisation and underlying-event effects.

The particle-level isolation variable on the photon was built from the transverse energy of all stable particles, except for muons and neutrinos, in a cone of size $\Delta R = 0.4$ around the photon direction after the contribution from the underlying event was subtracted; in this case, the same underlying-event subtraction procedure used on data was applied at the particle level. The isolation transverse energy at particle level is denoted by $E_{\mathrm{T,part}}^{\mathrm{iso}}$. The particle-level requirement on $E_{\mathrm{T,part}}^{\mathrm{iso}}$ was determined using the Pythia and Sherpa MC samples, by comparing the calorimeter isolation transverse energy with the particle-level isolation on an event-by-event basis. The effect of the experimental isolation requirement used in the data is close to a particle-level requirement of $E_{\mathrm{T,part}}^{\mathrm{iso}} < 10$ GeV over the measured E_{T}^{γ} range. The measured cross sections refer to particle-level jets and photons that are isolated by requiring $E_{\mathrm{T,part}}^{\mathrm{iso}} < 10$ GeV.

The MC predictions at particle level are normalised to the measured integrated cross sections. The normalisation factors are applied globally for each sample defined in Section 3.3 and are listed in Table 1.

Name	Matrix elements	PDF	Tune
PYTHIA 8.165	$2 \rightarrow 2$	LO CTEQ6L1	AU2 CTEQ6L1
SHERPA 1.4.0	$2 \rightarrow n, n = 2, ..., 5$	NLO CT10	CT10

Table 2: The generators used for correcting the data are listed, together with their matrix elements, the PDF and the tunes.

5 Signal extraction

5.1 Backgrounds

A non-negligible background contribution from jets remains in the selected sample, even after the application of the tight identification and isolation requirements on the photon. The background subtraction uses a data-driven method based on signal-suppressed control regions. The background contamination in the selected sample is estimated using the same two-dimensional sideband technique as in the previous analyses [3, 6, 7, 9, 12] and then subtracted bin-by-bin from the observed yield. In the two-dimensional plane formed by $E_{T,det}^{iso}$ and the photon identification variable, four regions are defined:

- *A*: the "signal" region, containing tight isolated photon candidates.

- *B*: the "non-isolated" background control region, containing tight non-isolated photon candidates. A candidate photon is considered to be non-isolated if $E_{T,det}^{iso} > (4.8 + 2) \, \text{GeV} + 4.2 \cdot 10^{-3} \cdot E_T^{\gamma}$ [GeV]; the threshold is 2 GeV higher than the isolation requirement for the signal region.

- *C*: the "non-tight" background control region, containing isolated non-tight photon candidates. A candidate photon is labelled as "non-tight" if it fails at least one among four of the tight requirements on the shower-shape variables computed from the energy deposits in the first layer of the electromagnetic calorimeter, but satisfies the tight requirement on the total lateral shower width [30] in the first layer and all the other tight identification criteria in other layers.

- *D*: the background control region containing non-isolated non-tight photon candidates.

The signal yield in region *A*, N_A^{sig}, is estimated from the numbers of events in regions *A*, *B*, *C* and *D* and takes into account the expected number of signal events in the three background control regions via signal leakage fractions, which are extracted from MC simulations of the signal. The only hypothesis is that the isolation and identification variables are uncorrelated in background events, thus $R^{bg} = (N_A^{bg} \cdot N_D^{bg})/(N_B^{bg} \cdot N_C^{bg}) = 1$, where N_K^{bg} with $K = A, B, C, D$ is the number of background events in each region. This assumption is verified [9] both in simulated background samples and in data in a background-dominated region. Deviations from unity are taken as systematic uncertainties (see Section 7). In addition, a systematic uncertainty is assigned to the modelling of the signal leakage fractions. Since the simulation does not accurately describe the electromagnetic shower profiles, a correction factor for each simulated shape variable is applied to better match the data [6, 7].

There is an additional background from electrons misidentified as photons, mainly produced in $Z \rightarrow e^+e^-$ and $W \rightarrow e\nu$ processes. Such misidentified electrons are largely suppressed by the photon selection. The remaining electron background is estimated using MC techniques and found to be negligible in the phase-space region of the analysis presented here.

5.2 Signal yield

The signal purity, defined as N_A^{sig}/N_A, is typically above 0.9 and is similar whether PYTHIA or SHERPA is used to extract the signal leakage fractions. The signal purity increases as E_{T}^{γ}, $p_{\mathrm{T}}^{\mathrm{jet1}}$ and $m^{\gamma-\mathrm{jet1}}$ increase and decreases as $|\cos\theta^*|$ increases.

For most of the distributions studied, the shapes of the hard and brem components in the signal MC simulated by PYTHIA are somewhat different. Therefore, in each case, the shape of the total MC distribution depends on the relative fraction of the two contributions. To improve the description of the data by the PYTHIA MC samples, a fit [3] to each data distribution is performed with the weight of the hard contribution, α, as the free parameter; the weight of the brem contribution is given by $1 - \alpha$. The fitted values of α are in the range 0.26–0.86. After these fits, a good description of the data is obtained from the PYTHIA MC simulations for all the observables, except for the distributions in the azimuthal angle between the jets. The simulations of SHERPA give a good description of the data, except for the tail of the distributions in E_{T}^{γ}.

The integrated efficiency, including the effects of trigger, reconstruction, particle identification and event selection, is evaluated from the simulated signal samples described in Section 4. The integrated efficiency is computed as $\varepsilon = N^{\mathrm{det,part}}/N^{\mathrm{part}}$, where $N^{\mathrm{det,part}}$ is the number of MC events that pass all the selection requirements at both the detector and particle levels and N^{part} is the number of MC events that pass the selection requirements at the particle level. The integrated efficiency using SHERPA (PYTHIA) is found to be 81.3% (81.5%) for the photon plus one-jet, 74.6% (75.3%) for the photon plus two-jet and 70.2% (70.6%) for the photon plus three-jet sample.

The bin-to-bin efficiency is computed as $\varepsilon_i = N_i^{\mathrm{det,part}}/N_i^{\mathrm{part}}$, where $N_i^{\mathrm{det,part}}$ is the number of MC events that pass all the selection requirements at both the detector and particle levels and are generated and reconstructed in bin i, and N_i^{part} is the number of MC events that pass the selection requirements at the particle level and are generated in bin i. The bin-to-bin efficiencies are typically above 50%, except for the $p_{\mathrm{T}}^{\mathrm{jet}}$ observables ($\gtrsim 40\%$) due to the resolution in these steeply falling distributions, and are similar for SHERPA and PYTHIA.

The bin-to-bin reconstruction purity is computed as $\kappa_i = N_i^{\mathrm{det,part}}/N_i^{\mathrm{det}}$, where N_i^{det} is the number of MC events that pass the selection requirements at the detector level and are reconstructed in bin i. The bin-to-bin reconstruction purities are typically above 55%, except for $p_{\mathrm{T}}^{\mathrm{jet}}$ ($\gtrsim 40\%$) for the same reason as the bin-to-bin efficiency, and are similar for SHERPA and PYTHIA.

6 Cross-section measurement procedure

The cross sections, after background subtraction, are corrected to the particle level using a bin-by-bin correction procedure. The bin-by-bin correction factors are determined using the MC samples; these correction factors take into account the efficiency of the selection criteria and the jet and photon reconstruction, as well as migration effects. The SHERPA samples are used to compute the nominal correction factors to the cross sections and the PYTHIA samples are used to estimate systematic uncertainties due to the modelling of the parton shower, hadronisation and signal (see Section 7).

The cross sections are corrected to the particle level via the formula

$$\frac{\mathrm{d}\sigma}{\mathrm{d}A}(i) = \frac{N_A^{\mathrm{sig}}(i)\, C^{\mathrm{MC}}(i)}{\mathcal{L}\, \Delta A(i)}, \tag{3}$$

where $(\mathrm{d}\sigma/\mathrm{d}A)(i)$ is the cross section as a function of observable A, $N_A^{\mathrm{sig}}(i)$ is the signal yield in bin i, $C^{\mathrm{MC}}(i)$ is the correction factor in bin i, $\mathcal{L}$ is the integrated luminosity and $\Delta A(i)$ is the width of bin i. The correction factors are computed as

$$C^{\mathrm{MC}}(i) = \frac{N_{\mathrm{part}}^{\mathrm{Sherpa}}(i)}{N_{\mathrm{det}}^{\mathrm{Sherpa}}(i)}, \tag{4}$$

where $N_{\mathrm{det\,(part)}}^{\mathrm{Sherpa}}(i)$ is the number of events in the Sherpa samples at detector (particle) level in bin i.

For the systematic uncertainties estimated with the Pythia samples, the acceptance correction factors are computed as

$$C^{\mathrm{MC}}(i) = \frac{\alpha\, N_{\mathrm{part}}^{\mathrm{Pythia,H}}(i) + (1-\alpha)\, N_{\mathrm{part}}^{\mathrm{Pythia,B}}(i)}{\alpha\, N_{\mathrm{det}}^{\mathrm{Pythia,H}}(i) + (1-\alpha)\, N_{\mathrm{det}}^{\mathrm{Pythia,B}}(i)}, \tag{5}$$

where α is the value obtained from the fit to the data distribution of each observable and $N_{\mathrm{det\,(part)}}^{\mathrm{Pythia}}(i)$ is the number of events in the Pythia samples at detector (particle) level in bin i. The indices H and B correspond to the hard and brem Pythia components, respectively. The correction factors from Pythia and Sherpa are very similar and differ from unity by typically $\lesssim 20\%$. The average correction factor for each distribution is listed in Table 3. The results of the bin-by-bin unfolding procedure are checked with a Bayesian unfolding method [48], giving consistent results.

Sample	Distribution: C^{MC} using Sherpa (Pythia)				
P1J	E_{T}^{γ}: 1.18 (1.17)	$p_{\mathrm{T}}^{\mathrm{jet1}}$: 1.20 (1.17)			
P1JM	$m^{\gamma-\mathrm{jet1}}$: 1.21 (1.18)	$\lvert\cos\theta^*\rvert$: 1.16 (1.14)			
P2J	E_{T}^{γ}: 1.17 (1.15)	$p_{\mathrm{T}}^{\mathrm{jet2}}$: 1.22 (1.15)	$\Delta\phi^{\gamma-\mathrm{jet2}}$: 1.13 (1.11)	$\Delta\phi^{\mathrm{jet1-jet2}}$: 1.13 (1.11)	
P3J	E_{T}^{γ}: 1.15 (1.13)	$p_{\mathrm{T}}^{\mathrm{jet3}}$: 1.19 (1.18)	$\Delta\phi^{\gamma-\mathrm{jet3}}$: 1.11 (1.09)	$\Delta\phi^{\mathrm{jet1-jet3}}$: 1.11 (1.09)	$\Delta\phi^{\mathrm{jet2-jet3}}$: 1.12 (1.10)

Table 3: Overview of the average correction factor C^{MC} for each distribution using the Sherpa and Pythia samples.

7 Systematic uncertainties

Several sources of systematic uncertainty are investigated. These sources include the photon energy scale and resolution, the jet energy scale and resolution, the parton-shower and hadronisation model dependence, the photon identification efficiency, the choice of background control regions, the signal modelling and the identification and isolation correlation in the background. Each source is discussed below. An overview of the systematic uncertainties in the cross sections is given in Table 4.

7.1 Photon energy scale and resolution

Differences between the photon energy scale and resolution in data and the simulations lead to systematic uncertainties. A total of 20 individual components [31] influencing the energy measurement of the photon are identified and varied within their uncertainties to assess the overall uncertainty in the energy measurement. These uncertainties are propagated through the analysis separately to maintain the full information about the correlations. The total relative photon energy-scale uncertainty is in the range (0.3–0.9)% for $|\eta^\gamma| < 1.37$, (1.3–2.4)% for $1.56 < |\eta^\gamma| < 1.81$ and (0.3–0.7)% for $1.81 < |\eta^\gamma| < 2.37$ depending on the photon transverse energy and whether the candidate is classified as an unconverted or converted photon.

Similarly to the energy scale uncertainty, the energy resolution is also influenced by different contributions (seven components), which are also propagated through the analysis separately to maintain the full information about the correlations.

The systematic uncertainties in the measured cross sections due to the effects mentioned above are estimated by varying each individual source of uncertainty separately in the MC simulations and then added in quadrature. The largest contribution arises from the uncertainty in the gain of the second layer of the electromagnetic calorimeter. The photon energy scale contributes an uncertainty in the cross section measured as a function of E_T^γ of ±1% (±4%) at low (high) E_T^γ, and typically less than ±2% when measured with the jet observables. The photon energy resolution contributes an uncertainty in the measured cross sections of less than ±1% for all observables.

7.2 Jet energy scale and resolution

The jet energy scale (JES) uncertainty contains a full treatment of bin-to-bin correlations for systematic uncertainties. A total of 67 individual components [37] influencing the energy measurement of the jets are identified and varied within their uncertainties to assess the overall uncertainty in the jet energy measurement. These parameters are propagated through the analysis separately to maintain the full information about the correlations. The total relative jet energy-scale uncertainty is $\lesssim \pm 3\%$ in the phase-space region of the measurements.

The jet energy resolution (JER) uncertainty accounts for the differences between data and simulated events. The impact of the JER uncertainty is estimated by smearing the MC simulated distributions and comparing the smeared and non-smeared results.

The systematic uncertainties in the measured cross sections due to the effects mentioned above are estimated by varying each individual source of uncertainty separately in the MC simulations and then added in quadrature. The major contributions arise from uncertainties in (a) the electron and photon energy scale, which affect the in situ corrections obtained from γ + jet and Z + jet events, (b) the modelling of the ambient transverse energy used in the subtraction of the underlying event and pile-up, and (c) the modelling of the quark and gluon composition of the jets. The resulting uncertainty due to the JES is the dominant effect on the measured cross sections, except for those as functions of E_T^γ. As an example, the effect on the measured cross section as a function of p_T^{jet1} is below ±6% for $p_T^{jet1} < 600$ GeV and grows to $\approx \pm 15\%$ for $p_T^{jet1} \sim 1$ TeV. The JER contributes an uncertainty in the measured cross sections which is smaller than ±1% for the photon plus one-jet observables; for the photon plus two-jet and photon plus three-jet observables it is below ±4%.

7.3 Parton-shower and hadronisation model dependence

The difference between the signal purities and the correction factors estimated in SHERPA and PYTHIA is taken as an estimate of the systematic uncertainty due to the parton-shower and hadronisation models. The resulting uncertainty in the measured cross sections is below ±3% for the photon plus one-jet measurements, except for p_T^{jet1} (for which the uncertainty increases to ±9% for $p_T^{\text{jet1}} \sim 1$ TeV), below ±6% for the photon plus two-jet measurements, except for p_T^{jet2} (for which the uncertainty increases to ±13% for $p_T^{\text{jet2}} \sim 1$ TeV), and below ±7% for the photon plus three-jet measurements.

7.4 Photon identification efficiency

Scale factors are applied to the MC events to match the "tight" identification efficiency between data and simulation [30]. The uncertainty in the photon identification is estimated by propagating the uncertainty in these scale factors through the analysis. These effects result in an uncertainty in the measured cross sections which is smaller than ±0.4% for all observables.

7.5 Choice of background control regions

The estimation of the background contamination in the signal region is affected by the choice of background control regions. The latter are defined by the lower limit on $E_{T,\text{det}}^{\text{iso}}$ in regions B and D and the choice of inverted photon identification variables used in the selection of non-tight photons. To study the dependence on the specific choices these definitions are varied over a wide range. The lower limit on $E_{T,\text{det}}^{\text{iso}}$ in regions B and D is varied by ±1 GeV, which is larger than any difference between data and simulations and still provides enough events to perform the data-driven subtraction. Likewise, the choice of inverted photon identification variables is varied. The analysis is repeated using different sets of variables: tighter (looser) identification criteria are defined by applying tight requirements to an extended (restricted) set of shower-shape variables in the first calorimeter layer [9]. The effects of these variations on the measured cross sections are typically smaller than ±1% for all observables.

7.6 Signal modelling

The simulation of the signal from the PYTHIA MC samples is used to estimate the systematic uncertainties arising from the modelling of the hard and bremsstrahlung components, which affect the signal leakage fractions in the two-dimensional sideband method for background subtraction and the bin-by-bin correction factors.

To estimate the effect of the signal modelling on the signal leakage fractions, the PYTHIA components are first mixed according to the default value given by the MC cross section to determine the signal yield. The uncertainty related to the simulation of the hard and brem components in the signal leakage fractions is estimated by performing the background subtraction using the admixture derived from the fit. For this estimation, the bin-by-bin correction factors are computed using Eq. (5).

To estimate the effect of the signal modelling on the bin-by-bin correction factors, the components in PYTHIA are mixed according to Eq. (5) but using $\alpha \pm \Delta\alpha$, where $\Delta\alpha$ is the error from the fit (see Section 5.2).

These effects result in an uncertainty in the measured cross sections which is typically smaller than $\pm 1\%$ for all observables.

7.7 Identification and isolation correlation in the background

The isolation and identification photon variables used to define the plane in the two-dimensional sideband method to subtract the background (see Section 5.1) are assumed to be uncorrelated for background events ($R^{\text{bg}} = 1$). Any correlation between these variables would affect the estimation of the purity of the signal and lead to systematic uncertainties in the background-subtraction procedure. It was shown that R^{bg} is consistent with unity within $\pm 10\%$ [9]. Therefore, $\pm 10\%$ is taken as the uncertainty in R^{bg} related to the identification and isolation correlation in the background. These effects result in an uncertainty in the measured cross sections which is typically smaller than $\pm 1\%$ for all observables.

7.8 Total systematic uncertainty

The total systematic uncertainty is computed by adding in quadrature the sources of uncertainty listed in the previous sections and the statistical uncertainty of the MC samples. The uncertainty in the integrated luminosity is $\pm 1.9\%$ [29]; this uncertainty is fully correlated in all bins of all the measured cross sections and is added in quadrature to the other uncertainties.

8 Fixed-order QCD calculations

8.1 Calculations for photon plus one-jet final state

The LO and NLO QCD calculations used in the photon plus one-jet analysis presented here are performed using the program JETPHOX 1.3.2 [23, 24]. This program includes a full NLO calculation of both the direct and fragmentation QCD contributions to the cross section for the $pp \rightarrow \gamma + \text{jet} + X$ reaction.

The calculation assumes five massless quark flavours. The renormalisation (μ_{R}), factorisation (μ_{F}) and fragmentation (μ_{f}) scales are chosen to be $\mu_{\text{R}} = \mu_{\text{F}} = \mu_{\text{f}} = E_{\text{T}}^{\gamma}$. The calculations are performed using the CT10 parameterisations of the proton PDF and the NLO BFG set II photon fragmentation function [49]. The strong coupling constant is calculated at two loops with $\alpha_{\text{s}}(m_Z) = 0.118$.

The calculations are performed using a parton-level isolation criterion which requires the total transverse energy from the partons inside a cone of $\Delta R = 0.4$ around the photon direction, called cone isolation henceforth, to be below 10 GeV. The anti-k_t algorithm with radius parameter $R = 0.6$ is applied to the partons in the events generated by this program to compute the cross-section predictions.

Source of uncertainty	Variable						
	Photon plus one-jet			Photon plus two-jet		Photon plus three-jet	
	E_{T}^{γ}	$p_{\mathrm{T}}^{\mathrm{jet1}}$	$\lvert\cos\theta^*\rvert$	$p_{\mathrm{T}}^{\mathrm{jet2}}$	$\Delta\phi$	$p_{\mathrm{T}}^{\mathrm{jet3}}$	$\Delta\phi$
Photon energy scale and resolution	(1–4)%	(0–3.5)%	(1–1.4)%	(0–2.5)%	(0–2.4)%	(0–1.9)%	(0–1.7)%
Jet energy scale	(0–1.7)%	(2.4–15)%	(1.8–2.3)%	(3.6–10)%	(1.8–9)%	(5.5–14)%	(4.5–11)%
Jet energy resolution	(0–0.3)%	(0.1–1.0)%	(0.1–0.4)%	(0.1–1.5)%	(0.2–2.0)%	(1.1–4.0)%	(0.1–2.5)%
Parton shower and hadronisation models	(0–0.8)%	(1.1–9)%	(0.6–1.3)%	(1–13)%	(0.8–4.6)%	(2.3–5.6)%	(2.1–7)%
Photon identification	(0–0.4)%	(0–0.4)%	(0–0.4)%	(0–0.4)%	(0–0.4)%	(0–0.4)%	(0–0.4)%
Background control regions	(0–1)%	(0–1.1)%	(0–0.6)%	(0–1.2)%	(0–0.5)%	(0–1.9)%	(0–1)%
Signal modelling	(0–0.1)%	(0–0.14)%	(0–0.4)%	(0–0.6)%	(0–0.7)%	(0–0.5)%	(0–1.2)%
Correlation in background	(0–0.8)%	(0–0.7)%	(0–0.9)%	(0–0.6)%	(0–0.6)%	(0–0.6)%	(0–0.5)%

Table 4: Overview of the relative systematic uncertainties in the cross sections.

8.2 Calculations for photon plus two-jet and photon plus three-jet final states

NLO QCD calculations are performed separately for photon plus two-jet and photon plus three-jet final states using the program BLACKHAT+SHERPA [25, 26]. This program includes a full NLO QCD calculation of only the direct contribution to the cross section for the $pp \rightarrow \gamma + 2$ jets + X and $pp \rightarrow \gamma + 3$ jets + X reactions. Therefore, the highest-order calculation used in this paper corresponds to that of photon plus three-jet production and it is up to $O(\alpha_{\mathrm{em}}\alpha_{\mathrm{s}}^4)$. The μ_{R} and μ_{F} scales are chosen to be $\mu_{\mathrm{R}} = \mu_{\mathrm{F}} = E_{\mathrm{T}}^{\gamma}$. The settings for the number of flavours, $\alpha_{\mathrm{s}}(m_Z)$ and proton PDF are the same as for JETPHOX. The calculations are performed using a parton-level isolation on the photon based on the Frixione method [50], called Frixione isolation henceforth. As with JETPHOX, the anti-k_t algorithm with radius parameter $R = 0.6$ is applied to the final-state partons.

8.3 Hadronisation and underlying-event corrections to the NLO QCD calculations

Since the measurements refer to jets of hadrons and include underlying-event (UE) effects, whereas the NLO QCD calculations refer to jets of partons without such effects, the cross-section predictions are corrected to include UE effects at particle level using the MC models. The correction factor, C_{NLO}, is defined as the ratio of the cross section for jets of hadrons with UE to that for jets of partons. The correction factors

for the photon plus one-jet predictions are estimated using the PYTHIA samples (using cone isolation) and those for the photon plus two/three-jet predictions are estimated using the SHERPA samples; in the latter case, the cone (Frixione) isolation is used at the particle (parton) level to match the measurements (predictions). The MC samples of PYTHIA (SHERPA) are suited for estimating the correction factors for JETPHOX (BLACKHAT) since these NLO QCD calculations include (do not include) the fragmentation contribution. These factors are close to unity for the photon plus one-jet observables, except for $p_{\mathrm{T}}^{\mathrm{jet1}} \gtrsim 500$ GeV, where they can differ by up to 30% from unity due to the dominance of the bremsstrahlung component in that region. For photon plus two-jet (three-jet) observables the average correction factor is 1.10 (1.14).

8.4 Theoretical uncertainties

The following sources of uncertainty in the theoretical predictions are considered:

- The uncertainty due to the scales is estimated by repeating the calculations using values of μ_{R} and μ_{F} scaled by factors 0.5 and 2. The two scales are varied individually. In the case of photon plus one-jet calculations, the μ_{f} scale is also varied.

- The uncertainty due to the proton PDF is estimated by repeating the calculations using the 52 additional sets from the CT10 error analysis and taking the sum in quadrature of all the uncertainty components. A scaling factor of 1/1.645 is applied to produce the uncertainty for the 68% confidence-level (CL) interval.

- The uncertainty due to the value of $\alpha_{\mathrm{s}}(m_Z)$ is estimated by repeating the calculations using two additional sets of proton PDFs, for which different values of $\alpha_{\mathrm{s}}(m_Z)$ are assumed in the fits, namely $\alpha_{\mathrm{s}}(m_Z) = 0.116$ and 0.120. In addition, the same scaling factor mentioned above is also applied to obtain the uncertainty for the 68% CL interval.

- The uncertainty on the hadronisation and underlying-event corrections is negligible compared to the other uncertainties on the theoretical predictions [3].

The dominant theoretical uncertainty is that arising from the scale variations. The total theoretical uncertainty is obtained by adding in quadrature the individual uncertainties listed above.

9 Results

9.1 Fiducial regions and integrated cross sections

The measurements presented here refer to isolated prompt photons with $E_{\mathrm{T,part}}^{\mathrm{iso}} < 10$ GeV (see Section 4) and jets of hadrons (see Section 3.2). The details of the phase-space regions are given in Table 1. The integrated cross sections for the photon plus one-jet, photon plus two-jet and photon plus three-jet final states are shown in Table 5. The measured and predicted integrated cross sections are consistent within the experimental and theoretical uncertainties.

Final state	Measured cross section [pb]	NLO QCD prediction JETPHOX/ BLACKHAT [pb]	PYTHIA prediction [pb]	SHERPA prediction [pb]
Photon plus one-jet	134 ± 4	128^{+11}_{-9} (J)	120	132
Photon plus two-jet	30.4 ± 1.8	$29.2^{+2.8}_{-2.7}$ (B)	26.4	27.4
Photon plus three-jet	8.7 ± 0.8	$9.5^{+0.9}_{-1.2}$ (B)	8.2	7.9

Table 5: Measured and predicted integrated cross sections.

9.2 Cross sections for isolated-photon plus one-jet production

The measured cross-section $d\sigma/dE_T^\gamma$, shown in Figure 3(a), decreases by five orders of magnitude as E_T^γ increases over the measured range. Values of E_T^γ up to 1.1 TeV are measured. The experimental uncertainty is below 5% for $E_T^\gamma \lesssim 650$ GeV, dominated by the photon energy scale uncertainty, and grows to 15% at $E_T^\gamma \sim 1$ TeV, dominated by the statistical uncertainty in this region. The NLO QCD prediction from JETPHOX is compared with the measurement in Figure 3(a). The NLO QCD prediction gives a good description of the data within the experimental and theoretical uncertainties. The theoretical uncertainty varies from $\approx 7\%$ for $E_T^\gamma \sim 130$ GeV to $\approx 10\%$ for $E_T^\gamma \sim 1$ TeV; it is dominated by the contribution arising from scale uncertainties, in particular from the variation of μ_R (7% (5%) at low (high) E_T^γ), although for $E_T^\gamma \gtrsim 750$ GeV the uncertainty from the PDF grows to be of the same order and dominates for higher E_T^γ values ($\approx 8\%$ for $E_T^\gamma \sim 1$ TeV). The predictions from SHERPA and PYTHIA are compared with the measurements in Figure 4(a). Both predictions give an adequate description of the shape of the data distribution within the experimental and theoretical uncertainties; the theoretical uncertainties are necessarily at least as large as for the NLO QCD calculations.

The measured cross-section $d\sigma/dp_T^{jet1}$, shown in Figure 3(b), decreases by five orders of magnitude from $p_T^{jet1} \sim 120$ GeV to the highest transverse momentum available, $p_T^{jet1} \approx 1.2$ TeV; for $p_T^{jet1} < 120$ GeV the cross section decreases due to the kinematic analysis requirements. The total experimental uncertainty is below 6% for $p_T^{jet1} < 500$ GeV and grows to $\approx 25\%$ for $p_T^{jet1} \sim 1.1$ TeV. It is dominated by the uncertainty in the jet energy scale. The NLO QCD prediction gives a good description of the data except for $p_T^{jet1} < 120$ GeV, where in the calculation of $A \cdot \alpha_{em}\alpha_s + B \cdot \alpha_{em}\alpha_s^2$ [23, 24] the Born term is zero, i.e. $A = 0$. The theoretical uncertainty grows from $< 5\%$ at $p_T^{jet1} \sim 135$ GeV to $\approx 25\%$ for $p_T^{jet1} \sim 1.1$ TeV and is dominated by the variation of μ_R in the whole measured range. The predictions from SHERPA and PYTHIA give an adequate description of the data (see Figure 4(b)).

Figure 3(c) shows $d\sigma/dm^{\gamma-jet1}$; the measured cross section decreases by four orders of magnitude as $m^{\gamma-jet1}$ increases from about 0.5 TeV to the highest measured value, ≈ 2.45 TeV. The experimental

uncertainty ranges from $\approx 3\%$ to $\approx 22\%$ and is dominated by the jet energy scale uncertainty in most of the measured range; for $m^{\gamma-\text{jet1}} > 1.5$ TeV the statistical uncertainty dominates. The NLO QCD calculation gives a good description of the data and no significant deviation from the prediction from pQCD is observed. The theoretical uncertainty is $\approx 10\%$ (15%) at $m^{\gamma-\text{jet1}} \approx 490$ (2450) GeV; it is dominated by the contribution arising from scale uncertainties, in particular from the variation of μ_R ($\approx 10\%$), although for $m^{\gamma-\text{jet1}} \gtrsim 2.15$ TeV the uncertainty from the PDF grows to be of the same order and dominates for higher $m^{\gamma-\text{jet1}}$ values. The predictions from Pythia and Sherpa give a good description of the data (see Figure 4(c)), except for $m^{\gamma-\text{jet1}} > 1.8$ TeV where, nevertheless, the differences are covered by the theoretical uncertainties.

The measured cross-section $d\sigma/d|\cos\theta^*|$, shown in Figure 3(d), increases as $|\cos\theta^*|$ increases. The experimental uncertainty is $\approx 3\%$; the only significant contributions arise from the photon and jet energy scale uncertainties and the model dependence. The NLO QCD prediction gives a good description of the data. The theoretical uncertainty is $\approx 10\%$, dominated by the contribution arising from scale uncertainties, in particular from the variation of μ_R. The predictions from Pythia and Sherpa give a good description of the data (see Figure 4(d)).

To gain further insight into the dynamics of the photon–jet system, cross sections are measured as functions of $|\cos\theta^*|$ in different regions of $m^{\gamma-\text{jet1}}$. Figure 5 shows the measured cross sections and NLO QCD predictions in nine regions of $m^{\gamma-\text{jet1}}$. The NLO QCD predictions describe well the scale evolution of the measured cross sections. The LO QCD predictions of the direct and fragmentation contributions to the cross section are compared with the measurements in Figure 6. Even though at NLO the two components are no longer distinguishable, the LO calculations are useful in illustrating the basic differences in the dynamics of the two processes. The contribution from fragmentation shows a steeper increase as $|\cos\theta^*| \to 1$ than that from direct processes. This different behaviour is due to the different spin of the exchanged particle dominating each of the processes: a quark in the case of direct processes and a gluon in the case of fragmentation processes. The shape of the measured cross-section $d\sigma/d|\cos\theta^*|$ is much closer to that of the direct-photon processes than that of fragmentation in all $m^{\gamma-\text{jet1}}$ regions. This is consistent with the dominance of processes in which the exchanged particle is a quark. The predictions[4] from Pythia and Sherpa are compared with the data in Figure 7 and also give an adequate description of the measurements.

---

[4] The MC predictions for every region in $m^{\gamma-\text{jet1}}$ are normalised using the same factors as for $d\sigma/dm^{\gamma-\text{jet1}}$.
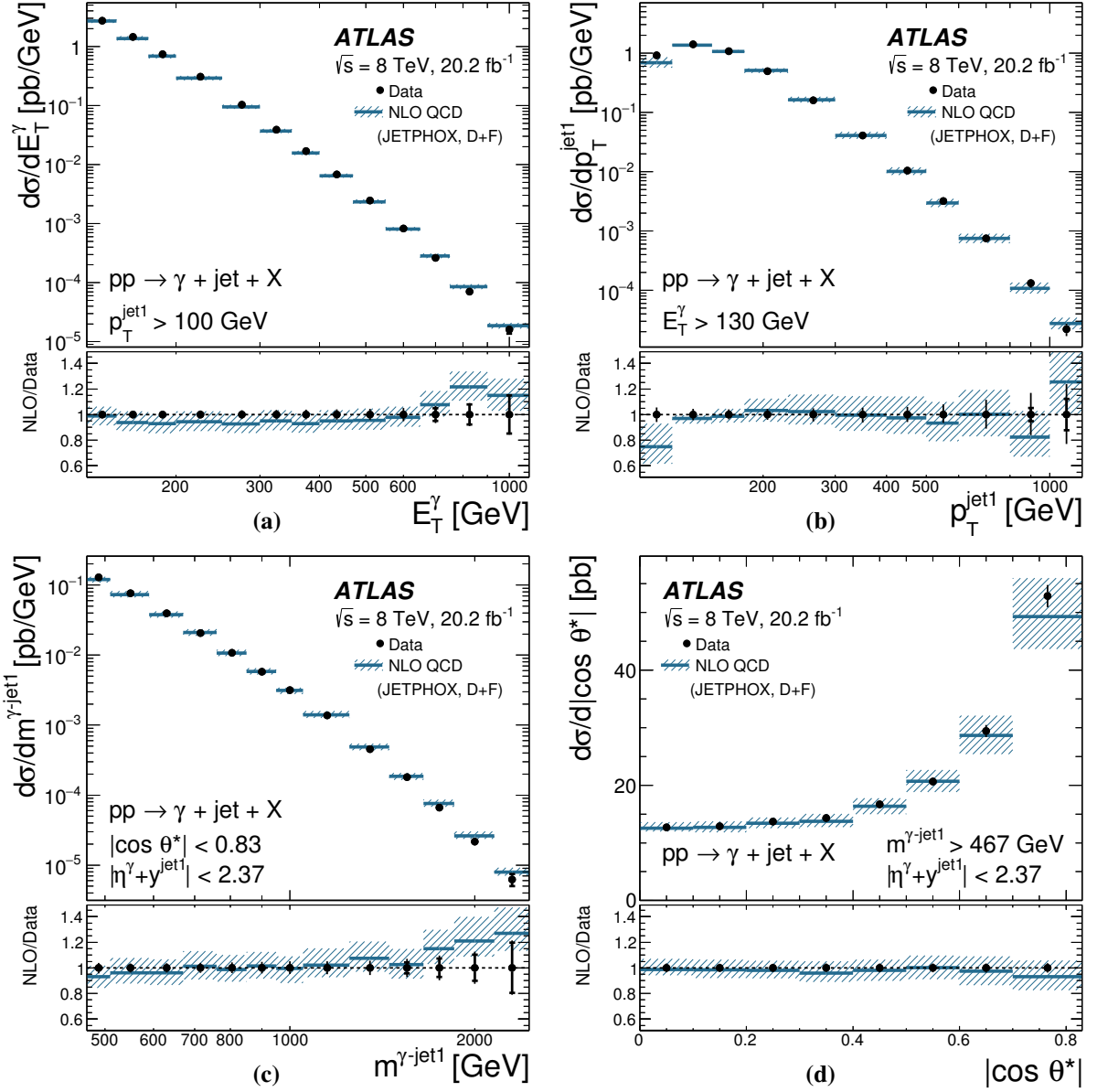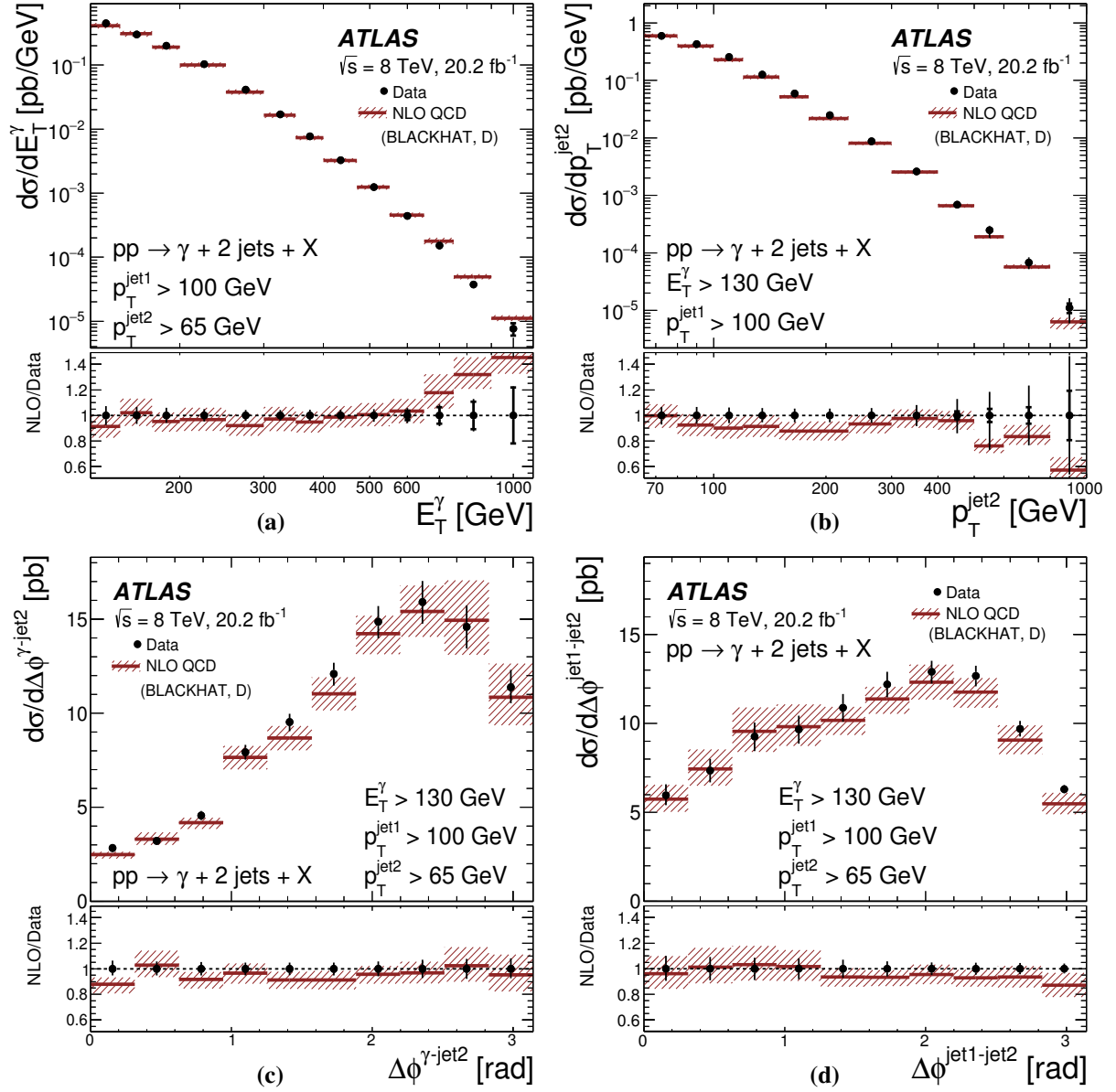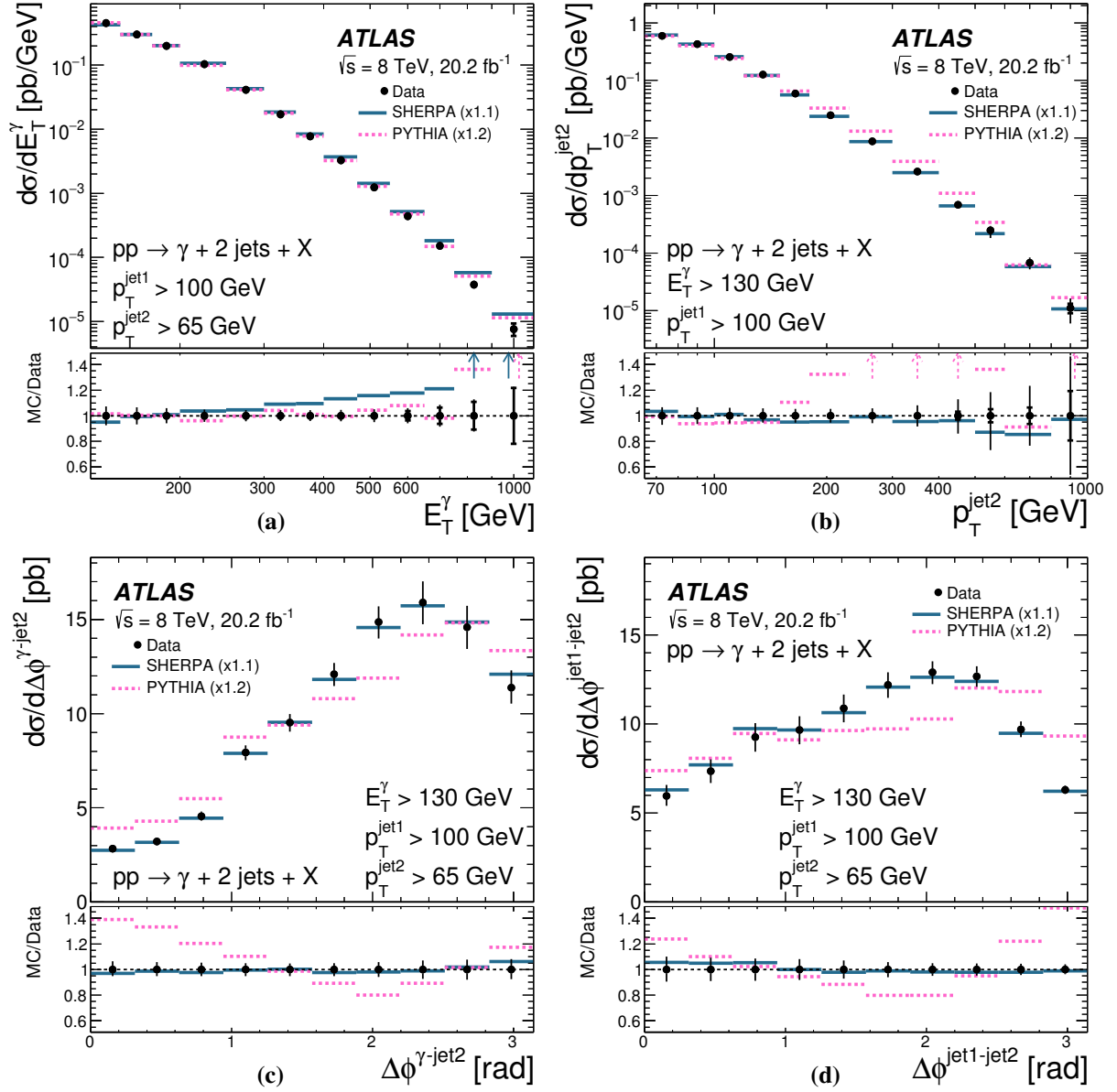
Figure 3: Measured cross sections for isolated-photon plus one-jet production (dots) as functions of (a) E_T^γ, (b) p_T^{jet1}, (c) $m^{\gamma-jet1}$ and (d) $|\cos\theta^*|$. The NLO QCD predictions from JETPHOX corrected for hadronisation and underlying-event effects and using the CT10 PDF set (solid lines) are also shown. These predictions include direct and fragmentation contributions (D+F). The bottom part of each figure shows the ratio of the NLO QCD prediction to the measured cross section. The inner (outer) error bars represent the statistical uncertainties (the statistical and systematic uncertainties added in quadrature) and the shaded band represents the theoretical uncertainty. For most of the points, the inner error bars are smaller than the marker size and, thus, not visible.
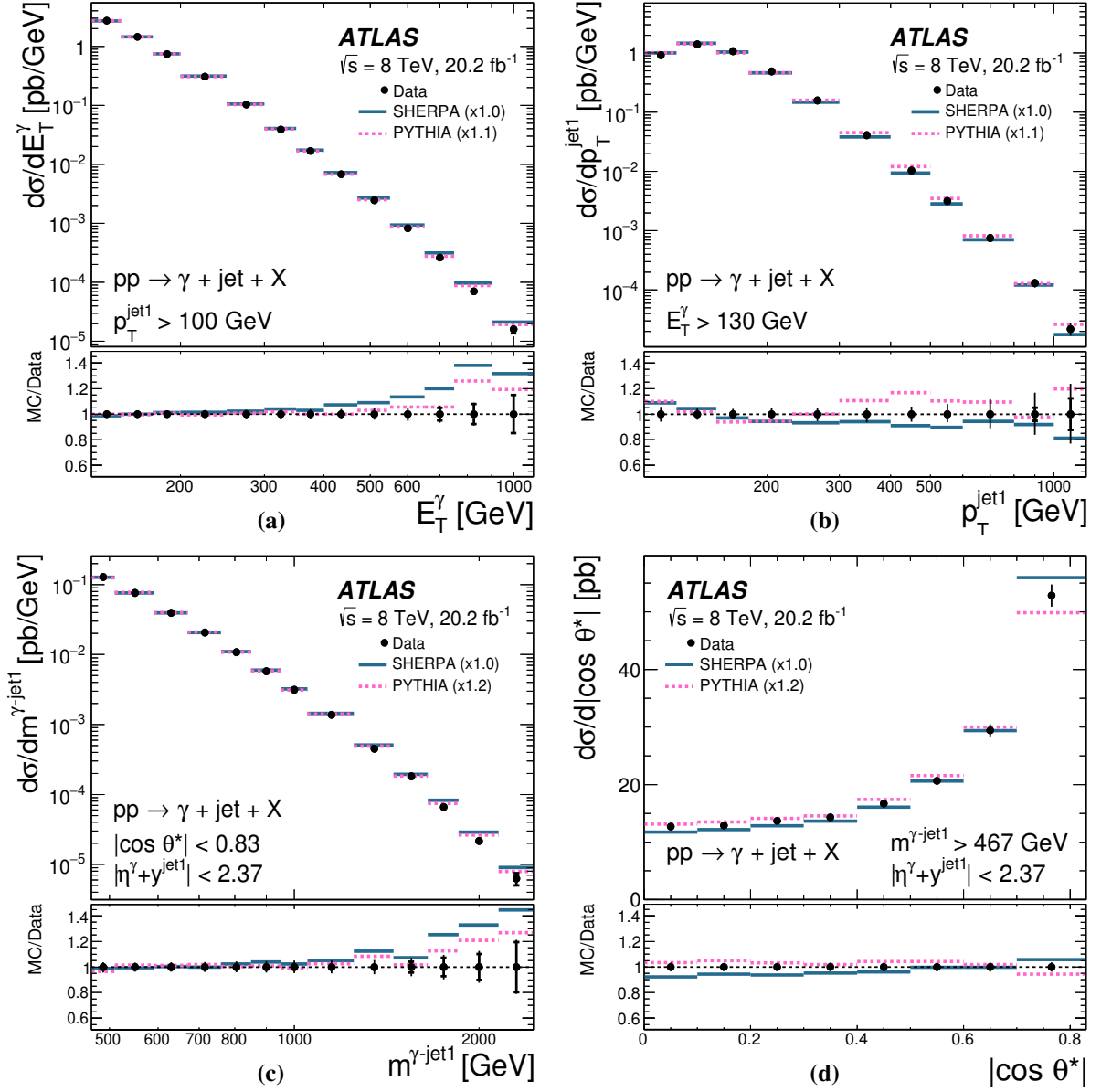
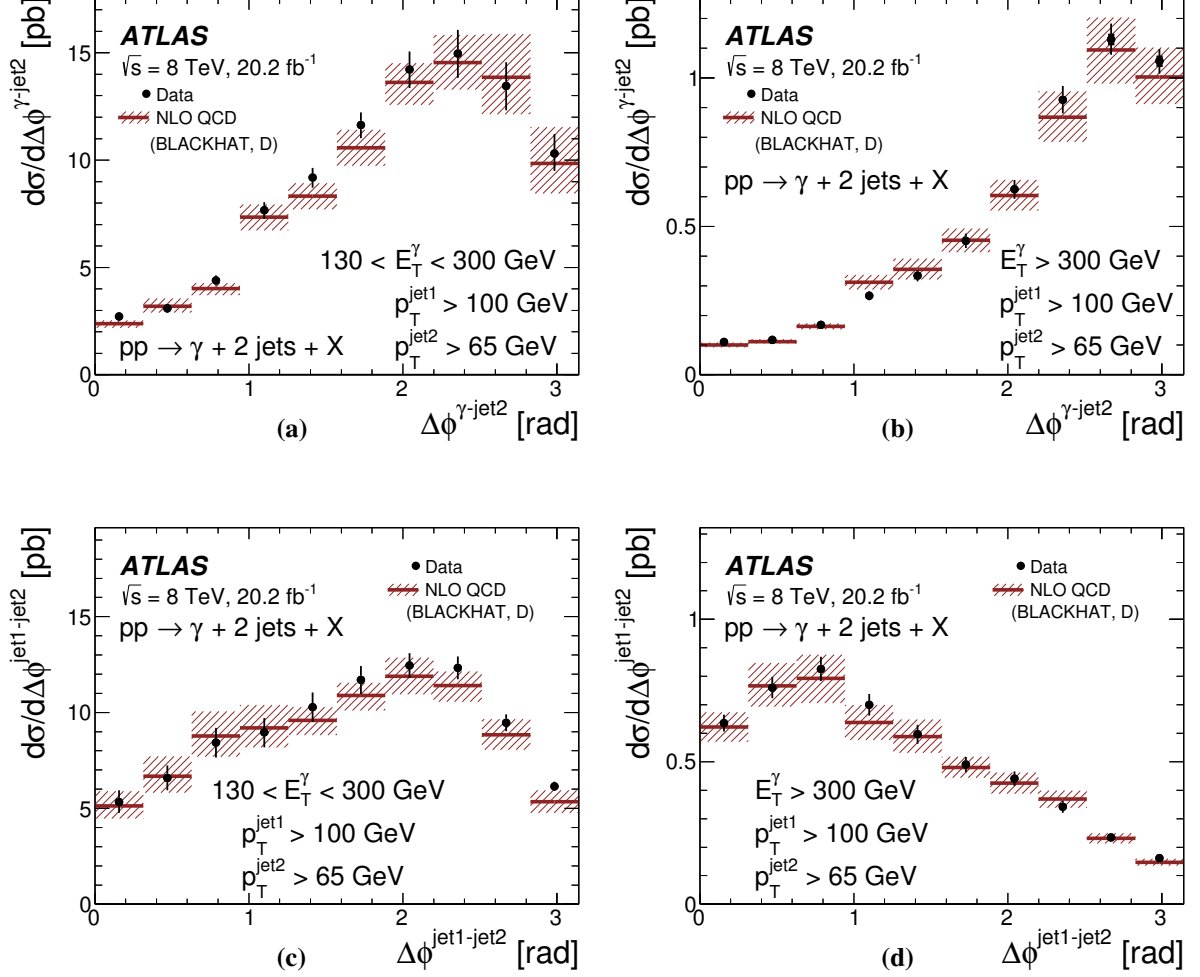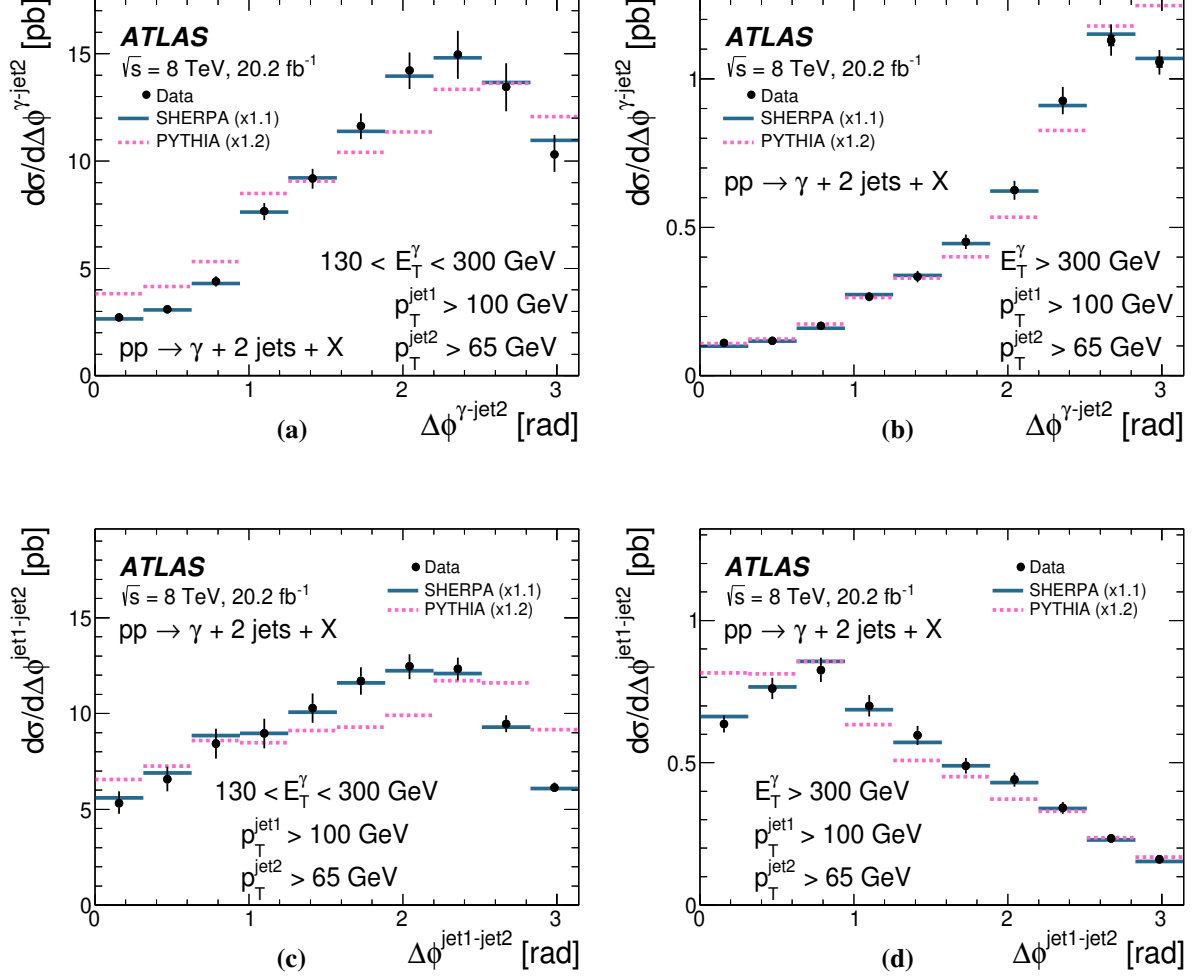Figure 4: Measured cross sections for isolated-photon plus one-jet production (dots) as functions of (a) E_T^γ, (b) p_T^{jet1}, (c) $m^{\gamma-jet1}$ and (d) $|\cos\theta^*|$, presented in Figure 3. For comparison, the predictions from SHERPA (solid lines) and PYTHIA (dashed lines) normalised to the integrated measured cross sections (using the factors indicated in parentheses) are also shown. The bottom part of each figure shows the ratios of the MC predictions to the measured cross section. The inner (outer) error bars represent the statistical uncertainties (the statistical and systematic uncertainties added in quadrature). For most of the points, the inner error bars are smaller than the marker size and, thus, not visible.
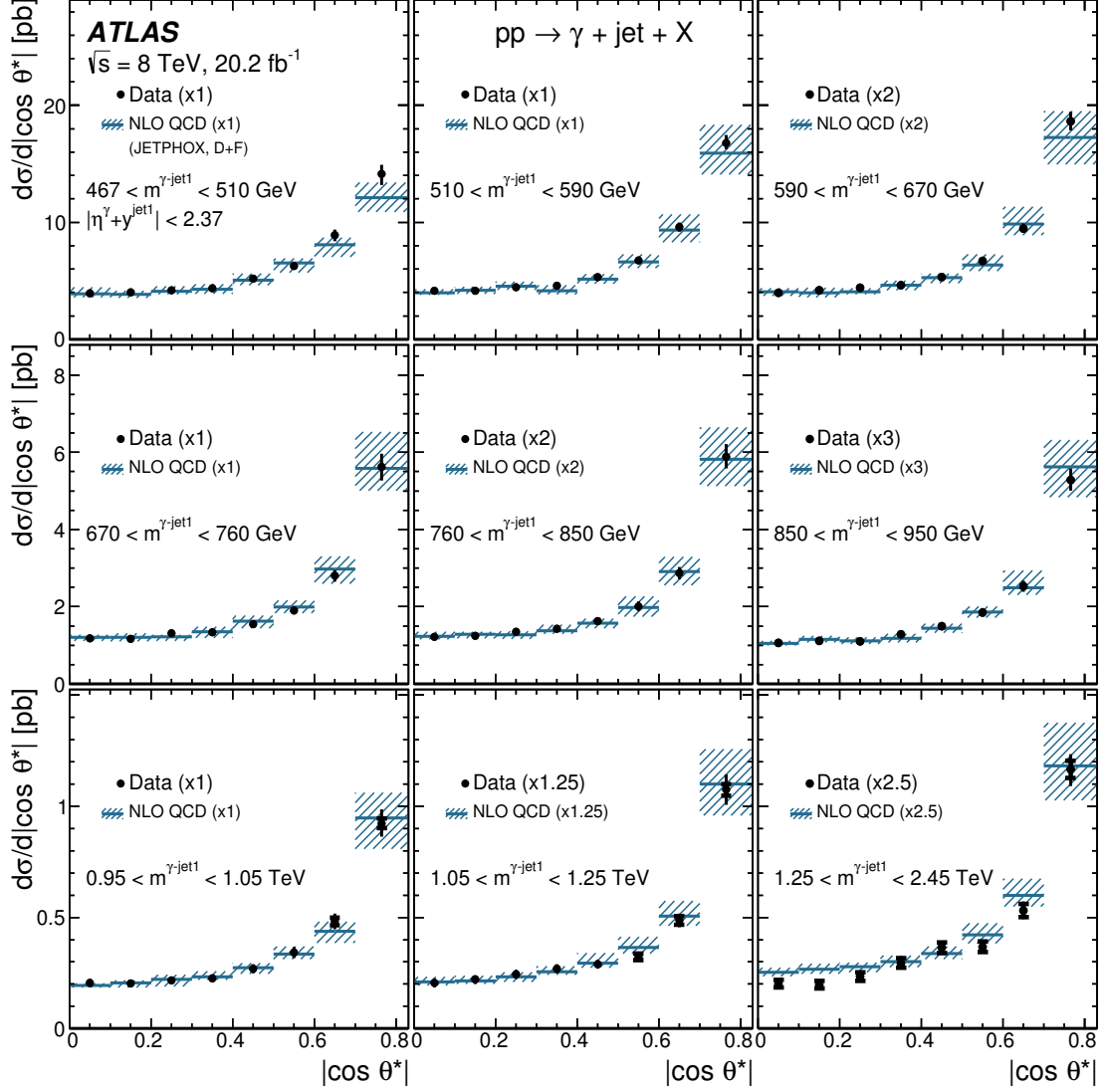
Figure 5: Measured cross sections for isolated-photon plus one-jet production (dots) as functions of $|\cos\theta^*|$ in different regions of $m^{\gamma-\mathrm{jet1}}$. The NLO QCD predictions from JETPHOX corrected for hadronisation and underlying-event effects and using the CT10 PDF set (solid lines) are also shown. These predictions include direct and fragmentation contributions (D+F). The inner (outer) error bars represent the statistical uncertainties (the statistical and systematic uncertainties added in quadrature) and the shaded band represents the theoretical uncertainty. For most of the points, the inner error bars are smaller than the marker size and, thus, not visible. For visibility, the measured and predicted cross sections are scaled by the factors indicated in parentheses.

24
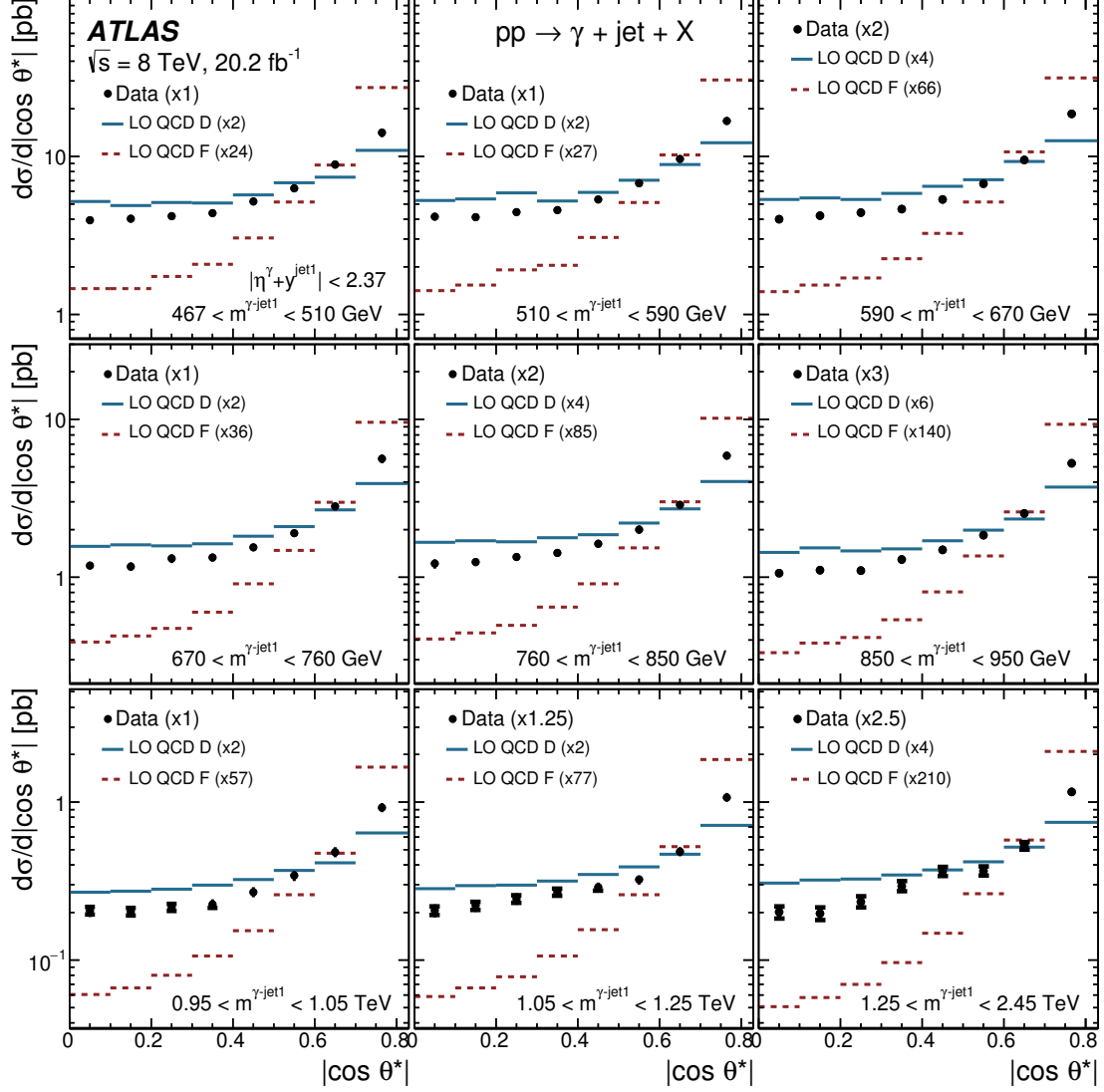
Figure 6: Measured cross sections for isolated-photon plus one-jet production (dots) as functions of $|\cos\theta^*|$ in different regions of $m^{\gamma-\mathrm{jet1}}$, presented in Figure 5. For visibility, the measured cross sections are scaled by the factors indicated in parentheses. For comparison, the LO QCD predictions from JETPHOX corrected for hadronisation and underlying-event effects and using the CT10 PDF set for direct (solid lines) and fragmentation (dashed lines) processes are shown separately. In each region of $m^{\gamma-\mathrm{jet1}}$, the predictions are normalised to the integrated measured cross section by the factors shown in parentheses, which include the visibility factor. The inner (outer) error bars represent the statistical uncertainties (the statistical and systematic uncertainties added in quadrature). For most of the points, the inner error bars are smaller than the marker size and, thus, not visible.
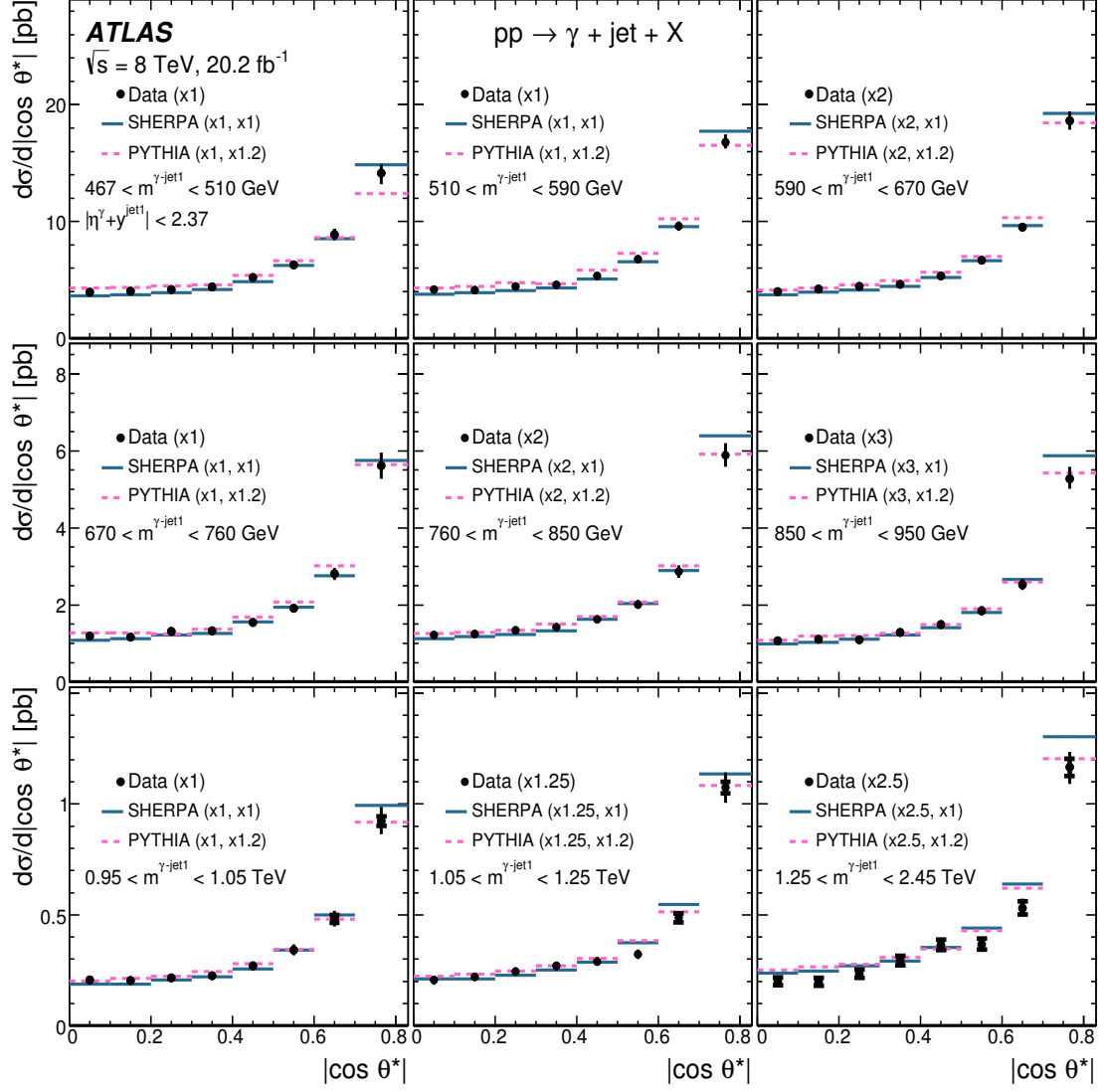
Figure 7: Measured cross sections for isolated-photon plus one-jet production (dots) as functions of $|\cos\theta^*|$ in different regions of $m^{\gamma-\mathrm{jet1}}$, presented in Figure 5. For comparison, the predictions from SHERPA (solid lines) and PYTHIA (dashed lines) are also shown; the predictions are normalised to the data by a global factor, which is shown as the second factor in parentheses. In addition, for visibility, the measured and predicted cross sections are scaled by the first factor indicated in parentheses. The inner (outer) error bars represent the statistical uncertainties (the statistical and systematic uncertainties added in quadrature). For most of the points, the inner error bars are smaller than the marker size and, thus, not visible.

9.3 Cross sections for isolated-photon plus two-jet production

The measured cross-section $d\sigma/dE_T^\gamma$ (Figure 8(a)) decreases by almost five orders of magnitude as E_T^γ increases over the measured range. Values of E_T^γ up to 1.1 TeV are measured. The experimental uncertainty ranges from 7% to 23%, dominated at low E_T^γ by the jet energy scale uncertainty and at high E_T^γ by the statistical uncertainty. The NLO QCD prediction from BLACKHAT is compared with the measurement in Figure 8(a). The NLO QCD prediction gives a good description of the data within the experimental and theoretical uncertainties for $E_T^\gamma < 750$ GeV. The theoretical uncertainty amounts to $\approx 10\%$; it is dominated by the contribution arising from scale uncertainties, in particular from the variation of μ_R for $E_T^\gamma \lesssim 500$ GeV, and by the uncertainty from the PDF for higher E_T^γ values.

The measured cross-section $d\sigma/dp_T^{\text{jet2}}$ (Figure 8(b)) decreases by almost five orders of magnitude within the measured range. The experimental uncertainty varies from 6% to 46% and is dominated by the jet energy scale uncertainty at low p_T^{jet2} and by the statistical uncertainty at high p_T^{jet2}. The NLO QCD prediction gives a good description of the data. No significant deviation from the prediction from NLO QCD is observed up to the highest value measured of $p_T^{\text{jet2}} \approx 1$ TeV. The theoretical uncertainty grows from 10% at $p_T^{\text{jet2}} \sim 70$ GeV to $\approx 26\%$ for $p_T^{\text{jet2}} \sim 1$ TeV and is dominated by the variation of μ_R for $p_T^{\text{jet2}} \lesssim 250$ GeV and by the uncertainty from the PDF for higher E_T^γ values.

The $d\sigma/d\Delta\phi^{\gamma-\text{jet2}}$ and $d\sigma/d\Delta\phi^{\text{jet1}-\text{jet2}}$ cross sections are shown in Figures 8(c) and 8(d), respectively. The measured cross sections display a maximum at 2–2.5 radians. The NLO QCD predictions give a good description of the data.

The prediction from PYTHIA gives a good description of the measured cross-section $d\sigma/dE_T^\gamma$ up to $E_T^\gamma \sim$ 750 GeV (see Figure 9(a)), whereas the prediction from SHERPA describes well the measured cross-section $d\sigma/dp_T^{\text{jet2}}$ (see Figure 9(b)). The predictions from SHERPA give a good description of the measured cross-section $d\sigma/d\Delta\phi^{\gamma-\text{jet2}}$ and $d\sigma/d\Delta\phi^{\text{jet1}-\text{jet2}}$, while the predictions from PYTHIA do not. In the predictions from PYTHIA a second jet can arise only from the parton shower, whereas in SHERPA, $2 \to n$ (with $n \geq 3$) matrix-element contributions are included as well, with a higher probability of producing a second hard jet.

The scale evolution of photon plus two-jet production is tested by measuring the azimuthal angle between jet2 and the photon or between jet2 and jet1 for E_T^γ below/above 300 GeV. Figure 10 shows the cross sections as functions of $\Delta\phi^{\gamma-\text{jet2}}$ and $\Delta\phi^{\text{jet1}-\text{jet2}}$ for the two E_T^γ ranges: both cross-section distributions have different shapes for E_T^γ below/above 300 GeV. The $d\sigma/d\Delta\phi^{\gamma-\text{jet2}}$ cross section is more peaked towards large values of $\Delta\phi^{\gamma-\text{jet2}}$ for $E_T^\gamma > 300$ GeV than that for $E_T^\gamma < 300$ GeV; the $d\sigma/d\Delta\phi^{\text{jet1}-\text{jet2}}$ cross section peaks at $\Delta\phi^{\text{jet1}-\text{jet2}} \sim 0.8$ rad (2.2 rad) for $E_T^\gamma > 300$ GeV ($E_T^\gamma < 300$ GeV). The NLO QCD predictions give a good description of the data and, in particular, reproduce the scale evolution of the measured cross sections. Figure 11 shows the comparison of the data and the predictions from PYTHIA and SHERPA. The predictions from PYTHIA fail to describe the data whereas those from SHERPA describe well the shape of the measured cross-section distributions and their evolution with the scale.
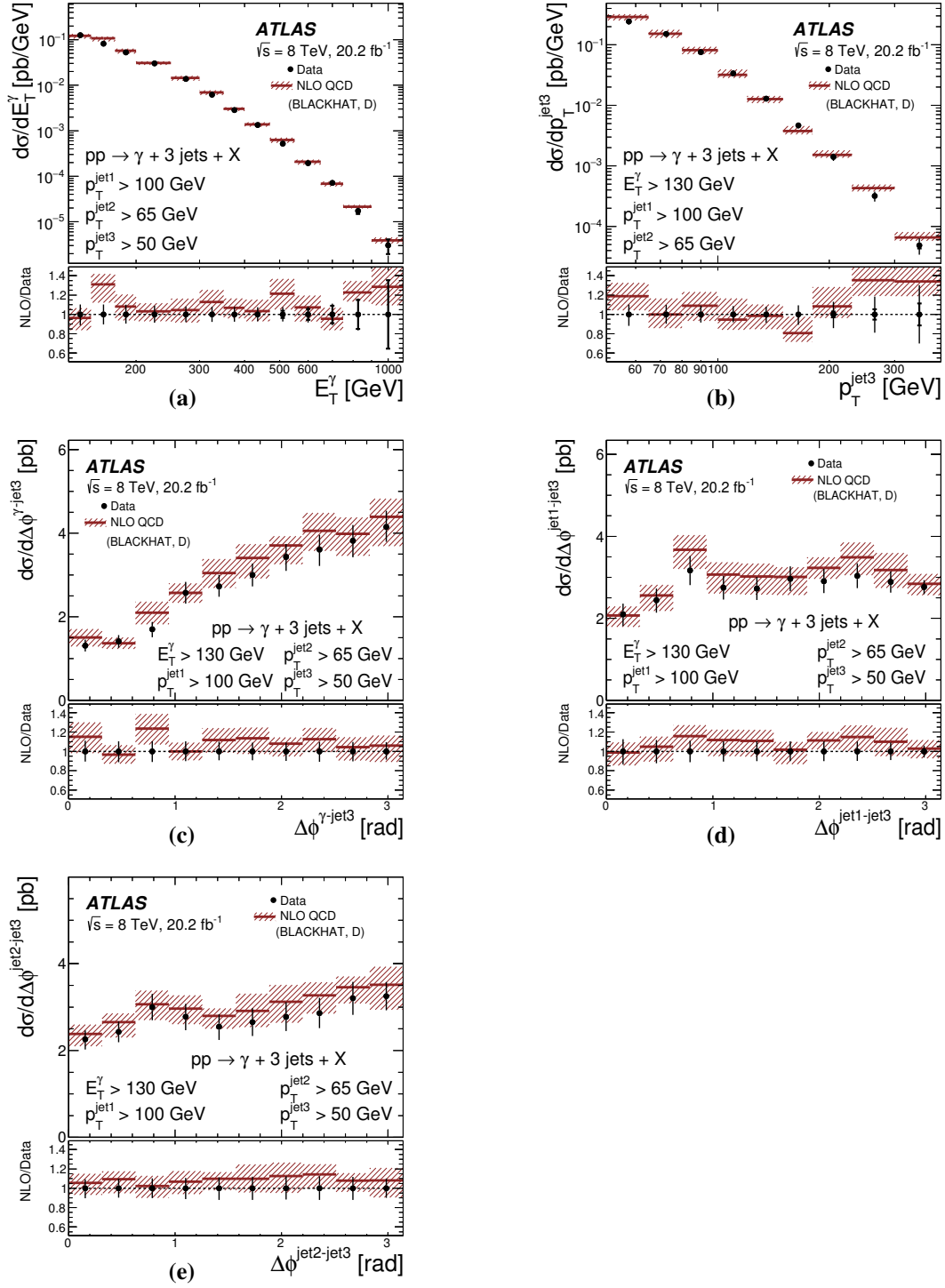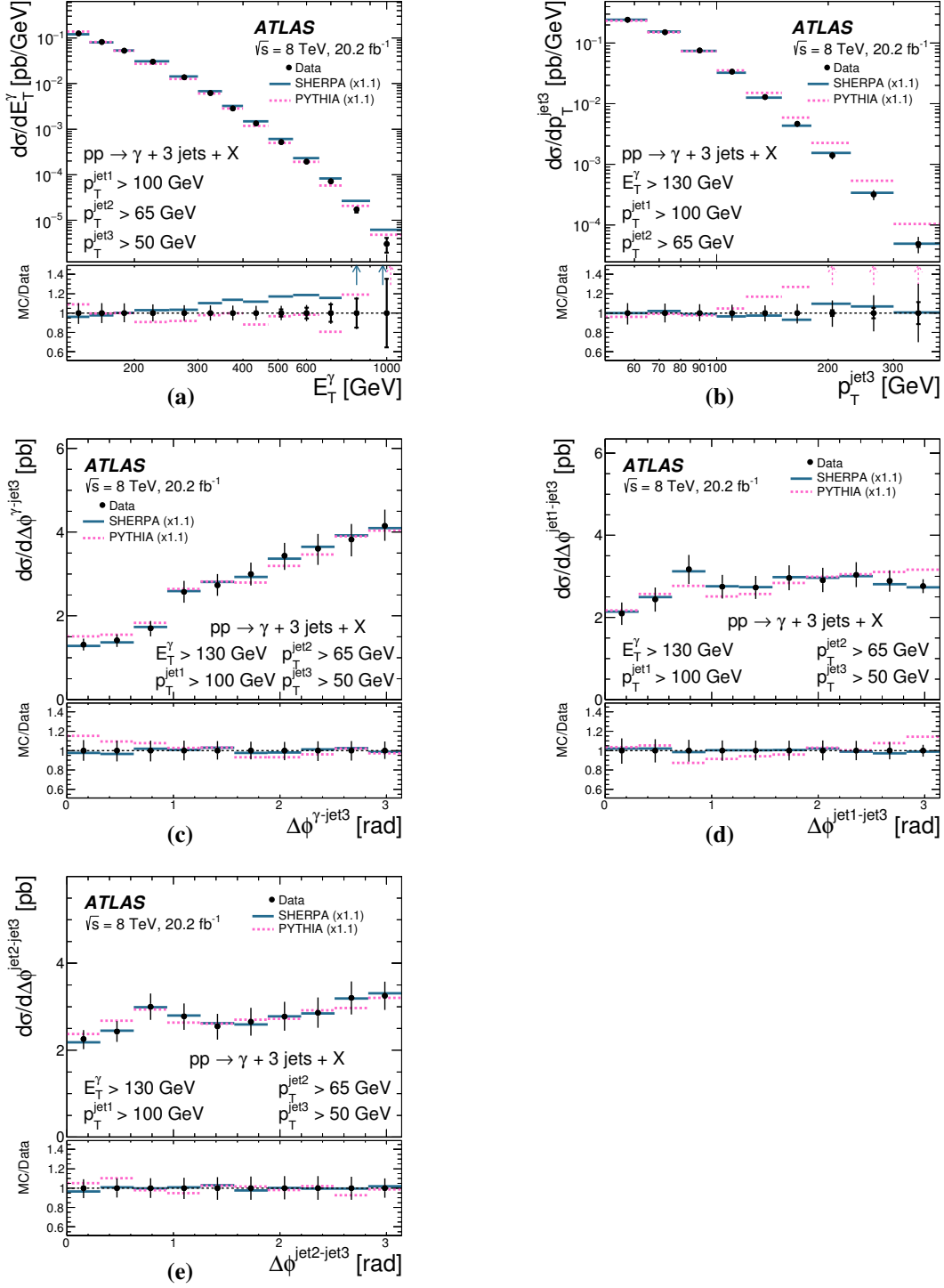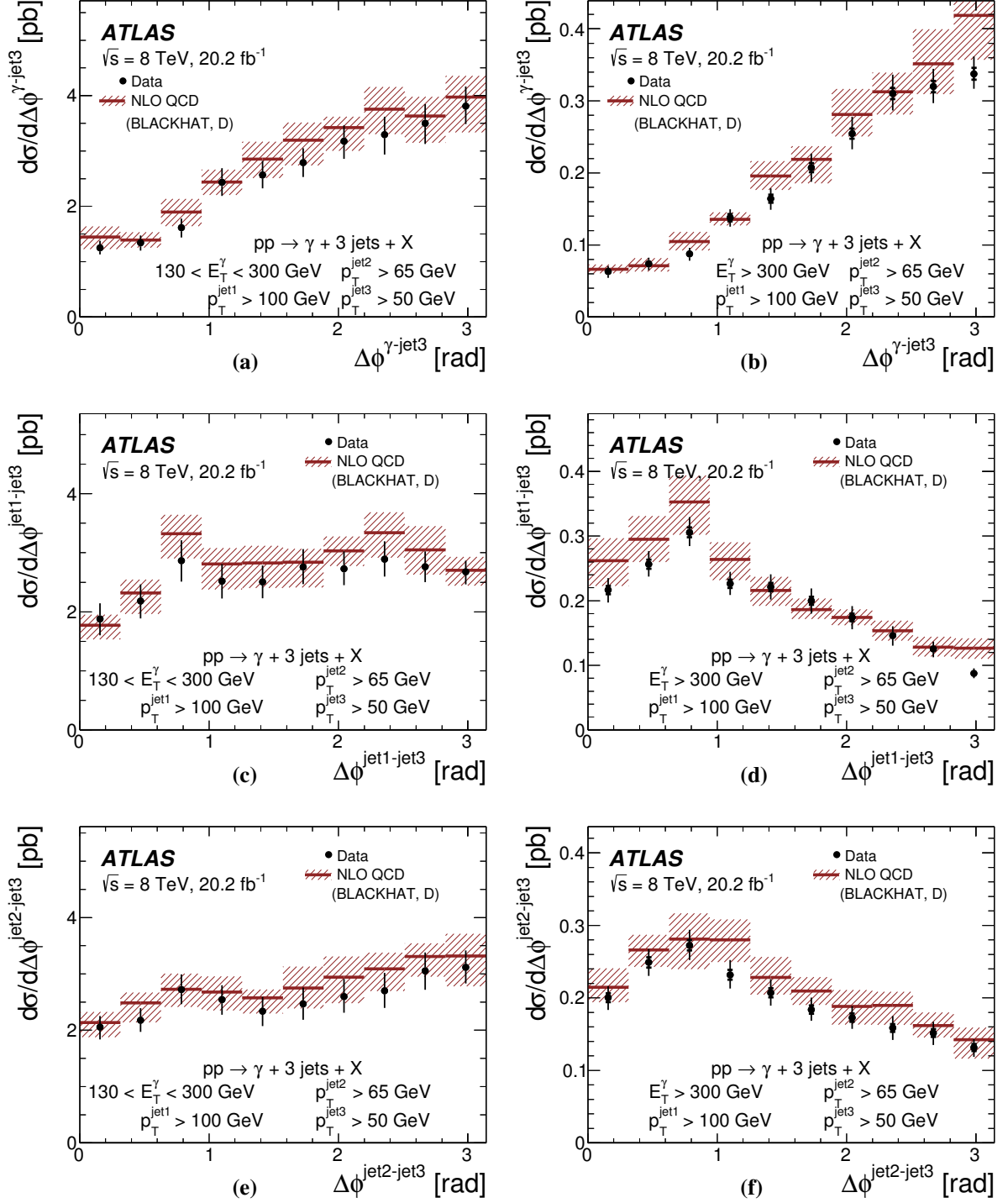
Figure 8: Measured cross sections for isolated-photon plus two-jet production (dots) as functions of (a) E_T^γ, (b) p_T^{jet2}, (c) $\Delta\phi^{\gamma-jet2}$ and (d) $\Delta\phi^{jet1-jet2}$. The NLO QCD predictions from BLACKHAT corrected for hadronisation and underlying-event effects and using the CT10 PDF set (solid lines) are also shown. These predictions include only the direct contribution (D). The bottom part of each figure shows the ratio of the NLO QCD prediction to the measured cross section. The inner (outer) error bars represent the statistical uncertainties (the statistical and systematic uncertainties added in quadrature) and the shaded band represents the theoretical uncertainty. For most of the points, the inner error bars are smaller than the marker size and, thus, not visible.
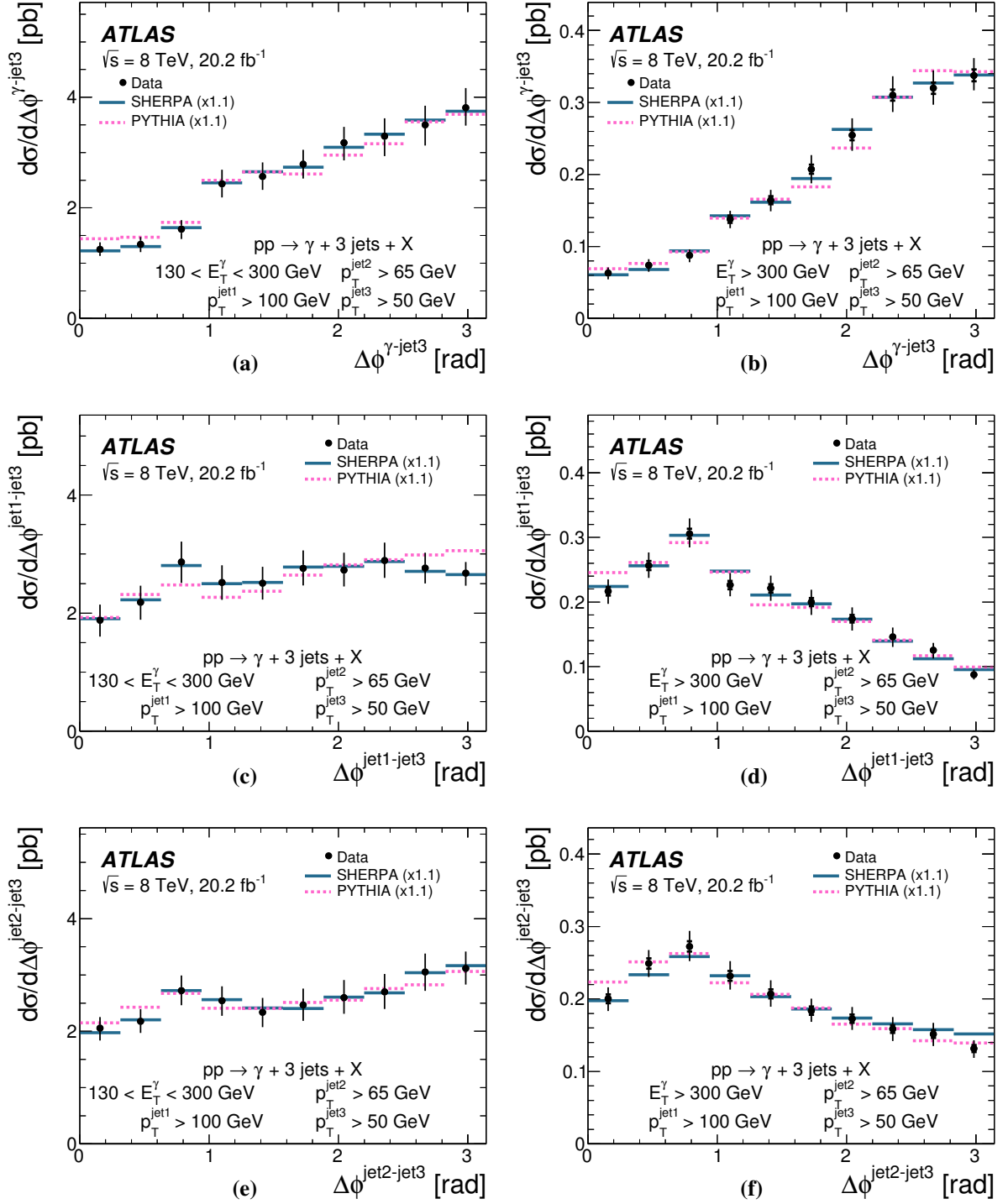
Figure 9: Measured cross sections for isolated-photon plus two-jet production (dots) as functions of (a) E_T^γ, (b) p_T^{jet2}, (c) $\Delta\phi^{\gamma-jet2}$ and (d) $\Delta\phi^{jet1-jet2}$. For comparison, the predictions from PYTHIA (dashed lines) and SHERPA (solid lines) normalised to the integrated measured cross sections (using the factors indicated in parentheses) are also shown. The bottom part of each figure shows the ratios of the MC predictions to the measured cross section. The inner (outer) error bars represent the statistical uncertainties (the statistical and systematic uncertainties added in quadrature). For most of the points, the inner error bars are smaller than the marker size and, thus, not visible.

29

Figure 10: Measured cross sections for isolated-photon plus two-jet production (dots) as functions of (a,b) $\Delta\phi^{\gamma-\text{jet2}}$ and (c,d) $\Delta\phi^{\text{jet1}-\text{jet2}}$ for (a,c) $E_T^\gamma < 300$ GeV and (b,d) $E_T^\gamma > 300$ GeV. The NLO QCD predictions from BLACKHAT corrected for hadronisation and underlying-event effects and using the CT10 PDF set are also shown as solid lines. These predictions include only the direct contribution (D). The inner (outer) error bars represent the statistical uncertainties (the statistical and systematic uncertainties added in quadrature) and the shaded band represents the theoretical uncertainty. For most of the points, the inner error bars are smaller than the marker size and, thus, not visible.

Figure 11: Measured cross sections for isolated-photon plus two-jet production (dots) as functions of (a,b) $\Delta\phi^{\gamma-\mathrm{jet2}}$ and (c,d) $\Delta\phi^{\mathrm{jet1}-\mathrm{jet2}}$ for (a,c) $E_T^\gamma < 300$ GeV and (b,d) $E_T^\gamma > 300$ GeV. For comparison, the predictions from PYTHIA (dashed lines) and SHERPA (solid lines) are also shown. The predictions are normalised to the data by a global factor, which is indicated in parentheses. The inner (outer) error bars represent the statistical uncertainties (the statistical and systematic uncertainties added in quadrature). For most of the points, the inner error bars are smaller than the marker size and, thus, not visible.

9.4 Comparison of jet production around the photon and jet1

Figure 12(a) shows the cross sections for photon plus two-jet production as functions of β^{jet1} and β^{γ}. The two measured cross sections have different shapes: the measured cross-section $d\sigma/d\beta^{\text{jet1}}$ increases monotonically as β^{jet1} increases, whereas the measured cross-section $d\sigma/d\beta^{\gamma}$ increases up to $\beta^{\gamma} \approx 1.8$ rad and then remains approximately constant. The predictions from SHERPA give a good description of the measured cross sections. To quantify the differences in the patterns of jet production around the photon and jet1, the ratio of the measured cross-sections $d\sigma/d\beta^{\text{jet1}}$ and $d\sigma/d\beta^{\gamma}$ is made. In the estimation of the systematic uncertainties of the ratio of the cross sections, the correlations between numerator and denominator are fully taken into account leading to complete or partial cancellations depending on the source of uncertainty. The ratio $(d\sigma/d\beta^{\text{jet1}})/(d\sigma/d\beta^{\gamma})$, shown in Figure 12(b), is enhanced at $\beta = 0$ and π rad with respect to the value of the ratio at $\beta = \pi/2$ rad. The measured ratio is tested against the hypothesis of being independent of β and the resulting p-value is 1.3%. Thus, it is observed that the patterns of QCD radiation around the photon and jet1 are different.
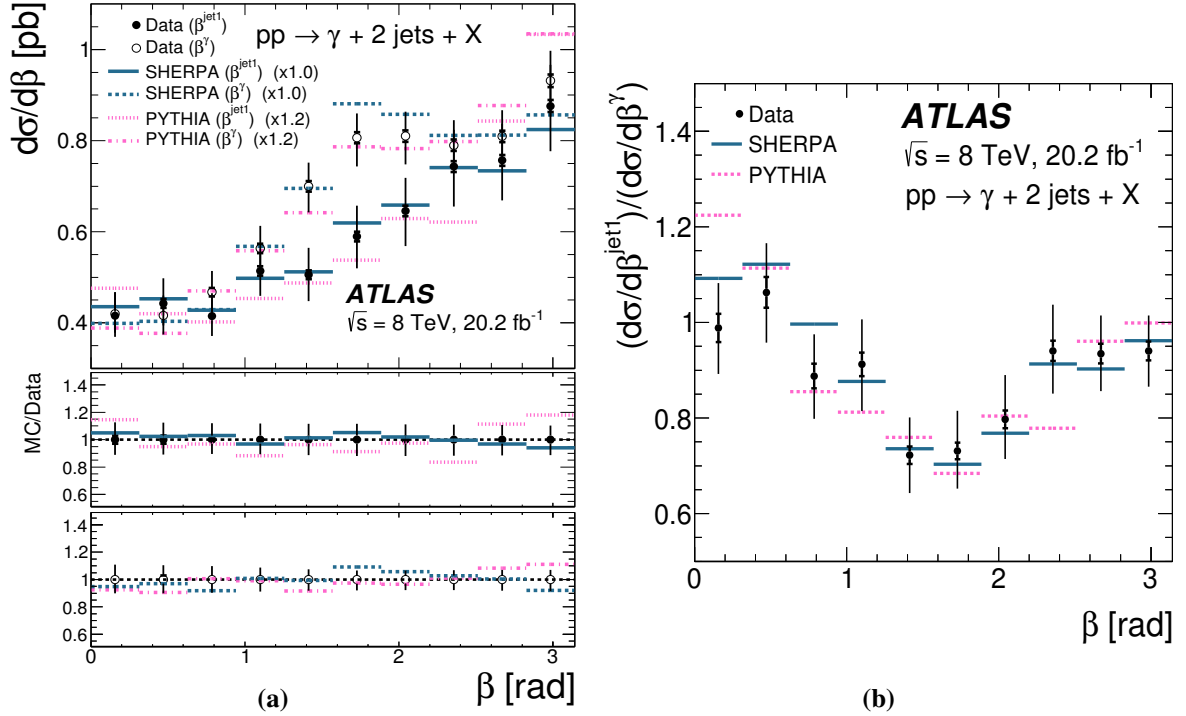
Figure 12: (a) Measured cross sections for isolated-photon plus two-jet production as functions of β^{jet1} (dots) and β^{γ} (open circles). For comparison, the predictions from SHERPA (blue solid and dashed lines) and PYTHIA (pink dash-dotted and dotted lines) normalised to the integrated measured cross sections (using the factors indicated in parentheses) are also shown. The bottom parts of the figure show the ratios of the MC predictions to the measured cross sections. (b) Ratio of the measured cross-section $d\sigma/d\beta^{\text{jet1}}$ and $d\sigma/d\beta^{\gamma}$ (dots); the ratios for the SHERPA and PYTHIA predictions are shown as solid and dashed lines, respectively. The inner (outer) error bars represent the statistical uncertainties (the statistical and systematic uncertainties added in quadrature). For some of the points, the inner error bars are smaller than the marker size and, thus, not visible.

9.5 Cross sections for isolated-photon plus three-jet production

The measured cross-section $d\sigma/dE_T^\gamma$ ($d\sigma/dp_T^{\rm jet3}$), shown in Figure 13(a) (Figure 13(b)), decreases by approximately five (three) orders of magnitude within the measured range. The measured cross-section $d\sigma/d\Delta\phi^{\gamma-\rm jet3}$ (Figure 13(c)) increases as $\Delta\phi^{\gamma-\rm jet3}$ increases whereas the measured cross sections as functions of $\Delta\phi^{\rm jet1-jet3}$ (Figure 13(d)) and $\Delta\phi^{\rm jet2-jet3}$ (Figure 13(e)) are approximately constant for $\Delta\phi^{\rm jet1-jet3}$, $\Delta\phi^{\rm jet2-jet3} > 1$ rad. The NLO QCD predictions from BLACKHAT give an adequate description of the data within the experimental and theoretical uncertainties; the predictions have a tendency to be systematically above the data.

The prediction from PYTHIA gives a good description of the measured cross-section $d\sigma/dE_T^\gamma$, whereas the prediction from SHERPA describes well the measured cross-section $d\sigma/dp_T^{\rm jet3}$ (see Figure 14). The predictions from SHERPA and PYTHIA give a good description of the measured cross sections as functions of $\Delta\phi^{\gamma-\rm jet3}$, $\Delta\phi^{\rm jet1-jet3}$ and $\Delta\phi^{\rm jet2-jet3}$.

The scale evolution of the photon plus three-jet production is tested by measuring the distributions of the azimuthal angle between jet3 and the photon, jet1 or jet2 for E_T^γ below/above 300 GeV. Figure 15 shows the cross sections as functions of $\Delta\phi^{\gamma-\rm jet3}$, $\Delta\phi^{\rm jet1-jet3}$ and $\Delta\phi^{\rm jet2-jet3}$ for the two E_T^γ ranges: the shape of the cross-section distributions is different for E_T^γ below/above 300 GeV. The $d\sigma/d\Delta\phi^{\gamma-\rm jet3}$ cross section is more peaked towards large values of $\Delta\phi^{\gamma-\rm jet3}$ for $E_T^\gamma > 300$ GeV than that for $E_T^\gamma < 300$ GeV; the $d\sigma/d\Delta\phi^{\rm jet1-jet3}$ ($d\sigma/d\Delta\phi^{\rm jet2-jet3}$) cross section decreases beyond the peak as $\Delta\phi^{\rm jet1-jet3}$ ($\Delta\phi^{\rm jet2-jet3}$) increases for $E_T^\gamma > 300$ GeV whereas it stays approximately constant for $E_T^\gamma < 300$ GeV. The NLO QCD predictions provide an adequate description of the measured cross sections and, thereby, of the observed scale evolution of the angular correlations. The predictions from PYTHIA and SHERPA, shown in Figure 16, give an adequate description of the shape of the measured cross sections.

Figure 13: Measured cross sections for isolated-photon plus three-jet production (dots) as functions of (a) E_T^γ, (b) p_T^{jet3}, (c) $\Delta\phi^{\gamma-jet3}$, (d) $\Delta\phi^{jet1-jet3}$ and (e) $\Delta\phi^{jet2-jet3}$. The NLO QCD predictions from BLACKHAT corrected for hadronisation and underlying-event effects and using the CT10 PDF set (solid lines) are also shown. These predictions include only the direct contribution (D). The bottom part of each figure shows the ratio of the NLO QCD prediction to the measured cross section. The inner (outer) error bars represent the statistical uncertainties (the statistical and systematic uncertainties added in quadrature) and the shaded band represents the theoretical uncertainty. For most of the points, the inner error bars are smaller than the marker size and, thus, not visible.

Figure 14: Measured cross sections for isolated-photon plus three-jet production (dots) as functions of (a) E_T^γ, (b) p_T^{jet3}, (c) $\Delta\phi^{\gamma-jet3}$, (d) $\Delta\phi^{jet1-jet3}$ and (e) $\Delta\phi^{jet2-jet3}$. For comparison, the predictions from SHERPA (solid lines) and PYTHIA (dashed lines) normalised to the integrated measured cross sections (using the factors indicated in parentheses) are also shown. The bottom part of each figure shows the ratios of the MC predictions to the measured cross section. The inner (outer) error bars represent the statistical uncertainties (the statistical and systematic uncertainties added in quadrature). For most of the points, the inner error bars are smaller than the marker size and, thus, not visible.

Figure 15: Measured cross sections for isolated-photon plus three-jet production (dots) as functions of (a,b) $\Delta\phi^{\gamma-\text{jet3}}$, (c,d) $\Delta\phi^{\text{jet1}-\text{jet3}}$ and (e,f) $\Delta\phi^{\text{jet2}-\text{jet3}}$ for (a,c,e) $E_T^\gamma < 300$ GeV and (b,d,f) $E_T^\gamma > 300$ GeV. The NLO QCD predictions from BLACKHAT corrected for hadronisation and underlying-event effects and using the CT10 PDF set are also shown as solid lines. These predictions include only the direct contribution (D). The inner (outer) error bars represent the statistical uncertainties (the statistical and systematic uncertainties added in quadrature) and the shaded band represents the theoretical uncertainty. For most of the points, the inner error bars are smaller than the marker size and, thus, not visible.

Figure 16: Measured cross sections for isolated-photon plus three-jet production (dots) as functions of (a,b) $\Delta\phi^{\gamma-\mathrm{jet}3}$, (c,d) $\Delta\phi^{\mathrm{jet}1-\mathrm{jet}3}$ and (e,f) $\Delta\phi^{\mathrm{jet}2-\mathrm{jet}3}$ for (a,c,e) $E_\mathrm{T}^\gamma < 300$ GeV and (b,d,f) $E_\mathrm{T}^\gamma > 300$ GeV. For comparison, the predictions from PYTHIA (dashed lines) and SHERPA (solid lines) are also shown. The predictions are normalised to the data by a global factor, which is indicated in parentheses. The inner (outer) error bars represent the statistical uncertainties (the statistical and systematic uncertainties added in quadrature). For most of the points, the inner error bars are smaller than the marker size and, thus, not visible.

10 Summary

Measurements of the cross sections for the production of an isolated photon in association with one, two or three jets in proton–proton collisions at $\sqrt{s}$ = 8 TeV, $pp \rightarrow \gamma$ + jet(s) + X, using a data set with an integrated luminosity of 20.2 fb^{-1} recorded by the ATLAS detector at the LHC are presented. The photon is required to have E_T^γ > 130 GeV and $|\eta^\gamma|$ < 2.37, excluding the region 1.37 < $|\eta^\gamma|$ < 1.56, and to be isolated with $E_{T,part}^{iso}$ < 10 GeV. The jets are reconstructed using the anti-k_t algorithm with radius parameter R = 0.6.

The cross sections for photon plus one-jet are measured as functions of E_T^γ and p_T^{jet1} with p_T^{jet1} > 100 GeV; the measurements extend up to values of E_T^γ (p_T^{jet1}) of 1.1 TeV (1.2 TeV). The dependence on $m^{\gamma-jet1}$ and $|\cos\theta^*|$ is also measured for $m^{\gamma-jet1}$ > 467 GeV and extends up to $m^{\gamma-jet1}$ of 2.45 TeV. The NLO QCD predictions from JETPHOX, corrected for hadronisation and underlying-event effects, give a good description of the measured cross-section distributions in both shape and normalisation. In particular, the measured dependence on $|\cos\theta^*|$ and its scale dependence is consistent with the dominance of processes in which a quark is being exchanged; the experimental (theoretical) uncertainty in $d\sigma/d|\cos\theta^*|$ amounts to $\approx$ 3% (10%).

Photon plus two-jet production is investigated by measuring cross sections as functions of E_T^γ and p_T^{jet2} and angular correlations between the final-state objects for p_T^{jet1} > 100 GeV and p_T^{jet2} > 65 GeV. The NLO QCD predictions from BLACKHAT provide a good description of the measurements except for E_T^γ > 750 GeV. The predictions from SHERPA, which include higher-order tree-level matrix elements, are found to be superior to those from PYTHIA, based on $2 \rightarrow 2$ processes, in describing the distributions in p_T^{jet2} and the angular correlations.

The patterns of QCD radiation around the photon and the leading jet are compared by measuring the production of the subleading jet in an annular region centred on the given final-state object. The cross sections as functions of β^γ and β^{jet1} are observed to be different. The ratio of the cross sections shows enhancements in the directions towards the beams, β = 0 and π rad.

Photon plus three-jet production is characterised by measurements of cross sections as functions of E_T^γ, p_T^{jet3} and angular correlations for p_T^{jet1} > 100 GeV, p_T^{jet2} > 65 GeV and p_T^{jet3} > 50 GeV. The NLO QCD predictions from BLACKHAT provide an adequate description of the measurements. Whereas the prediction from SHERPA for p_T^{jet3} is superior to that from PYTHIA, both give adequate descriptions of the angular correlations.

All these studies provide stringent tests of pQCD and scrutinise the description of the dynamics of isolated-photon plus jets production in pp collisions up to $O(\alpha_{em}\alpha_s^4)$.

Acknowledgements

References

[1] D. d'Enterria and J. Rojo, *Quantitative constraints on the gluon distribution function in the proton from collider isolated-photon data*, Nucl. Phys. B **860** (2012) 311, arXiv:`1202.1762 [hep-ph]`.

[2] L. Carminati et al., *Sensitivity of the LHC isolated-γ+jet data to the parton distribution functions of the proton*, Europhys. Lett. **101** (2013) 61002, arXiv:`1212.5511 [hep-ph]`.

[3] ATLAS Collaboration, *Dynamics of isolated-photon plus jet production in pp collisions at $\sqrt{s} = 7$ TeV with the ATLAS detector*, Nucl. Phys. B **875** (2013) 483, arXiv:`1307.6795 [hep-ex]`.

[4] T. Pietrycki and A. Szczurek, *Photon-jet correlations in pp and pp̄ collisions*, Phys. Rev. D **76** (2007) 034003, arXiv:`0704.2158 [hep-ph]`.

[5] Z. Belghobsi et al., *Photon-jet correlations and constraints on fragmentation functions*, Phys. Rev. D **79** (2009) 114024, arXiv:`0903.4834 [hep-ph]`.

[6] ATLAS Collaboration, *Measurement of the inclusive isolated prompt photon cross section in pp collisions at $\sqrt{s} = 7$ TeV with the ATLAS detector*, Phys. Rev. D **83** (2011) 052005, arXiv:`1012.4389 [hep-ex]`.

[7] ATLAS Collaboration, *Measurement of the inclusive isolated prompt photon cross-section in pp collisions at $\sqrt{s} = 7$ TeV using 35 pb^{-1} of ATLAS data*, Phys. Lett. B **706** (2011) 150, arXiv:`1108.0253 [hep-ex]`.

[8] ATLAS Collaboration, *Measurement of the inclusive isolated prompt photons cross section in pp collisions at* $\sqrt{s}$ = 7 *TeV with the ATLAS detector using* 4.6 *fb*$^{-1}$, Phys. Rev. D **89** (2014) 052004, arXiv:1311.1440 [hep-ex].

[9] ATLAS Collaboration, *Measurement of the inclusive isolated prompt photon cross section in pp collisions at* $\sqrt{s}$ = 8 *TeV with the ATLAS detector*, JHEP **1608** (2016) 005, arXiv:1605.03495 [hep-ex].

[10] CMS Collaboration, *Measurement of the isolated prompt photon production cross section in pp collisions at* $\sqrt{s}$ = 7 *TeV*, Phys. Rev. Lett. **106** (2011) 082001, arXiv:1012.0799 [hep-ex].

[11] CMS Collaboration, *Measurement of the differential cross section for isolated prompt photon production in pp collisions at 7 TeV*, Phys. Rev. D **84** (2011) 052011, arXiv:1108.2044 [hep-ex].

[12] ATLAS Collaboration, *Measurement of the production cross section of an isolated photon associated with jets in proton-proton collisions at* $\sqrt{s}$ = 7 *TeV with the ATLAS detector*, Phys. Rev. D **85** (2012) 092014, arXiv:1203.3161 [hep-ex].

[13] CMS Collaboration, *Rapidity distributions in exclusive Z + jet and γ + jet events in pp collisions at* $\sqrt{s}$ = 7 *TeV*, Phys. Rev. D **88** (2013) 112009, arXiv:1310.3082 [hep-ex].

[14] CMS Collaboration, *Measurement of the triple-differential cross section for photon+jets production in proton-proton collisions at* $\sqrt{s}$ = 7 *TeV*, JHEP **1406** (2014) 009, arXiv:1311.6141 [hep-ex].

[15] CMS Collaboration, *Comparison of the Z/γ* + jets to γ + jets cross sections in pp collisions at* $\sqrt{s}$ = 8 *TeV*, JHEP **1510** (2015) 128, arXiv:1505.06520 [hep-ex].

[16] CDF Collaboration, F. Abe et al., *Evidence for color coherence in pp collisions at* $\sqrt{s}$ = 1.8 *TeV*, Phys. Rev. D **50** (1994) 5562.

[17] DØ Collaboration, B. Abbott et al., *Color coherent radiation in multijet events from pp collisions at* $\sqrt{s}$ = 1.8 *TeV*, Phys. Lett. B **414** (1997) 419, arXiv:hep-ex/9706012.

[18] S. Keller and J.F. Owens, *Event structure in photon plus two jet final states*, Phys. Lett. B **269** (1991) 445.

[19] Z. Bern et al., *Driving Missing Data at Next-to-Leading Order*, Phys. Rev. D **84** (2011) 114002, arXiv:1106.1423 [hep-ph].

[20] Z. Bern et al., *Missing Energy and Jets for Supersymmetry Searches*, Phys. Rev. D **87** (2013) 034026, arXiv:1206.6064 [hep-ph].

[21] T. Sjöstrand, S. Mrenna and P.Z. Skands, *A Brief Introduction to PYTHIA 8.1*, Comput. Phys. Commun. **178** (2008) 852, arXiv:0710.3820 [hep-ph].

[22] T. Gleisberg et al., *Event generation with SHERPA 1.1*, JHEP **0902** (2009) 007, arXiv:0811.4622 [hep-ph].

[23] S. Catani, M. Fontannaz, J. Ph. Guillet and E. Pilon, *Cross section of isolated prompt photons in hadron-hadron collisions*, JHEP **0205** (2002) 028, arXiv:hep-ph/0204023.

[24] P. Aurenche, M. Fontannaz, J. Ph. Guillet, E. Pilon and M. Werlen,
A new critical study of photon production in hadronic collisions, Phys. Rev. D **73** (2006) 094007,
arXiv:hep-ph/0602133.

[25] C.F. Berger et al., *An Automated Implementation of On-Shell Methods for One-Loop Amplitudes*,
Phys. Rev. D **78** (2008) 036003, arXiv:0803.4180 [hep-ph].

[26] Z. Bern et al.,
Four-Jet Production at the Large Hadron Collider at Next-to-Leading Order in QCD,
Phys. Rev. Lett. **109** (2012) 042001, arXiv:1112.3940 [hep-ph].

[27] ATLAS Collaboration, *The ATLAS Experiment at the CERN Large Hadron Collider*,
JINST **3** (2008) S08003.

[28] ATLAS Collaboration, *Performance of the ATLAS Trigger System in 2010*,
Eur. Phys. J. C **72** (2012) 1849, arXiv:1110.1530 [hep-ex].

[29] ATLAS Collaboration,
Luminosity determination in pp collisions at $\sqrt{s}$ = 8 TeV using the ATLAS detector at the LHC,
(2016), arXiv:1608.03953 [hep-ex].

[30] ATLAS Collaboration, *Measurement of the photon identification efficiencies with the ATLAS
detector using LHC Run-1 data*, (2016), arXiv:1606.01813 [hep-ex].

[31] ATLAS Collaboration,
Electron and photon energy calibration with the ATLAS detector using LHC Run 1 data,
Eur. Phys. J. C **74** (2014) 3071, arXiv:1407.5063 [hep-ex].

[32] ATLAS Collaboration,
Topological cell clustering in the ATLAS calorimeters and its performance in LHC Run 1, (2016),
arXiv:1603.02934 [hep-ex].

[33] M. Cacciari, G.P. Salam and G. Soyez, *The Catchment Area of Jets*, JHEP **0804** (2008) 005,
arXiv:0802.1188 [hep-ph].

[34] M. Cacciari, G. Salam and G. Soyez, *The anti-k_t jet clustering algorithm*, JHEP **0804** (2008) 063,
arXiv:0802.1189 [hep-ph].

[35] ATLAS Collaboration, *Jet energy measurement and its systematic uncertainty in proton-proton
collisions at $\sqrt{s}$ = 7 TeV with the ATLAS detector*, Eur. Phys. J. C **75** (2015) 17,
arXiv:1406.0076 [hep-ex].

[36] ATLAS Collaboration, *Jet global sequential corrections with the ATLAS detector in
proton-proton collisions at $\sqrt{s}$ = 8 TeV*, ATLAS-CONF-2015-002, 2015,
URL: http://cds.cern.ch/record/2001682.

[37] ATLAS Collaboration, *Monte Carlo Calibration and Combination of In-situ Measurements of Jet
Energy Scale, Jet Energy Resolution and Jet Mass in ATLAS*, ATLAS-CONF-2015-037, 2015,
URL: http://cds.cern.ch/record/2044941.

[38] ATLAS Collaboration,
Jet energy measurement with the ATLAS detector in proton-proton collisions at $\sqrt{s}$ = 7 TeV,
Eur. Phys. J. C **73** (2013) 2304, arXiv:1112.6426 [hep-ex].

[39] S. Frixione and G. Ridolfi, *Jet photoproduction at HERA*, Nucl. Phys. B **507** (1997) 315,
arXiv:hep-ph/9707345.

[40] B. Andersson, G. Gustafson, G. Ingelman and T. Sjöstrand,
Parton Fragmentation and String Dynamics, Phys. Rept. **97** (1983) 31.

[41] C. Winter, F. Krauss and G. Soff, *A modified cluster hadronisation model*,
Eur. Phys. J. C **36** (2004) 381, arXiv:hep-ph/0311085.

[42] J. Pumplin et al.,
New generation of parton distributions with uncertainties from global QCD analysis,
JHEP **0207** (2002) 012, arXiv:hep-ph/0201195.

[43] H.-L. Lai et al., *New parton distributions for collider physics*, Phys. Rev. D **82** (2010) 074024,
arXiv:1007.2241 [hep-ph].

[44] ATLAS Collaboration, *Summary of ATLAS Pythia 8 tunes*, ATL-PHYS-PUB-2012-003, 2012,
URL: http://cds.cern.ch/record/1474107.

[45] S. Agostinelli et al., *GEANT4 - a simulation toolkit*, Nucl. Instrum. Meth. A **506** (2003) 250.

[46] ATLAS Collaboration, *The ATLAS simulation infrastructure*, Eur. Phys. J. C **70** (2010) 823,
arXiv:1005.4568 [physics.ins-det].

[47] A.D. Martin, W.J. Stirling, R.S. Thorne and G. Watt, *Uncertainties on α_s in global PDF analyses
and implications for predicted hadronic cross sections*, Eur. Phys. J. C **64** (2009) 653,
arXiv:0905.3531 [hep-ph].

[48] G. D'Agostini, *A Multidimensional unfolding method based on Bayes' theorem*,
Nucl. Instrum. Meth. A **362** (1995) 487.

[49] L. Bourhis, M. Fontannaz and J.Ph. Guillet,
Quark and gluon fragmentation functions into photons, Eur. Phys. J. C **2** (1998) 529,
arXiv:hep-ph/9704447.

[50] S. Frixione, *Isolated photons in perturbative QCD*, Phys. Lett. B **429** (1998) 369,
arXiv:hep-ph/9801442.

[51] ATLAS Collaboration, *ATLAS Computing Acknowledgements 2016-2017*,
ATL-GEN-PUB-2016-002, 2016, URL: http://cds.cern.ch/record/2202407.

The ATLAS Collaboration

M. Aaboud[137d], G. Aad[88], B. Abbott[115], J. Abdallah[8], O. Abdinov[12], B. Abeloos[119], O.S. AbouZeid[139], N.L. Abraham[151], H. Abramowicz[155], H. Abreu[154], R. Abreu[118], Y. Abulaiti[148a,148b], B.S. Acharya[167a,167b,a], S. Adachi[157], L. Adamczyk[41a], D.L. Adams[27], J. Adelman[110], S. Adomeit[102], T. Adye[133], A.A. Affolder[139], T. Agatonovic-Jovin[14], J.A. Aguilar-Saavedra[128a,128f], S.P. Ahlen[24], F. Ahmadov[68,b], G. Aielli[135a,135b], H. Akerstedt[148a,148b], T.P.A. Åkesson[84], A.V. Akimov[98], G.L. Alberghi[22a,22b], J. Albert[172], S. Albrand[58], M.J. Alconada Verzini[74], M. Aleksa[32], I.N. Aleksandrov[68], C. Alexa[28b], G. Alexander[155], T. Alexopoulos[10], M. Alhroob[115], B. Ali[130], M. Aliev[76a,76b], G. Alimonti[94a], J. Alison[33], S.P. Alkire[38], B.M.M. Allbrooke[151], B.W. Allen[118], P.P. Allport[19], A. Aloisio[106a,106b], A. Alonso[39], F. Alonso[74], C. Alpigiani[140], A.A. Alshehri[56], M. Alstaty[88], B. Alvarez Gonzalez[32], D. Álvarez Piqueras[170], M.G. Alviggi[106a,106b], B.T. Amadio[16], Y. Amaral Coutinho[26a], C. Amelung[25], D. Amidei[92], S.P. Amor Dos Santos[128a,128c], A. Amorim[128a,128b], S. Amoroso[32], G. Amundsen[25], C. Anastopoulos[141], L.S. Ancu[52], N. Andari[19], T. Andeen[11], C.F. Anders[60b], J.K. Anders[77], K.J. Anderson[33], A. Andreazza[94a,94b], V. Andrei[60a], S. Angelidakis[9], I. Angelozzi[109], A. Angerami[38], F. Anghinolfi[32], A.V. Anisenkov[111,c], N. Anjos[13], A. Annovi[126a,126b], C. Antel[60a], M. Antonelli[50], A. Antonov[100,*], D.J. Antrim[166], F. Anulli[134a], M. Aoki[69], L. Aperio Bella[19], G. Arabidze[93], Y. Arai[69], J.P. Araque[128a], A.T.H. Arce[48], F.A. Arduh[74], J-F. Arguin[97], S. Argyropoulos[66], M. Arik[20a], A.J. Armbruster[145], L.J. Armitage[79], O. Arnaez[32], H. Arnold[51], M. Arratia[30], O. Arslan[23], A. Artamonov[99], G. Artoni[122], S. Artz[86], S. Asai[157], N. Asbah[45], A. Ashkenazi[155], B. Åsman[148a,148b], L. Asquith[151], K. Assamagan[27], R. Astalos[146a], M. Atkinson[169], N.B. Atlay[143], K. Augsten[130], G. Avolio[32], B. Axen[16], M.K. Ayoub[119], G. Azuelos[97,d], M.A. Baak[32], A.E. Baas[60a], M.J. Baca[19], H. Bachacou[138], K. Bachas[76a,76b], M. Backes[122], M. Backhaus[32], P. Bagiacchi[134a,134b], P. Bagnaia[134a,134b], Y. Bai[35a], J.T. Baines[133], M. Bajic[39], O.K. Baker[179], E.M. Baldin[111,c], P. Balek[175], T. Balestri[150], F. Balli[138], W.K. Balunas[124], E. Banas[42], Sw. Banerjee[176,e], A.A.E. Bannoura[178], L. Barak[32], E.L. Barberio[91], D. Barberis[53a,53b], M. Barbero[88], T. Barillari[103], M-S Barisits[32], T. Barklow[145], N. Barlow[30], S.L. Barnes[87], B.M. Barnett[133], R.M. Barnett[16], Z. Barnovska-Blenessy[36a], A. Baroncelli[136a], G. Barone[25], A.J. Barr[122], L. Barranco Navarro[170], F. Barreiro[85], J. Barreiro Guimarães da Costa[35a], R. Bartoldus[145], A.E. Barton[75], P. Bartos[146a], A. Basalaev[125], A. Bassalat[119,f], R.L. Bates[56], S.J. Batista[161], J.R. Batley[30], M. Battaglia[139], M. Bauce[134a,134b], F. Bauer[138], H.S. Bawa[145,g], J.B. Beacham[113], M.D. Beattie[75], T. Beau[83], P.H. Beauchemin[165], P. Bechtle[23], H.P. Beck[18,h], K. Becker[122], M. Becker[86], M. Beckingham[173], C. Becot[112], A.J. Beddall[20e], A. Beddall[20b], V.A. Bednyakov[68], M. Bedognetti[109], C.P. Bee[150], L.J. Beemster[109], T.A. Beermann[32], M. Begel[27], J.K. Behr[45], A.S. Bell[81], G. Bella[155], L. Bellagamba[22a], A. Bellerive[31], M. Bellomo[89], K. Belotskiy[100], O. Beltramello[32], N.L. Belyaev[100], O. Benary[155,*], D. Benchekroun[137a], M. Bender[102], K. Bendtz[148a,148b], N. Benekos[10], Y. Benhammou[155], E. Benhar Noccioli[179], J. Benitez[66], D.P. Benjamin[48], J.R. Bensinger[25], S. Bentvelsen[109], L. Beresford[122], M. Beretta[50], D. Berge[109], E. Bergeaas Kuutmann[168], N. Berger[5], J. Beringer[16], S. Berlendis[58], N.R. Bernard[89], C. Bernius[112], F.U. Bernlochner[23], T. Berry[80], P. Berta[131], C. Bertella[86], G. Bertoli[148a,148b], F. Bertolucci[126a,126b], I.A. Bertram[75], C. Bertsche[45], D. Bertsche[115], G.J. Besjes[39], O. Bessidskaia Bylund[148a,148b], M. Bessner[45], N. Besson[138], C. Betancourt[51], A. Bethani[58], S. Bethke[103], A.J. Bevan[79], R.M. Bianchi[127], M. Bianco[32], O. Biebel[102], D. Biedermann[17], R. Bielski[87], N.V. Biesuz[126a,126b], M. Biglietti[136a], J. Bilbao De Mendizabal[52], T.R.V. Billoud[97], H. Bilokon[50], M. Bindi[57], A. Bingul[20b], C. Bini[134a,134b], S. Biondi[22a,22b], T. Bisanz[57], D.M. Bjergaard[48], C.W. Black[152], J.E. Black[145], K.M. Black[24], D. Blackburn[140], R.E. Blair[6], T. Blazek[146a], I. Bloch[45], C. Blocker[25], A. Blue[56], W. Blum[86,*], U. Blumenschein[57], S. Blunier[34a], G.J. Bobbink[109],

V.S. Bobrovnikov[111,c], S.S. Bocchetta[84], A. Bocci[48], C. Bock[102], M. Boehler[51], D. Boerner[178],
J.A. Bogaerts[32], D. Bogavac[102], A.G. Bogdanchikov[111], C. Bohm[148a], V. Boisvert[80], P. Bokan[14],
T. Bold[41a], A.S. Boldyrev[101], M. Bomben[83], M. Bona[79], M. Boonekamp[138], A. Borisov[132],
G. Borissov[75], J. Bortfeldt[32], D. Bortoletto[122], V. Bortolotto[62a,62b,62c], K. Bos[109], D. Boscherini[22a],
M. Bosman[13], J.D. Bossio Sola[29], J. Boudreau[127], J. Bouffard[2], E.V. Bouhova-Thacker[75],
D. Boumediene[37], C. Bourdarios[119], S.K. Boutle[56], A. Boveia[32], J. Boyd[32], I.R. Boyko[68], J. Bracinik[19],
A. Brandt[8], G. Brandt[57], O. Brandt[60a], U. Bratzler[158], B. Brau[89], J.E. Brau[118], W.D. Breaden Madden[56],
K. Brendlinger[124], A.J. Brennan[91], L. Brenner[109], R. Brenner[168], S. Bressler[175], T.M. Bristow[49],
D. Britton[56], D. Britzger[45], F.M. Brochu[30], I. Brock[23], R. Brock[93], G. Brooijmans[38], T. Brooks[80],
W.K. Brooks[34b], J. Brosamer[16], E. Brost[110], J.H Broughton[19], P.A. Bruckman de Renstrom[42],
D. Bruncko[146b], R. Bruneliere[51], A. Bruni[22a], G. Bruni[22a], L.S. Bruni[109], BH Brunt[30], M. Bruschi[22a],
N. Bruscino[23], P. Bryant[33], L. Bryngemark[84], T. Buanes[15], Q. Buat[144], P. Buchholz[143], A.G. Buckley[56],
I.A. Budagov[68], F. Buehrer[51], M.K. Bugge[121], O. Bulekov[100], D. Bullock[8], H. Burckhart[32], S. Burdin[77],
C.D. Burgard[51], A.M. Burger[5], B. Burghgrave[110], K. Burka[42], S. Burke[133], I. Burmeister[46],
J.T.P. Burr[122], E. Busato[37], D. Büscher[51], V. Büscher[86], P. Bussey[56], J.M. Butler[24], C.M. Buttar[56],
J.M. Butterworth[81], P. Butti[109], W. Buttinger[27], A. Buzatu[56], A.R. Buzykaev[111,c], S. Cabrera Urbán[170],
D. Caforio[130], V.M. Cairo[40a,40b], O. Cakir[4a], N. Calace[52], P. Calafiura[16], A. Calandri[88], G. Calderini[83],
P. Calfayan[64], G. Callea[40a,40b], L.P. Caloba[26a], S. Calvente Lopez[85], D. Calvet[37], S. Calvet[37],
T.P. Calvet[88], R. Camacho Toro[33], S. Camarda[32], P. Camarri[135a,135b], D. Cameron[121],
R. Caminal Armadans[169], C. Camincher[58], S. Campana[32], M. Campanelli[81], A. Camplani[94a,94b],
A. Campoverde[143], V. Canale[106a,106b], A. Canepa[163a], M. Cano Bret[36c], J. Cantero[116], T. Cao[155],
M.D.M. Capeans Garrido[32], I. Caprini[28b], M. Caprini[28b], M. Capua[40a,40b], R.M. Carbone[38],
R. Cardarelli[135a], F. Cardillo[51], I. Carli[131], T. Carli[32], G. Carlino[106a], B.T. Carlson[127],
L. Carminati[94a,94b], R.M.D. Carney[148a,148b], S. Caron[108], E. Carquin[34b], G.D. Carrillo-Montoya[32],
J.R. Carter[30], J. Carvalho[128a,128c], D. Casadei[19], M.P. Casado[13,i], M. Casolino[13], D.W. Casper[166],
E. Castaneda-Miranda[147a], R. Castelijn[109], A. Castelli[109], V. Castillo Gimenez[170], N.F. Castro[128a,j],
A. Catinaccio[32], J.R. Catmore[121], A. Cattai[32], J. Caudron[23], V. Cavaliere[169], E. Cavallaro[13],
D. Cavalli[94a], M. Cavalli-Sforza[13], V. Cavasinni[126a,126b], F. Ceradini[136a,136b], L. Cerda Alberich[170],
A.S. Cerqueira[26b], A. Cerri[151], L. Cerrito[135a,135b], F. Cerutti[16], A. Cervelli[18], S.A. Cetin[20d],
A. Chafaq[137a], D. Chakraborty[110], S.K. Chan[59], Y.L. Chan[62a], P. Chang[169], J.D. Chapman[30],
D.G. Charlton[19], A. Chatterjee[52], C.C. Chau[161], C.A. Chavez Barajas[151], S. Che[113],
S. Cheatham[167a,167c], A. Chegwidden[93], S. Chekanov[6], S.V. Chekulaev[163a], G.A. Chelkov[68,k],
M.A. Chelstowska[92], C. Chen[67], H. Chen[27], S. Chen[35b], S. Chen[157], X. Chen[35c,l], Y. Chen[70],
H.C. Cheng[92], H.J. Cheng[35a], Y. Cheng[33], A. Cheplakov[68], E. Cheremushkina[132],
R. Cherkaoui El Moursli[137e], V. Chernyatin[27,*], E. Cheu[7], L. Chevalier[138], V. Chiarella[50],
G. Chiarelli[126a,126b], G. Chiodini[76a], A.S. Chisholm[32], A. Chitan[28b], M.V. Chizhov[68], K. Choi[64],
A.R. Chomont[37], S. Chouridou[9], B.K.B. Chow[102], V. Christodoulou[81], D. Chromek-Burckhart[32],
J. Chudoba[129], A.J. Chuinard[90], J.J. Chwastowski[42], L. Chytka[117], G. Ciapetti[134a,134b], A.K. Ciftci[4a],
D. Cinca[46], V. Cindro[78], I.A. Cioara[23], C. Ciocca[22a,22b], A. Ciocio[16], F. Cirotto[106a,106b], Z.H. Citron[175],
M. Citterio[94a], M. Ciubancan[28b], A. Clark[52], B.L. Clark[59], M.R. Clark[38], P.J. Clark[49], R.N. Clarke[16],
C. Clement[148a,148b], Y. Coadou[88], M. Cobal[167a,167c], A. Coccaro[52], J. Cochran[67], L. Colasurdo[108],
B. Cole[38], A.P. Colijn[109], J. Collot[58], T. Colombo[166], S. Comotti[94a,94b], P. Conde Muiño[128a,128b],
E. Coniavitis[51], S.H. Connell[147b], I.A. Connelly[80], V. Consorti[51], S. Constantinescu[28b], G. Conti[32],
F. Conventi[106a,m], M. Cooke[16], B.D. Cooper[81], A.M. Cooper-Sarkar[122], F. Cormier[171],
K.J.R. Cormier[161], T. Cornelissen[178], M. Corradi[134a,134b], F. Corriveau[90,n], A. Cortes-Gonzalez[32],
G. Cortiana[103], G. Costa[94a], M.J. Costa[170], D. Costanzo[141], G. Cottin[30], G. Cowan[80], B.E. Cox[87],
K. Cranmer[112], S.J. Crawley[56], G. Cree[31], S. Crépé-Renaudin[58], F. Crescioli[83], W.A. Cribbs[148a,148b],

44

M. Crispin Ortuzar[122], M. Cristinziani[23], V. Croft[108], G. Crosetti[40a,40b], A. Cueto[85],
T. Cuhadar Donszelmann[141], J. Cummings[179], M. Curatolo[50], J. Cúth[86], H. Czirr[143], P. Czodrowski[3],
G. D'amen[22a,22b], S. D'Auria[56], M. D'Onofrio[77], M.J. Da Cunha Sargedas De Sousa[128a,128b],
C. Da Via[87], W. Dabrowski[41a], T. Dado[146a], T. Dai[92], O. Dale[15], F. Dallaire[97], C. Dallapiccola[89],
M. Dam[39], J.R. Dandoy[33], N.P. Dang[51], A.C. Daniells[19], N.S. Dann[87], M. Danninger[171],
M. Dano Hoffmann[138], V. Dao[51], G. Darbo[53a], S. Darmora[8], J. Dassoulas[3], A. Dattagupta[118],
W. Davey[23], C. David[45], T. Davidek[131], M. Davies[155], P. Davison[81], E. Dawe[91], I. Dawson[141], K. De[8],
R. de Asmundis[106a], A. De Benedetti[115], S. De Castro[22a,22b], S. De Cecco[83], N. De Groot[108],
P. de Jong[109], H. De la Torre[93], F. De Lorenzi[67], A. De Maria[57], D. De Pedis[134a], A. De Salvo[134a],
U. De Sanctis[151], A. De Santo[151], J.B. De Vivie De Regie[119], W.J. Dearnaley[75], R. Debbe[27],
C. Debenedetti[139], D.V. Dedovich[68], N. Dehghanian[3], I. Deigaard[109], M. Del Gaudio[40a,40b],
J. Del Peso[85], T. Del Prete[126a,126b], D. Delgove[119], F. Deliot[138], C.M. Delitzsch[52], A. Dell'Acqua[32],
L. Dell'Asta[24], M. Dell'Orso[126a,126b], M. Della Pietra[106a,m], D. della Volpe[52], M. Delmastro[5],
P.A. Delsart[58], D.A. DeMarco[161], S. Demers[179], M. Demichev[68], A. Demilly[83], S.P. Denisov[132],
D. Denysiuk[138], D. Derendarz[42], J.E. Derkaoui[137d], F. Derue[83], P. Dervan[77], K. Desch[23], C. Deterre[45],
K. Dette[46], P.O. Deviveiros[32], A. Dewhurst[133], S. Dhaliwal[25], A. Di Ciaccio[135a,135b], L. Di Ciaccio[5],
W.K. Di Clemente[124], C. Di Donato[106a,106b], A. Di Girolamo[32], B. Di Girolamo[32], B. Di Micco[136a,136b],
R. Di Nardo[32], K.F. Di Petrillo[59], A. Di Simone[51], R. Di Sipio[161], D. Di Valentino[31], C. Diaconu[88],
M. Diamond[161], F.A. Dias[49], M.A. Diaz[34a], E.B. Diehl[92], J. Dietrich[17], S. Díez Cornell[45],
A. Dimitrievska[14], J. Dingfelder[23], P. Dita[28b], S. Dita[28b], F. Dittus[32], F. Djama[88], T. Djobava[54b],
J.I. Djuvsland[60a], M.A.B. do Vale[26c], D. Dobos[32], M. Dobre[28b], C. Doglioni[84], J. Dolejsi[131],
Z. Dolezal[131], M. Donadelli[26d], S. Donati[126a,126b], P. Dondero[123a,123b], J. Donini[37], J. Dopke[133],
A. Doria[106a], M.T. Dova[74], A.T. Doyle[56], E. Drechsler[57], M. Dris[10], Y. Du[36b], J. Duarte-Campderros[155],
E. Duchovni[175], G. Duckeck[102], O.A. Ducu[97,o], D. Duda[109], A. Dudarev[32], A.Chr. Dudder[86],
E.M. Duffield[16], L. Duflot[119], M. Dührssen[32], M. Dumancic[175], A.K. Duncan[56], M. Dunford[60a],
H. Duran Yildiz[4a], M. Düren[55], A. Durglishvili[54b], D. Duschinger[47], B. Dutta[45], M. Dyndal[45],
C. Eckardt[45], K.M. Ecker[103], R.C. Edgar[92], N.C. Edwards[49], T. Eifert[32], G. Eigen[15], K. Einsweiler[16],
T. Ekelof[168], M. El Kacimi[137c], V. Ellajosyula[88], M. Ellert[168], S. Elles[5], F. Ellinghaus[178], A.A. Elliot[172],
N. Ellis[32], J. Elmsheuser[27], M. Elsing[32], D. Emeliyanov[133], Y. Enari[157], O.C. Endner[86], J.S. Ennis[173],
J. Erdmann[46], A. Ereditato[18], G. Ernis[178], J. Ernst[2], M. Ernst[27], S. Errede[169], E. Ertel[86], M. Escalier[119],
H. Esch[46], C. Escobar[127], B. Esposito[50], A.I. Etienvre[138], E. Etzion[155], H. Evans[64], A. Ezhilov[125],
M. Ezzi[137e], F. Fabbri[22a,22b], L. Fabbri[22a,22b], G. Facini[33], R.M. Fakhrutdinov[132], S. Falciano[134a],
R.J. Falla[81], J. Faltova[32], Y. Fang[35a], M. Fanti[94a,94b], A. Farbin[8], A. Farilla[136a], C. Farina[127],
E.M. Farina[123a,123b], T. Farooque[13], S. Farrell[16], S.M. Farrington[173], P. Farthouat[32], F. Fassi[137e],
P. Fassnacht[32], D. Fassouliotis[9], M. Faucci Giannelli[80], A. Favareto[53a,53b], W.J. Fawcett[122], L. Fayard[119],
O.L. Fedin[125,p], W. Fedorko[171], S. Feigl[121], L. Feligioni[88], C. Feng[36b], E.J. Feng[32], H. Feng[92],
A.B. Fenyuk[132], L. Feremenga[8], P. Fernandez Martinez[170], S. Fernandez Perez[13], J. Ferrando[45],
A. Ferrari[168], P. Ferrari[109], R. Ferrari[123a], D.E. Ferreira de Lima[60b], A. Ferrer[170], D. Ferrere[52],
C. Ferretti[92], F. Fiedler[86], A. Filipčič[78], M. Filipuzzi[45], F. Filthaut[108], M. Fincke-Keeler[172],
K.D. Finelli[152], M.C.N. Fiolhais[128a,128c], L. Fiorini[170], A. Fischer[2], C. Fischer[13], J. Fischer[178],
W.C. Fisher[93], N. Flaschel[45], I. Fleck[143], P. Fleischmann[92], G.T. Fletcher[141], R.R.M. Fletcher[124],
T. Flick[178], B.M. Flierl[102], L.R. Flores Castillo[62a], M.J. Flowerdew[103], G.T. Forcolin[87], A. Formica[138],
A. Forti[87], A.G. Foster[19], D. Fournier[119], H. Fox[75], S. Fracchia[13], P. Francavilla[83], M. Franchini[22a,22b],
D. Francis[32], L. Franconi[121], M. Franklin[59], M. Frate[166], M. Fraternali[123a,123b], D. Freeborn[81],
S.M. Fressard-Batraneanu[32], F. Friedrich[47], D. Froidevaux[32], J.A. Frost[122], C. Fukunaga[158],
E. Fullana Torregrosa[86], T. Fusayasu[104], J. Fuster[170], C. Gabaldon[58], O. Gabizon[154], A. Gabrielli[22a,22b],
A. Gabrielli[16], G.P. Gach[41a], S. Gadatsch[32], G. Gagliardi[53a,53b], L.G. Gagnon[97], P. Gagnon[64],

45

C. Galea[108], B. Galhardo[128a,128c], E.J. Gallas[122], B.J. Gallop[133], P. Gallus[130], G. Galster[39], K.K. Gan[113],
S. Ganguly[37], J. Gao[36a], Y. Gao[49], Y.S. Gao[145,g], F.M. Garay Walls[49], C. García[170],
J.E. García Navarro[170], M. Garcia-Sciveres[16], R.W. Gardner[33], N. Garelli[145], V. Garonne[121],
A. Gascon Bravo[45], K. Gasnikova[45], C. Gatti[50], A. Gaudiello[53a,53b], G. Gaudio[123a], L. Gauthier[97],
I.L. Gavrilenko[98], C. Gay[171], G. Gaycken[23], E.N. Gazis[10], Z. Gecse[171], C.N.P. Gee[133],
Ch. Geich-Gimbel[23], M. Geisen[86], M.P. Geisler[60a], K. Gellerstedt[148a,148b], C. Gemme[53a],
M.H. Genest[58], C. Geng[36a,q], S. Gentile[134a,134b], C. Gentsos[156], S. George[80], D. Gerbaudo[13],
A. Gershon[155], S. Ghasemi[143], M. Ghneimat[23], B. Giacobbe[22a], S. Giagu[134a,134b], P. Giannetti[126a,126b],
S.M. Gibson[80], M. Gignac[171], M. Gilchriese[16], T.P.S. Gillam[30], D. Gillberg[31], G. Gilles[178],
D.M. Gingrich[3,d], N. Giokaris[9,*], M.P. Giordani[167a,167c], F.M. Giorgi[22a], P.F. Giraud[138], P. Giromini[59],
D. Giugni[94a], F. Giuli[122], C. Giuliani[103], M. Giulini[60b], B.K. Gjelsten[121], S. Gkaitatzis[156], I. Gkialas[9],
E.L. Gkougkousis[139], L.K. Gladilin[101], C. Glasman[85], J. Glatzer[13], P.C.F. Glaysher[49], A. Glazov[45],
M. Goblirsch-Kolb[25], J. Godlewski[42], S. Goldfarb[91], T. Golling[52], D. Golubkov[132],
A. Gomes[128a,128b,128d], R. Gonçalo[128a], J. Goncalves Pinto Firmino Da Costa[138], G. Gonella[51],
L. Gonella[19], A. Gongadze[68], S. González de la Hoz[170], S. Gonzalez-Sevilla[52], L. Goossens[32],
P.A. Gorbounov[99], H.A. Gordon[27], I. Gorelov[107], B. Gorini[32], E. Gorini[76a,76b], A. Gorišek[78],
A.T. Goshaw[48], C. Gössling[46], M.I. Gostkin[68], C.R. Goudet[119], D. Goujdami[137c], A.G. Goussiou[140],
N. Govender[147b,r], E. Gozani[154], L. Graber[57], I. Grabowska-Bold[41a], P.O.J. Gradin[58],
P. Grafström[22a,22b], J. Gramling[52], E. Gramstad[121], S. Grancagnolo[17], V. Gratchev[125], P.M. Gravila[28e],
H.M. Gray[32], E. Graziani[136a], Z.D. Greenwood[82,s], C. Grefe[23], K. Gregersen[81], I.M. Gregor[45],
P. Grenier[145], K. Grevtsov[5], J. Griffiths[8], A.A. Grillo[139], K. Grimm[75], S. Grinstein[13,t], Ph. Gris[37],
J.-F. Grivaz[119], S. Groh[86], E. Gross[175], J. Grosse-Knetter[57], G.C. Grossi[82], Z.J. Grout[81], L. Guan[92],
W. Guan[176], J. Guenther[65], F. Guescini[52], D. Guest[166], O. Gueta[155], B. Gui[113], E. Guido[53a,53b],
T. Guillemin[5], S. Guindon[2], U. Gul[56], C. Gumpert[32], J. Guo[36c], W. Guo[92], Y. Guo[36a,q], R. Gupta[43],
S. Gupta[122], G. Gustavino[134a,134b], P. Gutierrez[115], N.G. Gutierrez Ortiz[81], C. Gutschow[81], C. Guyot[138],
C. Gwenlan[122], C.B. Gwilliam[77], A. Haas[112], C. Haber[16], H.K. Hadavand[8], N. Haddad[137e], A. Hadef[88],
S. Hageböck[23], M. Hagihara[164], Z. Hajduk[42], H. Hakobyan[180,*], M. Haleem[45], J. Haley[116],
G. Halladjian[93], G.D. Hallewell[88], K. Hamacher[178], P. Hamal[117], K. Hamano[172], A. Hamilton[147a],
G.N. Hamity[141], P.G. Hamnett[45], L. Han[36a], S. Han[35a], K. Hanagaki[69,u], K. Hanawa[157], M. Hance[139],
B. Haney[124], P. Hanke[60a], R. Hanna[138], J.B. Hansen[39], J.D. Hansen[39], M.C. Hansen[23], P.H. Hansen[39],
K. Hara[164], A.S. Hard[176], T. Harenberg[178], F. Hariri[119], S. Harkusha[95], R.D. Harrington[49],
P.F. Harrison[173], F. Hartjes[109], N.M. Hartmann[102], M. Hasegawa[70], Y. Hasegawa[142], A. Hasib[115],
S. Hassani[138], S. Haug[18], R. Hauser[93], L. Hauswald[47], M. Havranek[129], C.M. Hawkes[19],
R.J. Hawkings[32], D. Hayakawa[159], D. Hayden[93], C.P. Hays[122], J.M. Hays[79], H.S. Hayward[77],
S.J. Haywood[133], S.J. Head[19], T. Heck[86], V. Hedberg[84], L. Heelan[8], S. Heim[124], T. Heim[16],
B. Heinemann[45,v], J.J. Heinrich[102], L. Heinrich[112], C. Heinz[55], J. Hejbal[129], L. Helary[32],
S. Hellman[148a,148b], C. Helsens[32], J. Henderson[122], R.C.W. Henderson[75], Y. Heng[176], S. Henkelmann[171],
A.M. Henriques Correia[32], S. Henrot-Versille[119], G.H. Herbert[17], H. Herde[25], V. Herget[177],
Y. Hernández Jiménez[147c], G. Herten[51], R. Hertenberger[102], L. Hervas[32], G.G. Hesketh[81],
N.P. Hessey[109], J.W. Hetherly[43], E. Higón-Rodriguez[170], E. Hill[172], J.C. Hill[30], K.H. Hiller[45],
S.J. Hillier[19], I. Hinchliffe[16], E. Hines[124], M. Hirose[51], D. Hirschbuehl[178], O. Hladik[129], X. Hoad[49],
J. Hobbs[150], N. Hod[163a], M.C. Hodgkinson[141], P. Hodgson[141], A. Hoecker[32], M.R. Hoeferkamp[107],
F. Hoenig[102], D. Hohn[23], T.R. Holmes[16], M. Homann[46], S. Honda[164], T. Honda[69], T.M. Hong[127],
B.H. Hooberman[169], W.H. Hopkins[118], Y. Horii[105], A.J. Horton[144], J-Y. Hostachy[58], S. Hou[153],
A. Hoummada[137a], J. Howarth[45], J. Hoya[74], M. Hrabovsky[117], I. Hristova[17], J. Hrivnac[119], T. Hryn'ova[5],
A. Hrynevich[96], P.J. Hsu[63], S.-C. Hsu[140], Q. Hu[36a], S. Hu[36c], Y. Huang[45], Z. Hubacek[130], F. Hubaut[88],
F. Huegging[23], T.B. Huffman[122], E.W. Hughes[38], G. Hughes[75], M. Huhtinen[32], P. Huo[150],

46

N. Huseynov[68,b], J. Huston[93], J. Huth[59], G. Iacobucci[52], G. Iakovidis[27], I. Ibragimov[143],
L. Iconomidou-Fayard[119], E. Ideal[179], Z. Idrissi[137e], P. Iengo[32], O. Igonkina[109,w], T. Iizawa[174],
Y. Ikegami[69], M. Ikeno[69], Y. Ilchenko[11,x], D. Iliadis[156], N. Ilic[145], G. Introzzi[123a,123b], P. Ioannou[9,*],
M. Iodice[136a], K. Iordanidou[38], V. Ippolito[59], N. Ishijima[120], M. Ishino[157], M. Ishitsuka[159], C. Issever[122],
S. Istin[20a], F. Ito[164], J.M. Iturbe Ponce[87], R. Iuppa[162a,162b], H. Iwasaki[69], J.M. Izen[44], V. Izzo[106a],
S. Jabbar[3], B. Jackson[124], P. Jackson[1], V. Jain[2], K.B. Jakobi[86], K. Jakobs[51], S. Jakobsen[32],
T. Jakoubek[129], D.O. Jamin[116], D.K. Jana[82], R. Jansky[65], J. Janssen[23], M. Janus[57], P.A. Janus[41a],
G. Jarlskog[84], N. Javadov[68,b], T. Javůrek[51], M. Javurkova[51], F. Jeanneau[138], L. Jeanty[16], J. Jejelava[54a,y],
G.-Y. Jeng[152], P. Jenni[51,z], C. Jeske[173], S. Jézéquel[5], H. Ji[176], J. Jia[150], H. Jiang[67], Y. Jiang[36a],
Z. Jiang[145], S. Jiggins[81], J. Jimenez Pena[170], S. Jin[35a], A. Jinaru[28b], O. Jinnouchi[159], H. Jivan[147c],
P. Johansson[141], K.A. Johns[7], C.A. Johnson[64], W.J. Johnson[140], K. Jon-And[148a,148b], G. Jones[173],
R.W.L. Jones[75], S. Jones[7], T.J. Jones[77], J. Jongmanns[60a], P.M. Jorge[128a,128b], J. Jovicevic[163a], X. Ju[176],
A. Juste Rozas[13,t], M.K. Köhler[175], A. Kaczmarska[42], M. Kado[119], H. Kagan[113], M. Kagan[145],
S.J. Kahn[88], T. Kaji[174], E. Kajomovitz[48], C.W. Kalderon[122], A. Kaluza[86], S. Kama[43],
A. Kamenshchikov[132], N. Kanaya[157], S. Kaneti[30], L. Kanjir[78], V.A. Kantserov[100], J. Kanzaki[69],
B. Kaplan[112], L.S. Kaplan[176], A. Kapliy[33], D. Kar[147c], K. Karakostas[10], A. Karamaoun[3],
N. Karastathis[10], M.J. Kareem[57], E. Karentzos[10], M. Karnevskiy[86], S.N. Karpov[68], Z.M. Karpova[68],
K. Karthik[112], V. Kartvelishvili[75], A.N. Karyukhin[132], K. Kasahara[164], L. Kashif[176], R.D. Kass[113],
A. Kastanas[149], Y. Kataoka[157], C. Kato[157], A. Katre[52], J. Katzy[45], K. Kawade[105], K. Kawagoe[73],
T. Kawamoto[157], G. Kawamura[57], V.F. Kazanin[111,c], R. Keeler[172], R. Kehoe[43], J.S. Keller[45],
J.J. Kempster[80], H. Keoshkerian[161], O. Kepka[129], B.P. Kerševan[78], S. Kersten[178], R.A. Keyes[90],
M. Khader[169], F. Khalil-zada[12], A. Khanov[116], A.G. Kharlamov[111,c], T. Kharlamova[111,c], T.J. Khoo[52],
V. Khovanskiy[99], E. Khramov[68], J. Khubua[54b,aa], S. Kido[70], C.R. Kilby[80], H.Y. Kim[8], S.H. Kim[164],
Y.K. Kim[33], N. Kimura[156], O.M. Kind[17], B.T. King[77], M. King[170], J. Kirk[133], A.E. Kiryunin[103],
T. Kishimoto[157], D. Kisielewska[41a], F. Kiss[51], K. Kiuchi[164], O. Kivernyk[138], E. Kladiva[146b],
M.H. Klein[38], M. Klein[77], U. Klein[77], K. Kleinknecht[86], P. Klimek[110], A. Klimentov[27],
R. Klingenberg[46], T. Klioutchnikova[32], E.-E. Kluge[60a], P. Kluit[109], S. Kluth[103], J. Knapik[42],
E. Kneringer[65], E.B.F.G. Knoops[88], A. Knue[103], A. Kobayashi[157], D. Kobayashi[159], T. Kobayashi[157],
M. Kobel[47], M. Kocian[145], P. Kodys[131], T. Koffas[31], E. Koffeman[109], N.M. Köhler[103], T. Koi[145],
H. Kolanoski[17], M. Kolb[60b], I. Koletsou[5], A.A. Komar[98,*], Y. Komori[157], T. Kondo[69],
N. Kondrashova[36c], K. Köneke[51], A.C. König[108], T. Kono[69,ab], R. Konoplich[112,ac], N. Konstantinidis[81],
R. Kopeliansky[64], S. Koperny[41a], A.K. Kopp[51], K. Korcyl[42], K. Kordas[156], A. Korn[81], A.A. Korol[111,c],
I. Korolkov[13], E.V. Korolkova[141], O. Kortner[103], S. Kortner[103], T. Kosek[131], V.V. Kostyukhin[23],
A. Kotwal[48], A. Koulouris[10], A. Kourkoumeli-Charalampidi[123a,123b], C. Kourkoumelis[9],
V. Kouskoura[27], A.B. Kowalewska[42], R. Kowalewski[172], T.Z. Kowalski[41a], C. Kozakai[157],
W. Kozanecki[138], A.S. Kozhin[132], V.A. Kramarenko[101], G. Kramberger[78], D. Krasnopevtsev[100],
M.W. Krasny[83], A. Krasznahorkay[32], A. Kravchenko[27], M. Kretz[60c], J. Kretzschmar[77], K. Kreutzfeldt[55],
P. Krieger[161], K. Krizka[33], K. Kroeninger[46], H. Kroha[103], J. Kroll[124], J. Kroseberg[23], J. Krstic[14],
U. Kruchonak[68], H. Krüger[23], N. Krumnack[67], M.C. Kruse[48], M. Kruskal[24], T. Kubota[91], H. Kucuk[81],
S. Kuday[4b], J.T. Kuechler[178], S. Kuehn[51], A. Kugel[60c], F. Kuger[177], T. Kuhl[45], V. Kukhtin[68],
R. Kukla[138], Y. Kulchitsky[95], S. Kuleshov[34b], M. Kuna[134a,134b], T. Kunigo[71], A. Kupco[129],
O. Kuprash[155], H. Kurashige[70], L.L. Kurchaninov[163a], Y.A. Kurochkin[95], M.G. Kurth[44], V. Kus[129],
E.S. Kuwertz[172], M. Kuze[159], J. Kvita[117], T. Kwan[172], D. Kyriazopoulos[141], A. La Rosa[103],
J.L. La Rosa Navarro[26d], L. La Rotonda[40a,40b], C. Lacasta[170], F. Lacava[134a,134b], J. Lacey[31], H. Lacker[17],
D. Lacour[83], E. Ladygin[68], R. Lafaye[5], B. Laforge[83], T. Lagouri[179], S. Lai[57], S. Lammers[64], W. Lampl[7],
E. Lançon[138], U. Landgraf[51], M.P.J. Landon[79], M.C. Lanfermann[52], V.S. Lang[60a], J.C. Lange[13],
A.J. Lankford[166], F. Lanni[27], K. Lantzsch[23], A. Lanza[123a], S. Laplace[83], C. Lapoire[32], J.F. Laporte[138],

47

T. Lari[94a], F. Lasagni Manghi[22a,22b], M. Lassnig[32], P. Laurelli[50], W. Lavrijsen[16], A.T. Law[139], P. Laycock[77], T. Lazovich[59], M. Lazzaroni[94a,94b], B. Le[91], O. Le Dortz[83], E. Le Guirriec[88], E.P. Le Quilleuc[138], M. LeBlanc[172], T. LeCompte[6], F. Ledroit-Guillon[58], C.A. Lee[27], S.C. Lee[153], L. Lee[1], B. Lefebvre[90], G. Lefebvre[83], M. Lefebvre[172], F. Legger[102], C. Leggett[16], A. Lehan[77], G. Lehmann Miotto[32], X. Lei[7], W.A. Leight[31], A.G. Leister[179], M.A.L. Leite[26d], R. Leitner[131], D. Lellouch[175], B. Lemmer[57], K.J.C. Leney[81], T. Lenz[23], B. Lenzi[32], R. Leone[7], S. Leone[126a,126b], C. Leonidopoulos[49], S. Leontsinis[10], G. Lerner[151], C. Leroy[97], A.A.J. Lesage[138], C.G. Lester[30], M. Levchenko[125], J. Levêque[5], D. Levin[92], L.J. Levinson[175], M. Levy[19], D. Lewis[79], M. Leyton[44], B. Li[36a,q], C. Li[36a], H. Li[150], L. Li[48], L. Li[36c], Q. Li[35a], S. Li[48], X. Li[87], Y. Li[143], Z. Liang[35a], B. Liberti[135a], A. Liblong[161], P. Lichard[32], K. Lie[169], J. Liebal[23], W. Liebig[15], A. Limosani[152], S.C. Lin[153,ad], T.H. Lin[86], B.E. Lindquist[150], A.E. Lionti[52], E. Lipeles[124], A. Lipniacka[15], M. Lisovyi[60b], T.M. Liss[169], A. Lister[171], A.M. Litke[139], B. Liu[153,ae], D. Liu[153], H. Liu[92], H. Liu[27], J. Liu[36b], J.B. Liu[36a], K. Liu[88], L. Liu[169], M. Liu[36a], Y.L. Liu[36a], Y. Liu[36a], M. Livan[123a,123b], A. Lleres[58], J. Llorente Merino[35a], S.L. Lloyd[79], F. Lo Sterzo[153], E.M. Lobodzinska[45], P. Loch[7], F.K. Loebinger[87], K.M. Loew[25], A. Loginov[179,*], T. Lohse[17], K. Lohwasser[45], M. Lokajicek[129], B.A. Long[24], J.D. Long[169], R.E. Long[75], L. Longo[76a,76b], K.A. Looper[113], J.A. Lopez[34b], D. Lopez Mateos[59], B. Lopez Paredes[141], I. Lopez Paz[13], A. Lopez Solis[83], J. Lorenz[102], N. Lorenzo Martinez[64], M. Losada[21], P.J. Lösel[102], X. Lou[35a], A. Lounis[119], J. Love[6], P.A. Love[75], H. Lu[62a], N. Lu[92], H.J. Lubatti[140], C. Luci[134a,134b], A. Lucotte[58], C. Luedtke[51], F. Luehring[64], W. Lukas[65], L. Luminari[134a], O. Lundberg[148a,148b], B. Lund-Jensen[149], P.M. Luzi[83], D. Lynn[27], R. Lysak[129], E. Lytken[84], V. Lyubushkin[68], H. Ma[27], L.L. Ma[36b], Y. Ma[36b], G. Maccarrone[50], A. Macchiolo[103], C.M. Macdonald[141], B. Maček[78], J. Machado Miguens[124,128b], D. Madaffari[88], R. Madar[37], H.J. Maddocks[168], W.F. Mader[47], A. Madsen[45], J. Maeda[70], S. Maeland[15], T. Maeno[27], A. Maevskiy[101], E. Magradze[57], J. Mahlstedt[109], C. Maiani[119], C. Maidantchik[26a], A.A. Maier[103], T. Maier[102], A. Maio[128a,128b,128d], S. Majewski[118], Y. Makida[69], N. Makovec[119], B. Malaescu[83], Pa. Malecki[42], V.P. Maleev[125], F. Malek[58], U. Mallik[66], D. Malon[6], C. Malone[30], S. Maltezos[10], S. Malyukov[32], J. Mamuzic[170], G. Mancini[50], L. Mandelli[94a], I. Mandić[78], J. Maneira[128a,128b], L. Manhaes de Andrade Filho[26b], J. Manjarres Ramos[163b], A. Mann[102], A. Manousos[32], B. Mansoulie[138], J.D. Mansour[35a], R. Mantifel[90], M. Mantoani[57], S. Manzoni[94a,94b], L. Mapelli[32], G. Marceca[29], L. March[52], G. Marchiori[83], M. Marcisovsky[129], M. Marjanovic[14], D.E. Marley[92], F. Marroquim[26a], S.P. Marsden[87], Z. Marshall[16], S. Marti-Garcia[170], B. Martin[93], T.A. Martin[173], V.J. Martin[49], B. Martin dit Latour[15], M. Martinez[13,t], V.I. Martinez Outschoorn[169], S. Martin-Haugh[133], V.S. Martoiu[28b], A.C. Martyniuk[81], A. Marzin[32], L. Masetti[86], T. Mashimo[157], R. Mashinistov[98], J. Masik[87], A.L. Maslennikov[111,c], I. Massa[22a,22b], L. Massa[22a,22b], P. Mastrandrea[5], A. Mastroberardino[40a,40b], T. Masubuchi[157], P. Mättig[178], J. Mattmann[86], J. Maurer[28b], S.J. Maxfield[77], D.A. Maximov[111,c], R. Mazini[153], I. Maznas[156], S.M. Mazza[94a,94b], N.C. Mc Fadden[107], G. Mc Goldrick[161], S.P. Mc Kee[92], A. McCarn[92], R.L. McCarthy[150], T.G. McCarthy[103], L.I. McClymont[81], E.F. McDonald[91], J.A. Mcfayden[81], G. Mchedlidze[57], S.J. McMahon[133], R.A. McPherson[172,n], M. Medinnis[45], S. Meehan[140], S. Mehlhase[102], A. Mehta[77], K. Meier[60a], C. Meineck[102], B. Meirose[44], D. Melini[170,af], B.R. Mellado Garcia[147c], M. Melo[146a], F. Meloni[18], S.B. Menary[87], L. Meng[77], X.T. Meng[92], A. Mengarelli[22a,22b], S. Menke[103], E. Meoni[165], S. Mergelmeyer[17], P. Mermod[52], L. Merola[106a,106b], C. Meroni[94a], F.S. Merritt[33], A. Messina[134a,134b], J. Metcalfe[6], A.S. Mete[166], C. Meyer[86], C. Meyer[124], J-P. Meyer[138], J. Meyer[109], H. Meyer Zu Theenhausen[60a], F. Miano[151], R.P. Middleton[133], S. Miglioranzi[53a,53b], L. Mijović[49], G. Mikenberg[175], M. Mikestikova[129], M. Mikuž[78], M. Milesi[91], A. Milic[27], D.W. Miller[33], C. Mills[49], A. Milov[175], D.A. Milstead[148a,148b], A.A. Minaenko[132], Y. Minami[157], I.A. Minashvili[68], A.I. Mincer[112], B. Mindur[41a], M. Mineev[68], Y. Minegishi[157], Y. Ming[176], L.M. Mir[13], K.P. Mistry[124], T. Mitani[174],

J. Mitrevski[102], V.A. Mitsou[170], A. Miucci[18], P.S. Miyagawa[141], A. Mizukami[69], J.U. Mjörnmark[84],
M. Mlynarikova[131], T. Moa[148a,148b], K. Mochizuki[97], P. Mogg[51], S. Mohapatra[38], S. Molander[148a,148b],
R. Moles-Valls[23], R. Monden[71], M.C. Mondragon[93], K. Mönig[45], J. Monk[39], E. Monnier[88],
A. Montalbano[150], J. Montejo Berlingen[32], F. Monticelli[74], S. Monzani[94a,94b], R.W. Moore[3],
N. Morange[119], D. Moreno[21], M. Moreno Llácer[57], P. Morettini[53a], S. Morgenstern[32], D. Mori[144],
T. Mori[157], M. Morii[59], M. Morinaga[157], V. Morisbak[121], S. Moritz[86], A.K. Morley[152], G. Mornacchi[32],
J.D. Morris[79], L. Morvaj[150], P. Moschovakos[10], M. Mosidze[54b], H.J. Moss[141], J. Moss[145,ag],
K. Motohashi[159], R. Mount[145], E. Mountricha[27], E.J.W. Moyse[89], S. Muanza[88], R.D. Mudd[19],
F. Mueller[103], J. Mueller[127], R.S.P. Mueller[102], T. Mueller[30], D. Muenstermann[75], P. Mullen[56],
G.A. Mullier[18], F.J. Munoz Sanchez[87], J.A. Murillo Quijada[19], W.J. Murray[173,133], H. Musheghyan[57],
M. Muškinja[78], A.G. Myagkov[132,ah], M. Myska[130], B.P. Nachman[16], O. Nackenhorst[52], K. Nagai[122],
R. Nagai[69,ab], K. Nagano[69], Y. Nagasaka[61], K. Nagata[164], M. Nagel[51], E. Nagy[88], A.M. Nairz[32],
Y. Nakahama[105], K. Nakamura[69], T. Nakamura[157], I. Nakano[114], R.F. Naranjo Garcia[45], R. Narayan[11],
D.I. Narrias Villar[60a], I. Naryshkin[125], T. Naumann[45], G. Navarro[21], R. Nayyar[7], H.A. Neal[92],
P.Yu. Nechaeva[98], T.J. Neep[87], A. Negri[123a,123b], M. Negrini[22a], S. Nektarijevic[108], C. Nellist[119],
A. Nelson[166], S. Nemecek[129], P. Nemethy[112], A.A. Nepomuceno[26a], M. Nessi[32,ai], M.S. Neubauer[169],
M. Neumann[178], R.M. Neves[112], P. Nevski[27], P.R. Newman[19], D.H. Nguyen[6], T. Nguyen Manh[97],
R.B. Nickerson[122], R. Nicolaidou[138], J. Nielsen[139], V. Nikolaenko[132,ah], I. Nikolic-Audit[83],
K. Nikolopoulos[19], J.K. Nilsen[121], P. Nilsson[27], Y. Ninomiya[157], A. Nisati[134a], R. Nisius[103], T. Nobe[157],
M. Nomachi[120], I. Nomidis[31], T. Nooney[79], S. Norberg[115], M. Nordberg[32], N. Norjoharuddeen[122],
O. Novgorodova[47], S. Nowak[103], M. Nozaki[69], L. Nozka[117], K. Ntekas[166], E. Nurse[81], F. Nuti[91],
F. O'grady[7], D.C. O'Neil[144], A.A. O'Rourke[45], V. O'Shea[56], F.G. Oakham[31,d], H. Oberlack[103],
T. Obermann[23], J. Ocariz[83], A. Ochi[70], I. Ochoa[38], J.P. Ochoa-Ricoux[34a], S. Oda[73], S. Odaka[69],
H. Ogren[64], A. Oh[87], S.H. Oh[48], C.C. Ohm[16], H. Ohman[168], H. Oide[53a,53b], H. Okawa[164],
Y. Okumura[157], T. Okuyama[69], A. Olariu[28b], L.F. Oleiro Seabra[128a], S.A. Olivares Pino[49],
D. Oliveira Damazio[27], A. Olszewski[42], J. Olszowska[42], A. Onofre[128a,128e], K. Onogi[105],
P.U.E. Onyisi[11,x], M.J. Oreglia[33], Y. Oren[155], D. Orestano[136a,136b], N. Orlando[62b], R.S. Orr[161],
B. Osculati[53a,53b,*], R. Ospanov[87], G. Otero y Garzon[29], H. Otono[73], M. Ouchrif[137d], F. Ould-Saada[121],
A. Ouraou[138], K.P. Oussoren[109], Q. Ouyang[35a], M. Owen[56], R.E. Owen[19], V.E. Ozcan[20a], N. Ozturk[8],
K. Pachal[144], A. Pacheco Pages[13], L. Pacheco Rodriguez[138], C. Padilla Aranda[13], S. Pagan Griso[16],
M. Paganini[179], F. Paige[27], P. Pais[89], K. Pajchel[121], G. Palacino[64], S. Palazzo[40a,40b], S. Palestini[32],
M. Palka[41b], D. Pallin[37], E.St. Panagiotopoulou[10], I. Panagoulias[10], C.E. Pandini[83],
J.G. Panduro Vazquez[80], P. Pani[148a,148b], S. Panitkin[27], D. Pantea[28b], L. Paolozzi[52],
Th.D. Papadopoulou[10], K. Papageorgiou[9], A. Paramonov[6], D. Paredes Hernandez[179], A.J. Parker[75],
M.A. Parker[30], K.A. Parker[141], F. Parodi[53a,53b], J.A. Parsons[38], U. Parzefall[51], V.R. Pascuzzi[161],
E. Pasqualucci[134a], S. Passaggio[53a], Fr. Pastore[80], G. Pásztor[31,aj], S. Pataraia[178], J.R. Pater[87], T. Pauly[32],
J. Pearce[172], B. Pearson[115], L.E. Pedersen[39], M. Pedersen[121], S. Pedraza Lopez[170], R. Pedro[128a,128b],
S.V. Peleganchuk[111,c], O. Penc[129], C. Peng[35a], H. Peng[36a], J. Penwell[64], B.S. Peralva[26b],
M.M. Perego[138], D.V. Perepelitsa[27], E. Perez Codina[163a], L. Perini[94a,94b], H. Pernegger[32],
S. Perrella[106a,106b], R. Peschke[45], V.D. Peshekhonov[68], K. Peters[45], R.F.Y. Peters[87], B.A. Petersen[32],
T.C. Petersen[39], E. Petit[58], A. Petridis[1], C. Petridou[156], P. Petroff[119], E. Petrolo[134a], M. Petrov[122],
F. Petrucci[136a,136b], N.E. Pettersson[89], A. Peyaud[138], R. Pezoa[34b], P.W. Phillips[133], G. Piacquadio[145,ak],
E. Pianori[173], A. Picazio[89], E. Piccaro[79], M. Piccinini[22a,22b], M.A. Pickering[122], R. Piegaia[29],
J.E. Pilcher[33], A.D. Pilkington[87], A.W.J. Pin[87], M. Pinamonti[167a,167c,al], J.L. Pinfold[3], A. Pingel[39],
S. Pires[83], H. Pirumov[45], M. Pitt[175], L. Plazak[146a], M.-A. Pleier[27], V. Pleskot[86], E. Plotnikova[68],
D. Pluth[67], R. Poettgen[148a,148b], L. Poggioli[119], D. Pohl[23], G. Polesello[123a], A. Poley[45],
A. Policicchio[40a,40b], R. Polifka[161], A. Polini[22a], C.S. Pollard[56], V. Polychronakos[27], K. Pommès[32],

49

L. Pontecorvo[134a], B.G. Pope[93], G.A. Popeneciu[28c], A. Poppleton[32], S. Pospisil[130], K. Potamianos[16], I.N. Potrap[68], C.J. Potter[30], C.T. Potter[118], G. Poulard[32], J. Poveda[32], V. Pozdnyakov[68], M.E. Pozo Astigarraga[32], P. Pralavorio[88], A. Pranko[16], S. Prell[67], D. Price[87], L.E. Price[6], M. Primavera[76a], S. Prince[90], K. Prokofiev[62c], F. Prokoshin[34b], S. Protopopescu[27], J. Proudfoot[6], M. Przybycien[41a], D. Puddu[136a,136b], M. Purohit[27,am], P. Puzo[119], J. Qian[92], G. Qin[56], Y. Qin[87], A. Quadt[57], W.B. Quayle[167a,167b], M. Queitsch-Maitland[45], D. Quilty[56], S. Raddum[121], V. Radeka[27], V. Radescu[122], S.K. Radhakrishnan[150], P. Radloff[118], P. Rados[91], F. Ragusa[94a,94b], G. Rahal[181], J.A. Raine[87], S. Rajagopalan[27], M. Rammensee[32], C. Rangel-Smith[168], M.G. Ratti[94a,94b], D.M. Rauch[45], F. Rauscher[102], S. Rave[86], T. Ravenscroft[56], I. Ravinovich[175], M. Raymond[32], A.L. Read[121], N.P. Readioff[77], M. Reale[76a,76b], D.M. Rebuzzi[123a,123b], A. Redelbach[177], G. Redlinger[27], R. Reece[139], R.G. Reed[147c], K. Reeves[44], L. Rehnisch[17], J. Reichert[124], A. Reiss[86], C. Rembser[32], H. Ren[35a], M. Rescigno[134a], S. Resconi[94a], E.D. Resseguie[124], O.L. Rezanova[111,c], P. Reznicek[131], R. Rezvani[97], R. Richter[103], S. Richter[81], E. Richter-Was[41b], O. Ricken[23], M. Ridel[83], P. Rieck[103], C.J. Riegel[178], J. Rieger[57], O. Rifki[115], M. Rijssenbeek[150], A. Rimoldi[123a,123b], M. Rimoldi[18], L. Rinaldi[22a], B. Ristić[52], E. Ritsch[32], I. Riu[13], F. Rizatdinova[116], E. Rizvi[79], C. Rizzi[13], R.T. Roberts[87], S.H. Robertson[90,n], A. Robichaud-Veronneau[90], D. Robinson[30], J.E.M. Robinson[45], A. Robson[56], C. Roda[126a,126b], Y. Rodina[88,an], A. Rodriguez Perez[13], D. Rodriguez Rodriguez[170], S. Roe[32], C.S. Rogan[59], O. Røhne[121], J. Roloff[59], A. Romaniouk[100], M. Romano[22a,22b], S.M. Romano Saez[37], E. Romero Adam[170], N. Rompotis[140], M. Ronzani[51], L. Roos[83], E. Ros[170], S. Rosati[134a], K. Rosbach[51], P. Rose[139], N.-A. Rosien[57], V. Rossetti[148a,148b], E. Rossi[106a,106b], L.P. Rossi[53a], J.H.N. Rosten[30], R. Rosten[140], M. Rotaru[28b], I. Roth[175], J. Rothberg[140], D. Rousseau[119], A. Rozanov[88], Y. Rozen[154], X. Ruan[147c], F. Rubbo[145], M.S. Rudolph[161], F. Rühr[51], A. Ruiz-Martinez[31], Z. Rurikova[51], N.A. Rusakovich[68], A. Ruschke[102], H.L. Russell[140], J.P. Rutherfoord[7], N. Ruthmann[32], Y.F. Ryabov[125], M. Rybar[169], G. Rybkin[119], S. Ryu[6], A. Ryzhov[132], G.F. Rzehorz[57], A.F. Saavedra[152], G. Sabato[109], S. Sacerdoti[29], H.F-W. Sadrozinski[139], R. Sadykov[68], F. Safai Tehrani[134a], P. Saha[110], M. Sahinsoy[60a], M. Saimpert[138], T. Saito[157], H. Sakamoto[157], Y. Sakurai[174], G. Salamanna[136a,136b], A. Salamon[135a,135b], J.E. Salazar Loyola[34b], D. Salek[109], P.H. Sales De Bruin[140], D. Salihagic[103], A. Salnikov[145], J. Salt[170], D. Salvatore[40a,40b], F. Salvatore[151], A. Salvucci[62a,62b,62c], A. Salzburger[32], D. Sammel[51], D. Sampsonidis[156], J. Sánchez[170], V. Sanchez Martinez[170], A. Sanchez Pineda[106a,106b], H. Sandaker[121], R.L. Sandbach[79], M. Sandhoff[178], C. Sandoval[21], D.P.C. Sankey[133], M. Sannino[53a,53b], A. Sansoni[50], C. Santoni[37], R. Santonico[135a,135b], H. Santos[128a], I. Santoyo Castillo[151], K. Sapp[127], A. Sapronov[68], J.G. Saraiva[128a,128d], B. Sarrazin[23], O. Sasaki[69], K. Sato[164], E. Sauvan[5], G. Savage[80], P. Savard[161,d], N. Savic[103], C. Sawyer[133], L. Sawyer[82,s], J. Saxon[33], C. Sbarra[22a], A. Sbrizzi[22a,22b], T. Scanlon[81], D.A. Scannicchio[166], M. Scarcella[152], V. Scarfone[40a,40b], J. Schaarschmidt[175], P. Schacht[103], B.M. Schachtner[102], D. Schaefer[32], L. Schaefer[124], R. Schaefer[45], J. Schaeffer[86], S. Schaepe[23], S. Schaetzel[60b], U. Schäfer[86], A.C. Schaffer[119], D. Schaile[102], R.D. Schamberger[150], V. Scharf[60a], V.A. Schegelsky[125], D. Scheirich[131], M. Schernau[166], C. Schiavi[53a,53b], S. Schier[139], C. Schillo[51], M. Schioppa[40a,40b], S. Schlenker[32], K.R. Schmidt-Sommerfeld[103], K. Schmieden[32], C. Schmitt[86], S. Schmitt[45], S. Schmitz[86], B. Schneider[163a], U. Schnoor[51], L. Schoeffel[138], A. Schoening[60b], B.D. Schoenrock[93], E. Schopf[23], M. Schott[86], J.F.P. Schouwenberg[108], J. Schovancova[8], S. Schramm[52], M. Schreyer[177], N. Schuh[86], A. Schulte[86], M.J. Schultens[23], H.-C. Schultz-Coulon[60a], H. Schulz[17], M. Schumacher[51], B.A. Schumm[139], Ph. Schune[138], A. Schwartzman[145], T.A. Schwarz[92], H. Schweiger[87], Ph. Schwemling[138], R. Schwienhorst[93], J. Schwindling[138], T. Schwindt[23], G. Sciolla[25], F. Scuri[126a,126b], F. Scutti[91], J. Searcy[92], P. Seema[23], S.C. Seidel[107], A. Seiden[139], F. Seifert[130], J.M. Seixas[26a], G. Sekhniaidze[106a], K. Sekhon[92], S.J. Sekula[43], D.M. Seliverstov[125,*], N. Semprini-Cesari[22a,22b], C. Serfon[121], L. Serin[119], L. Serkin[167a,167b], M. Sessa[136a,136b], R. Seuster[172], H. Severini[115], T. Sfiligoj[78], F. Sforza[32], A. Sfyrla[52], E. Shabalina[57], N.W. Shaikh[148a,148b], L.Y. Shan[35a],

R. Shang[169], J.T. Shank[24], M. Shapiro[16], P.B. Shatalov[99], K. Shaw[167a,167b], S.M. Shaw[87],
A. Shcherbakova[148a,148b], C.Y. Shehu[151], P. Sherwood[81], L. Shi[153,ao], S. Shimizu[70], C.O. Shimmin[166],
M. Shimojima[104], S. Shirabe[73], M. Shiyakova[68,ap], A. Shmeleva[98], D. Shoaleh Saadi[97], M.J. Shochet[33],
S. Shojaii[94a], D.R. Shope[115], S. Shrestha[113], E. Shulga[100], M.A. Shupe[7], P. Sicho[129], A.M. Sickles[169],
P.E. Sidebo[149], E. Sideras Haddad[147c], O. Sidiropoulou[177], D. Sidorov[116], A. Sidoti[22a,22b], F. Siegert[47],
Dj. Sijacki[14], J. Silva[128a,128d], S.B. Silverstein[148a], V. Simak[130], Lj. Simic[14], S. Simion[119], E. Simioni[86],
B. Simmons[81], D. Simon[37], M. Simon[86], P. Sinervo[161], N.B. Sinev[118], M. Sioli[22a,22b], G. Siragusa[177],
I. Siral[92], S.Yu. Sivoklokov[101], J. Sjölin[148a,148b], M.B. Skinner[75], H.P. Skottowe[59], P. Skubic[115],
M. Slater[19], T. Slavicek[130], M. Slawinska[109], K. Sliwa[165], R. Slovak[131], V. Smakhtin[175], B.H. Smart[5],
L. Smestad[15], J. Smiesko[146a], S.Yu. Smirnov[100], Y. Smirnov[100], L.N. Smirnova[101,aq], O. Smirnova[84],
J.W. Smith[57], M.N.K. Smith[38], R.W. Smith[38], M. Smizanska[75], K. Smolek[130], A.A. Snesarev[98],
I.M. Snyder[118], S. Snyder[27], R. Sobie[172,n], F. Socher[47], A. Soffer[155], D.A. Soh[153], G. Sokhrannyi[78],
C.A. Solans Sanchez[32], M. Solar[130], E.Yu. Soldatov[100], U. Soldevila[170], A.A. Solodkov[132],
A. Soloshenko[68], O.V. Solovyanov[132], V. Solovyev[125], P. Sommer[51], H. Son[165], H.Y. Song[36a,ar],
A. Sood[16], A. Sopczak[130], V. Sopko[130], V. Sorin[13], D. Sosa[60b], C.L. Sotiropoulou[126a,126b],
R. Soualah[167a,167c], A.M. Soukharev[111,c], D. South[45], B.C. Sowden[80], S. Spagnolo[76a,76b],
M. Spalla[126a,126b], M. Spangenberg[173], F. Spanò[80], D. Sperlich[17], F. Spettel[103], R. Spighi[22a], G. Spigo[32],
L.A. Spiller[91], M. Spousta[131], R.D. St. Denis[56,*], A. Stabile[94a], R. Stamen[60a], S. Stamm[17],
E. Stanecka[42], R.W. Stanek[6], C. Stanescu[136a], M. Stanescu-Bellu[45], M.M. Stanitzki[45], S. Stapnes[121],
E.A. Starchenko[132], G.H. Stark[33], J. Stark[58], S.H Stark[39], P. Staroba[129], P. Starovoitov[60a], S. Stärz[32],
R. Staszewski[42], P. Steinberg[27], B. Stelzer[144], H.J. Stelzer[32], O. Stelzer-Chilton[163a], H. Stenzel[55],
G.A. Stewart[56], J.A. Stillings[23], M.C. Stockton[90], M. Stoebe[90], G. Stoicea[28b], P. Stolte[57], S. Stonjek[103],
A.R. Stradling[8], A. Straessner[47], M.E. Stramaglia[18], J. Strandberg[149], S. Strandberg[148a,148b],
A. Strandlie[121], M. Strauss[115], P. Strizenec[146b], R. Ströhmer[177], D.M. Strom[118], R. Stroynowski[43],
A. Strubig[108], S.A. Stucci[27], B. Stugu[15], N.A. Styles[45], D. Su[145], J. Su[127], S. Suchek[60a], Y. Sugaya[120],
M. Suk[130], V.V. Sulin[98], S. Sultansoy[4c], T. Sumida[71], S. Sun[59], X. Sun[35a], J.E. Sundermann[51],
K. Suruliz[151], C.J.E. Suster[152], M.R. Sutton[151], S. Suzuki[69], M. Svatos[129], M. Swiatlowski[33],
S.P. Swift[2], I. Sykora[146a], T. Sykora[131], D. Ta[51], K. Tackmann[45], J. Taenzer[155], A. Taffard[166],
R. Tafirout[163a], N. Taiblum[155], H. Takai[27], R. Takashima[72], T. Takeshita[142], Y. Takubo[69], M. Talby[88],
A.A. Talyshev[111,c], J. Tanaka[157], M. Tanaka[159], R. Tanaka[119], S. Tanaka[69], R. Tanioka[70],
B.B. Tannenwald[113], S. Tapia Araya[34b], S. Tapprogge[86], S. Tarem[154], G.F. Tartarelli[94a], P. Tas[131],
M. Tasevsky[129], T. Tashiro[71], E. Tassi[40a,40b], A. Tavares Delgado[128a,128b], Y. Tayalati[137e], A.C. Taylor[107],
G.N. Taylor[91], P.T.E. Taylor[91], W. Taylor[163b], F.A. Teischinger[32], P. Teixeira-Dias[80], K.K. Temming[51],
D. Temple[144], H. Ten Kate[32], P.K. Teng[153], J.J. Teoh[120], F. Tepel[178], S. Terada[69], K. Terashi[157],
J. Terron[85], S. Terzo[13], M. Testa[50], R.J. Teuscher[161,n], T. Theveneaux-Pelzer[88], J.P. Thomas[19],
J. Thomas-Wilsker[80], P.D. Thompson[19], A.S. Thompson[56], L.A. Thomsen[179], E. Thomson[124],
M.J. Tibbetts[16], R.E. Ticse Torres[88], V.O. Tikhomirov[98,as], Yu.A. Tikhonov[111,c], S. Timoshenko[100],
P. Tipton[179], S. Tisserant[88], K. Todome[159], T. Todorov[5,*], S. Todorova-Nova[131], J. Tojo[73], S. Tokár[146a],
K. Tokushuku[69], E. Tolley[59], L. Tomlinson[87], M. Tomoto[105], L. Tompkins[145,at], K. Toms[107], B. Tong[59],
P. Tornambe[51], E. Torrence[118], H. Torres[144], E. Torró Pastor[140], J. Toth[88,au], F. Touchard[88],
D.R. Tovey[141], T. Trefzger[177], A. Tricoli[27], I.M. Trigger[163a], S. Trincaz-Duvoid[83], M.F. Tripiana[13],
W. Trischuk[161], B. Trocmé[58], A. Trofymov[45], C. Troncon[94a], M. Trottier-McDonald[16], M. Trovatelli[172],
L. Truong[167a,167c], M. Trzebinski[42], A. Trzupek[42], J.C-L. Tseng[122], P.V. Tsiareshka[95], G. Tsipolitis[10],
N. Tsirintanis[9], S. Tsiskaridze[13], V. Tsiskaridze[51], E.G. Tskhadadze[54a], K.M. Tsui[62a], I.I. Tsukerman[99],
V. Tsulaia[16], S. Tsuno[69], D. Tsybychev[150], Y. Tu[62b], A. Tudorache[28b], V. Tudorache[28b], T.T. Tulbure[28a],
A.N. Tuna[59], S.A. Tupputi[22a,22b], S. Turchikhin[68], D. Turgeman[175], I. Turk Cakir[4b,av], R. Turra[94a,94b],
P.M. Tuts[38], G. Ucchielli[22a,22b], I. Ueda[157], M. Ughetto[148a,148b], F. Ukegawa[164], G. Unal[32], A. Undrus[27],

51

G. Unel[166], F.C. Ungaro[91], Y. Unno[69], C. Unverdorben[102], J. Urban[146b], P. Urquijo[91], P. Urrejola[86],
G. Usai[8], J. Usui[69], L. Vacavant[88], V. Vacek[130], B. Vachon[90], C. Valderanis[102],
E. Valdes Santurio[148a,148b], N. Valencic[109], S. Valentinetti[22a,22b], A. Valero[170], L. Valery[13], S. Valkar[131],
J.A. Valls Ferrer[170], W. Van Den Wollenberg[109], P.C. Van Der Deijl[109], H. van der Graaf[109],
N. van Eldik[154], P. van Gemmeren[6], J. Van Nieuwkoop[144], I. van Vulpen[109], M.C. van Woerden[109],
M. Vanadia[134a,134b], W. Vandelli[32], R. Vanguri[124], A. Vaniachine[160], P. Vankov[109], G. Vardanyan[180],
R. Vari[134a], E.W. Varnes[7], T. Varol[43], D. Varouchas[83], A. Vartapetian[8], K.E. Varvell[152], J.G. Vasquez[179],
G.A. Vasquez[34b], F. Vazeille[37], T. Vazquez Schroeder[90], J. Veatch[57], V. Veeraraghavan[7], L.M. Veloce[161],
F. Veloso[128a,128c], S. Veneziano[134a], A. Ventura[76a,76b], M. Venturi[172], N. Venturi[161], A. Venturini[25],
V. Vercesi[123a], M. Verducci[134a,134b], W. Verkerke[109], J.C. Vermeulen[109], A. Vest[47,aw], M.C. Vetterli[144,d],
O. Viazlo[84], I. Vichou[169,*], T. Vickey[141], O.E. Vickey Boeriu[141], G.H.A. Viehhauser[122], S. Viel[16],
L. Vigani[122], M. Villa[22a,22b], M. Villaplana Perez[94a,94b], E. Vilucchi[50], M.G. Vincter[31],
V.B. Vinogradov[68], C. Vittori[22a,22b], I. Vivarelli[151], S. Vlachos[10], M. Vlasak[130], M. Vogel[178],
P. Vokac[130], G. Volpi[126a,126b], M. Volpi[91], H. von der Schmitt[103], E. von Toerne[23], V. Vorobel[131],
K. Vorobev[100], M. Vos[170], R. Voss[32], J.H. Vossebeld[77], N. Vranjes[14], M. Vranjes Milosavljevic[14],
V. Vrba[129], M. Vreeswijk[109], R. Vuillermet[32], I. Vukotic[33], P. Wagner[23], W. Wagner[178], H. Wahlberg[74],
S. Wahrmund[47], J. Wakabayashi[105], J. Walder[75], R. Walker[102], W. Walkowiak[143], V. Wallangen[148a,148b],
C. Wang[35b], C. Wang[36b,ax], F. Wang[176], H. Wang[16], H. Wang[43], J. Wang[45], J. Wang[152], K. Wang[90],
R. Wang[6], S.M. Wang[153], T. Wang[38], W. Wang[36a], C. Wanotayaroj[118], A. Warburton[90], C.P. Ward[30],
D.R. Wardrope[81], A. Washbrook[49], P.M. Watkins[19], A.T. Watson[19], M.F. Watson[19], G. Watts[140],
S. Watts[87], B.M. Waugh[81], S. Webb[86], M.S. Weber[18], S.W. Weber[177], S.A. Weber[31], J.S. Webster[6],
A.R. Weidberg[122], B. Weinert[64], J. Weingarten[57], C. Weiser[51], H. Weits[109], P.S. Wells[32], T. Wenaus[27],
T. Wengler[32], S. Wenig[32], N. Wermes[23], M.D. Werner[67], P. Werner[32], M. Wessels[60a], J. Wetter[165],
K. Whalen[118], N.L. Whallon[140], A.M. Wharton[75], A. White[8], M.J. White[1], R. White[34b], D. Whiteson[166],
F.J. Wickens[133], W. Wiedenmann[176], M. Wielers[133], C. Wiglesworth[39], L.A.M. Wiik-Fuchs[23],
A. Wildauer[103], F. Wilk[87], H.G. Wilkens[32], H.H. Williams[124], S. Williams[109], C. Willis[93], S. Willocq[89],
J.A. Wilson[19], I. Wingerter-Seez[5], F. Winklmeier[118], O.J. Winston[151], B.T. Winter[23], M. Wittgen[145],
T.M.H. Wolf[109], R. Wolff[88], M.W. Wolter[42], H. Wolters[128a,128c], S.D. Worm[133], B.K. Wosiek[42],
J. Wotschack[32], M.J. Woudstra[87], K.W. Wozniak[42], M. Wu[58], M. Wu[33], S.L. Wu[176], X. Wu[52], Y. Wu[92],
T.R. Wyatt[87], B.M. Wynne[49], S. Xella[39], Z. Xi[92], D. Xu[35a], L. Xu[27], B. Yabsley[152], S. Yacoob[147a],
D. Yamaguchi[159], Y. Yamaguchi[120], A. Yamamoto[69], S. Yamamoto[157], T. Yamanaka[157],
K. Yamauchi[105], Y. Yamazaki[70], Z. Yan[24], H. Yang[36c], H. Yang[176], Y. Yang[153], Z. Yang[15], W-M. Yao[16],
Y.C. Yap[83], Y. Yasu[69], E. Yatsenko[5], K.H. Yau Wong[23], J. Ye[43], S. Ye[27], I. Yeletskikh[68], E. Yildirim[86],
K. Yorita[174], R. Yoshida[6], K. Yoshihara[124], C. Young[145], C.J.S. Young[32], S. Youssef[24], D.R. Yu[16],
J. Yu[8], J.M. Yu[92], J. Yu[67], L. Yuan[70], S.P.Y. Yuen[23], I. Yusuff[30,ay], B. Zabinski[42], G. Zacharis[10],
R. Zaidan[66], A.M. Zaitsev[132,ah], N. Zakharchuk[45], J. Zalieckas[15], A. Zaman[150], S. Zambito[59],
L. Zanello[134a,134b], D. Zanzi[91], C. Zeitnitz[178], M. Zeman[130], A. Zemla[41a], J.C. Zeng[169], Q. Zeng[145],
O. Zenin[132], T. Ženiš[146a], D. Zerwas[119], D. Zhang[92], F. Zhang[176], G. Zhang[36a,ar], H. Zhang[35b],
J. Zhang[6], L. Zhang[51], L. Zhang[36a], M. Zhang[169], R. Zhang[23], R. Zhang[36a,ax], X. Zhang[36b], Z. Zhang[119],
X. Zhao[43], Y. Zhao[36b,az], Z. Zhao[36a], A. Zhemchugov[68], J. Zhong[122], B. Zhou[92], C. Zhou[176], L. Zhou[38],
L. Zhou[43], M. Zhou[150], N. Zhou[35c], C.G. Zhu[36b], H. Zhu[35a], J. Zhu[92], Y. Zhu[36a], X. Zhuang[35a],
K. Zhukov[98], A. Zibell[177], D. Zieminska[64], N.I. Zimine[68], C. Zimmermann[86], S. Zimmermann[51],
Z. Zinonos[57], M. Zinser[86], M. Ziolkowski[143], L. Živković[14], G. Zobernig[176], A. Zoccoli[22a,22b],
M. zur Nedden[17], L. Zwalinski[32].

[1] Department of Physics, University of Adelaide, Adelaide, Australia
[2] Physics Department, SUNY Albany, Albany NY, United States of America

[3] Department of Physics, University of Alberta, Edmonton AB, Canada

[4] [a] Department of Physics, Ankara University, Ankara; [b] Istanbul Aydin University, Istanbul; [c] Division of Physics, TOBB University of Economics and Technology, Ankara, Turkey

[5] LAPP, CNRS/IN2P3 and Université Savoie Mont Blanc, Annecy-le-Vieux, France

[6] High Energy Physics Division, Argonne National Laboratory, Argonne IL, United States of America

[7] Department of Physics, University of Arizona, Tucson AZ, United States of America

[8] Department of Physics, The University of Texas at Arlington, Arlington TX, United States of America

[9] Physics Department, National and Kapodistrian University of Athens, Athens, Greece

[10] Physics Department, National Technical University of Athens, Zografou, Greece

[11] Department of Physics, The University of Texas at Austin, Austin TX, United States of America

[12] Institute of Physics, Azerbaijan Academy of Sciences, Baku, Azerbaijan

[13] Institut de Física d'Altes Energies (IFAE), The Barcelona Institute of Science and Technology, Barcelona, Spain

[14] Institute of Physics, University of Belgrade, Belgrade, Serbia

[15] Department for Physics and Technology, University of Bergen, Bergen, Norway

[16] Physics Division, Lawrence Berkeley National Laboratory and University of California, Berkeley CA, United States of America

[17] Department of Physics, Humboldt University, Berlin, Germany

[18] Albert Einstein Center for Fundamental Physics and Laboratory for High Energy Physics, University of Bern, Bern, Switzerland

[19] School of Physics and Astronomy, University of Birmingham, Birmingham, United Kingdom

[20] [a] Department of Physics, Bogazici University, Istanbul; [b] Department of Physics Engineering, Gaziantep University, Gaziantep; [d] Istanbul Bilgi University, Faculty of Engineering and Natural Sciences, Istanbul,Turkey; [e] Bahcesehir University, Faculty of Engineering and Natural Sciences, Istanbul, Turkey, Turkey

[21] Centro de Investigaciones, Universidad Antonio Narino, Bogota, Colombia

[22] [a] INFN Sezione di Bologna; [b] Dipartimento di Fisica e Astronomia, Università di Bologna, Bologna, Italy

[23] Physikalisches Institut, University of Bonn, Bonn, Germany

[24] Department of Physics, Boston University, Boston MA, United States of America

[25] Department of Physics, Brandeis University, Waltham MA, United States of America

[26] [a] Universidade Federal do Rio De Janeiro COPPE/EE/IF, Rio de Janeiro; [b] Electrical Circuits Department, Federal University of Juiz de Fora (UFJF), Juiz de Fora; [c] Federal University of Sao Joao del Rei (UFSJ), Sao Joao del Rei; [d] Instituto de Fisica, Universidade de Sao Paulo, Sao Paulo, Brazil

[27] Physics Department, Brookhaven National Laboratory, Upton NY, United States of America

[28] [a] Transilvania University of Brasov, Brasov, Romania; [b] Horia Hulubei National Institute of Physics and Nuclear Engineering, Bucharest; [c] National Institute for Research and Development of Isotopic and Molecular Technologies, Physics Department, Cluj Napoca; [d] University Politehnica Bucharest, Bucharest; [e] West University in Timisoara, Timisoara, Romania

[29] Departamento de Física, Universidad de Buenos Aires, Buenos Aires, Argentina

[30] Cavendish Laboratory, University of Cambridge, Cambridge, United Kingdom

[31] Department of Physics, Carleton University, Ottawa ON, Canada

[32] CERN, Geneva, Switzerland

[33] Enrico Fermi Institute, University of Chicago, Chicago IL, United States of America

[34] [a] Departamento de Física, Pontificia Universidad Católica de Chile, Santiago; [b] Departamento de Física, Universidad Técnica Federico Santa María, Valparaíso, Chile

[35] [a] Institute of High Energy Physics, Chinese Academy of Sciences, Beijing; [b] Department of

Physics, Nanjing University, Jiangsu; [c] Physics Department, Tsinghua University, Beijing 100084, China

36 [a] Department of Modern Physics, University of Science and Technology of China, Anhui; [b] School of Physics, Shandong University, Shandong; [c] Department of Physics and Astronomy, Key Laboratory for Particle Physics, Astrophysics and Cosmology, Ministry of Education; Shanghai Key Laboratory for Particle Physics and Cosmology (SKLPPC), Shanghai Jiao Tong University, Shanghai;, China

37 Laboratoire de Physique Corpusculaire, Université Clermont Auvergne, Université Blaise Pascal, CNRS/IN2P3, Clermont-Ferrand, France

38 Nevis Laboratory, Columbia University, Irvington NY, United States of America

39 Niels Bohr Institute, University of Copenhagen, Kobenhavn, Denmark

40 [a] INFN Gruppo Collegato di Cosenza, Laboratori Nazionali di Frascati; [b] Dipartimento di Fisica, Università della Calabria, Rende, Italy

41 [a] AGH University of Science and Technology, Faculty of Physics and Applied Computer Science, Krakow; [b] Marian Smoluchowski Institute of Physics, Jagiellonian University, Krakow, Poland

42 Institute of Nuclear Physics Polish Academy of Sciences, Krakow, Poland

43 Physics Department, Southern Methodist University, Dallas TX, United States of America

44 Physics Department, University of Texas at Dallas, Richardson TX, United States of America

45 DESY, Hamburg and Zeuthen, Germany

46 Lehrstuhl für Experimentelle Physik IV, Technische Universität Dortmund, Dortmund, Germany

47 Institut für Kern- und Teilchenphysik, Technische Universität Dresden, Dresden, Germany

48 Department of Physics, Duke University, Durham NC, United States of America

49 SUPA - School of Physics and Astronomy, University of Edinburgh, Edinburgh, United Kingdom

50 INFN Laboratori Nazionali di Frascati, Frascati, Italy

51 Fakultät für Mathematik und Physik, Albert-Ludwigs-Universität, Freiburg, Germany

52 Departement de Physique Nucleaire et Corpusculaire, Université de Genève, Geneva, Switzerland

53 [a] INFN Sezione di Genova; [b] Dipartimento di Fisica, Università di Genova, Genova, Italy

54 [a] E. Andronikashvili Institute of Physics, Iv. Javakhishvili Tbilisi State University, Tbilisi; [b] High Energy Physics Institute, Tbilisi State University, Tbilisi, Georgia

55 II Physikalisches Institut, Justus-Liebig-Universität Giessen, Giessen, Germany

56 SUPA - School of Physics and Astronomy, University of Glasgow, Glasgow, United Kingdom

57 II Physikalisches Institut, Georg-August-Universität, Göttingen, Germany

58 Laboratoire de Physique Subatomique et de Cosmologie, Université Grenoble-Alpes, CNRS/IN2P3, Grenoble, France

59 Laboratory for Particle Physics and Cosmology, Harvard University, Cambridge MA, United States of America

60 [a] Kirchhoff-Institut für Physik, Ruprecht-Karls-Universität Heidelberg, Heidelberg; [b] Physikalisches Institut, Ruprecht-Karls-Universität Heidelberg, Heidelberg; [c] ZITI Institut für technische Informatik, Ruprecht-Karls-Universität Heidelberg, Mannheim, Germany

61 Faculty of Applied Information Science, Hiroshima Institute of Technology, Hiroshima, Japan

62 [a] Department of Physics, The Chinese University of Hong Kong, Shatin, N.T., Hong Kong; [b] Department of Physics, The University of Hong Kong, Hong Kong; [c] Department of Physics and Institute for Advanced Study, The Hong Kong University of Science and Technology, Clear Water Bay, Kowloon, Hong Kong, China

63 Department of Physics, National Tsing Hua University, Taiwan, Taiwan

64 Department of Physics, Indiana University, Bloomington IN, United States of America

65 Institut für Astro- und Teilchenphysik, Leopold-Franzens-Universität, Innsbruck, Austria

66 University of Iowa, Iowa City IA, United States of America

[67] Department of Physics and Astronomy, Iowa State University, Ames IA, United States of America
[68] Joint Institute for Nuclear Research, JINR Dubna, Dubna, Russia
[69] KEK, High Energy Accelerator Research Organization, Tsukuba, Japan
[70] Graduate School of Science, Kobe University, Kobe, Japan
[71] Faculty of Science, Kyoto University, Kyoto, Japan
[72] Kyoto University of Education, Kyoto, Japan
[73] Department of Physics, Kyushu University, Fukuoka, Japan
[74] Instituto de Física La Plata, Universidad Nacional de La Plata and CONICET, La Plata, Argentina
[75] Physics Department, Lancaster University, Lancaster, United Kingdom
[76] [a] INFN Sezione di Lecce; [b] Dipartimento di Matematica e Fisica, Università del Salento, Lecce, Italy
[77] Oliver Lodge Laboratory, University of Liverpool, Liverpool, United Kingdom
[78] Department of Experimental Particle Physics, Jožef Stefan Institute and Department of Physics, University of Ljubljana, Ljubljana, Slovenia
[79] School of Physics and Astronomy, Queen Mary University of London, London, United Kingdom
[80] Department of Physics, Royal Holloway University of London, Surrey, United Kingdom
[81] Department of Physics and Astronomy, University College London, London, United Kingdom
[82] Louisiana Tech University, Ruston LA, United States of America
[83] Laboratoire de Physique Nucléaire et de Hautes Energies, UPMC and Université Paris-Diderot and CNRS/IN2P3, Paris, France
[84] Fysiska institutionen, Lunds universitet, Lund, Sweden
[85] Departamento de Fisica Teorica C-15, Universidad Autonoma de Madrid, Madrid, Spain
[86] Institut für Physik, Universität Mainz, Mainz, Germany
[87] School of Physics and Astronomy, University of Manchester, Manchester, United Kingdom
[88] CPPM, Aix-Marseille Université and CNRS/IN2P3, Marseille, France
[89] Department of Physics, University of Massachusetts, Amherst MA, United States of America
[90] Department of Physics, McGill University, Montreal QC, Canada
[91] School of Physics, University of Melbourne, Victoria, Australia
[92] Department of Physics, The University of Michigan, Ann Arbor MI, United States of America
[93] Department of Physics and Astronomy, Michigan State University, East Lansing MI, United States of America
[94] [a] INFN Sezione di Milano; [b] Dipartimento di Fisica, Università di Milano, Milano, Italy
[95] B.I. Stepanov Institute of Physics, National Academy of Sciences of Belarus, Minsk, Republic of Belarus
[96] Research Institute for Nuclear Problems of Byelorussian State University, Minsk, Republic of Belarus
[97] Group of Particle Physics, University of Montreal, Montreal QC, Canada
[98] P.N. Lebedev Physical Institute of the Russian Academy of Sciences, Moscow, Russia
[99] Institute for Theoretical and Experimental Physics (ITEP), Moscow, Russia
[100] National Research Nuclear University MEPhI, Moscow, Russia
[101] D.V. Skobeltsyn Institute of Nuclear Physics, M.V. Lomonosov Moscow State University, Moscow, Russia
[102] Fakultät für Physik, Ludwig-Maximilians-Universität München, München, Germany
[103] Max-Planck-Institut für Physik (Werner-Heisenberg-Institut), München, Germany
[104] Nagasaki Institute of Applied Science, Nagasaki, Japan
[105] Graduate School of Science and Kobayashi-Maskawa Institute, Nagoya University, Nagoya, Japan
[106] [a] INFN Sezione di Napoli; [b] Dipartimento di Fisica, Università di Napoli, Napoli, Italy
[107] Department of Physics and Astronomy, University of New Mexico, Albuquerque NM, United States

of America

[108] Institute for Mathematics, Astrophysics and Particle Physics, Radboud University Nijmegen/Nikhef, Nijmegen, Netherlands

[109] Nikhef National Institute for Subatomic Physics and University of Amsterdam, Amsterdam, Netherlands

[110] Department of Physics, Northern Illinois University, DeKalb IL, United States of America

[111] Budker Institute of Nuclear Physics, SB RAS, Novosibirsk, Russia

[112] Department of Physics, New York University, New York NY, United States of America

[113] Ohio State University, Columbus OH, United States of America

[114] Faculty of Science, Okayama University, Okayama, Japan

[115] Homer L. Dodge Department of Physics and Astronomy, University of Oklahoma, Norman OK, United States of America

[116] Department of Physics, Oklahoma State University, Stillwater OK, United States of America

[117] Palacký University, RCPTM, Olomouc, Czech Republic

[118] Center for High Energy Physics, University of Oregon, Eugene OR, United States of America

[119] LAL, Univ. Paris-Sud, CNRS/IN2P3, Université Paris-Saclay, Orsay, France

[120] Graduate School of Science, Osaka University, Osaka, Japan

[121] Department of Physics, University of Oslo, Oslo, Norway

[122] Department of Physics, Oxford University, Oxford, United Kingdom

[123] [a] INFN Sezione di Pavia; [b] Dipartimento di Fisica, Università di Pavia, Pavia, Italy

[124] Department of Physics, University of Pennsylvania, Philadelphia PA, United States of America

[125] National Research Centre "Kurchatov Institute" B.P.Konstantinov Petersburg Nuclear Physics Institute, St. Petersburg, Russia

[126] [a] INFN Sezione di Pisa; [b] Dipartimento di Fisica E. Fermi, Università di Pisa, Pisa, Italy

[127] Department of Physics and Astronomy, University of Pittsburgh, Pittsburgh PA, United States of America

[128] [a] Laboratório de Instrumentação e Física Experimental de Partículas - LIP, Lisboa; [b] Faculdade de Ciências, Universidade de Lisboa, Lisboa; [c] Department of Physics, University of Coimbra, Coimbra; [d] Centro de Física Nuclear da Universidade de Lisboa, Lisboa; [e] Departamento de Fisica, Universidade do Minho, Braga; [f] Departamento de Fisica Teorica y del Cosmos and CAFPE, Universidad de Granada, Granada (Spain); [g] Dep Fisica and CEFITEC of Faculdade de Ciencias e Tecnologia, Universidade Nova de Lisboa, Caparica, Portugal

[129] Institute of Physics, Academy of Sciences of the Czech Republic, Praha, Czech Republic

[130] Czech Technical University in Prague, Praha, Czech Republic

[131] Charles University, Faculty of Mathematics and Physics, Prague, Czech Republic

[132] State Research Center Institute for High Energy Physics (Protvino), NRC KI, Russia

[133] Particle Physics Department, Rutherford Appleton Laboratory, Didcot, United Kingdom

[134] [a] INFN Sezione di Roma; [b] Dipartimento di Fisica, Sapienza Università di Roma, Roma, Italy

[135] [a] INFN Sezione di Roma Tor Vergata; [b] Dipartimento di Fisica, Università di Roma Tor Vergata, Roma, Italy

[136] [a] INFN Sezione di Roma Tre; [b] Dipartimento di Matematica e Fisica, Università Roma Tre, Roma, Italy

[137] [a] Faculté des Sciences Ain Chock, Réseau Universitaire de Physique des Hautes Energies - Université Hassan II, Casablanca; [b] Centre National de l'Energie des Sciences Techniques Nucleaires, Rabat; [c] Faculté des Sciences Semlalia, Université Cadi Ayyad, LPHEA-Marrakech; [d] Faculté des Sciences, Université Mohamed Premier and LPTPM, Oujda; [e] Faculté des sciences, Université Mohammed V, Rabat, Morocco

[138] DSM/IRFU (Institut de Recherches sur les Lois Fondamentales de l'Univers), CEA Saclay (Commissariat à l'Energie Atomique et aux Energies Alternatives), Gif-sur-Yvette, France

[139] Santa Cruz Institute for Particle Physics, University of California Santa Cruz, Santa Cruz CA, United States of America

[140] Department of Physics, University of Washington, Seattle WA, United States of America

[141] Department of Physics and Astronomy, University of Sheffield, Sheffield, United Kingdom

[142] Department of Physics, Shinshu University, Nagano, Japan

[143] Fachbereich Physik, Universität Siegen, Siegen, Germany

[144] Department of Physics, Simon Fraser University, Burnaby BC, Canada

[145] SLAC National Accelerator Laboratory, Stanford CA, United States of America

[146] [a] Faculty of Mathematics, Physics & Informatics, Comenius University, Bratislava; [b] Department of Subnuclear Physics, Institute of Experimental Physics of the Slovak Academy of Sciences, Kosice, Slovak Republic

[147] [a] Department of Physics, University of Cape Town, Cape Town; [b] Department of Physics, University of Johannesburg, Johannesburg; [c] School of Physics, University of the Witwatersrand, Johannesburg, South Africa

[148] [a] Department of Physics, Stockholm University; [b] The Oskar Klein Centre, Stockholm, Sweden

[149] Physics Department, Royal Institute of Technology, Stockholm, Sweden

[150] Departments of Physics & Astronomy and Chemistry, Stony Brook University, Stony Brook NY, United States of America

[151] Department of Physics and Astronomy, University of Sussex, Brighton, United Kingdom

[152] School of Physics, University of Sydney, Sydney, Australia

[153] Institute of Physics, Academia Sinica, Taipei, Taiwan

[154] Department of Physics, Technion: Israel Institute of Technology, Haifa, Israel

[155] Raymond and Beverly Sackler School of Physics and Astronomy, Tel Aviv University, Tel Aviv, Israel

[156] Department of Physics, Aristotle University of Thessaloniki, Thessaloniki, Greece

[157] International Center for Elementary Particle Physics and Department of Physics, The University of Tokyo, Tokyo, Japan

[158] Graduate School of Science and Technology, Tokyo Metropolitan University, Tokyo, Japan

[159] Department of Physics, Tokyo Institute of Technology, Tokyo, Japan

[160] Tomsk State University, Tomsk, Russia, Russia

[161] Department of Physics, University of Toronto, Toronto ON, Canada

[162] [a] INFN-TIFPA; [b] University of Trento, Trento, Italy, Italy

[163] [a] TRIUMF, Vancouver BC; [b] Department of Physics and Astronomy, York University, Toronto ON, Canada

[164] Faculty of Pure and Applied Sciences, and Center for Integrated Research in Fundamental Science and Engineering, University of Tsukuba, Tsukuba, Japan

[165] Department of Physics and Astronomy, Tufts University, Medford MA, United States of America

[166] Department of Physics and Astronomy, University of California Irvine, Irvine CA, United States of America

[167] [a] INFN Gruppo Collegato di Udine, Sezione di Trieste, Udine; [b] ICTP, Trieste; [c] Dipartimento di Chimica, Fisica e Ambiente, Università di Udine, Udine, Italy

[168] Department of Physics and Astronomy, University of Uppsala, Uppsala, Sweden

[169] Department of Physics, University of Illinois, Urbana IL, United States of America

[170] Instituto de Fisica Corpuscular (IFIC) and Departamento de Fisica Atomica, Molecular y Nuclear and Departamento de Ingeniería Electrónica and Instituto de Microelectrónica de Barcelona

(IMB-CNM), University of Valencia and CSIC, Valencia, Spain

[171] Department of Physics, University of British Columbia, Vancouver BC, Canada

[172] Department of Physics and Astronomy, University of Victoria, Victoria BC, Canada

[173] Department of Physics, University of Warwick, Coventry, United Kingdom

[174] Waseda University, Tokyo, Japan

[175] Department of Particle Physics, The Weizmann Institute of Science, Rehovot, Israel

[176] Department of Physics, University of Wisconsin, Madison WI, United States of America

[177] Fakultät für Physik und Astronomie, Julius-Maximilians-Universität, Würzburg, Germany

[178] Fakultät für Mathematik und Naturwissenschaften, Fachgruppe Physik, Bergische Universität Wuppertal, Wuppertal, Germany

[179] Department of Physics, Yale University, New Haven CT, United States of America

[180] Yerevan Physics Institute, Yerevan, Armenia

[181] Centre de Calcul de l'Institut National de Physique Nucléaire et de Physique des Particules (IN2P3), Villeurbanne, France

[a] Also at Department of Physics, King's College London, London, United Kingdom

[b] Also at Institute of Physics, Azerbaijan Academy of Sciences, Baku, Azerbaijan

[c] Also at Novosibirsk State University, Novosibirsk, Russia

[d] Also at TRIUMF, Vancouver BC, Canada

[e] Also at Department of Physics & Astronomy, University of Louisville, Louisville, KY, United States of America

[f] Also at Physics Department, An-Najah National University, Nablus, Palestine

[g] Also at Department of Physics, California State University, Fresno CA, United States of America

[h] Also at Department of Physics, University of Fribourg, Fribourg, Switzerland

[i] Also at Departament de Fisica de la Universitat Autonoma de Barcelona, Barcelona, Spain

[j] Also at Departamento de Fisica e Astronomia, Faculdade de Ciencias, Universidade do Porto, Portugal

[k] Also at Tomsk State University, Tomsk, Russia, Russia

[l] Also at The Collaborative Innovation Center of Quantum Matter (CICQM), Beijing, China

[m] Also at Universita di Napoli Parthenope, Napoli, Italy

[n] Also at Institute of Particle Physics (IPP), Canada

[o] Also at Horia Hulubei National Institute of Physics and Nuclear Engineering, Bucharest, Romania

[p] Also at Department of Physics, St. Petersburg State Polytechnical University, St. Petersburg, Russia

[q] Also at Department of Physics, The University of Michigan, Ann Arbor MI, United States of America

[r] Also at Centre for High Performance Computing, CSIR Campus, Rosebank, Cape Town, South Africa

[s] Also at Louisiana Tech University, Ruston LA, United States of America

[t] Also at Institucio Catalana de Recerca i Estudis Avancats, ICREA, Barcelona, Spain

[u] Also at Graduate School of Science, Osaka University, Osaka, Japan

[v] Also at Fakultät für Mathematik und Physik, Albert-Ludwigs-Universität, Freiburg, Germany

[w] Also at Institute for Mathematics, Astrophysics and Particle Physics, Radboud University Nijmegen/Nikhef, Nijmegen, Netherlands

[x] Also at Department of Physics, The University of Texas at Austin, Austin TX, United States of America

[y] Also at Institute of Theoretical Physics, Ilia State University, Tbilisi, Georgia

[z] Also at CERN, Geneva, Switzerland

[aa] Also at Georgian Technical University (GTU),Tbilisi, Georgia

[ab] Also at Ochadai Academic Production, Ochanomizu University, Tokyo, Japan

[ac] Also at Manhattan College, New York NY, United States of America

[ad] Also at Academia Sinica Grid Computing, Institute of Physics, Academia Sinica, Taipei, Taiwan

[ae] Also at School of Physics, Shandong University, Shandong, China

[af] Also at Departamento de Fisica Teorica y del Cosmos and CAFPE, Universidad de Granada, Granada (Spain), Portugal

[ag] Also at Department of Physics, California State University, Sacramento CA, United States of America

[ah] Also at Moscow Institute of Physics and Technology State University, Dolgoprudny, Russia

[ai] Also at Departement de Physique Nucleaire et Corpusculaire, Université de Genève, Geneva, Switzerland

[aj] Also at Eotvos Lorand University, Budapest, Hungary

[ak] Also at Departments of Physics & Astronomy and Chemistry, Stony Brook University, Stony Brook NY, United States of America

[al] Also at International School for Advanced Studies (SISSA), Trieste, Italy

[am] Also at Department of Physics and Astronomy, University of South Carolina, Columbia SC, United States of America

[an] Also at Institut de Física d'Altes Energies (IFAE), The Barcelona Institute of Science and Technology, Barcelona, Spain

[ao] Also at School of Physics, Sun Yat-sen University, Guangzhou, China

[ap] Also at Institute for Nuclear Research and Nuclear Energy (INRNE) of the Bulgarian Academy of Sciences, Sofia, Bulgaria

[aq] Also at Faculty of Physics, M.V.Lomonosov Moscow State University, Moscow, Russia

[ar] Also at Institute of Physics, Academia Sinica, Taipei, Taiwan

[as] Also at National Research Nuclear University MEPhI, Moscow, Russia

[at] Also at Department of Physics, Stanford University, Stanford CA, United States of America

[au] Also at Institute for Particle and Nuclear Physics, Wigner Research Centre for Physics, Budapest, Hungary

[av] Also at Giresun University, Faculty of Engineering, Turkey

[aw] Also at Flensburg University of Applied Sciences, Flensburg, Germany

[ax] Also at CPPM, Aix-Marseille Université and CNRS/IN2P3, Marseille, France

[ay] Also at University of Malaya, Department of Physics, Kuala Lumpur, Malaysia

[az] Also at LAL, Univ. Paris-Sud, CNRS/IN2P3, Université Paris-Saclay, Orsay, France

* Deceased